

ACC JOURNAL XXIV 1/2018

Issue A

Natural Sciences and Technology



TECHNICKÁ UNIVERZITA V LIBERCI

HOCHSCHULE ZITTAU/GÖRLITZ

INTERNATIONALES HOCHSCHULINSTITUT ZITTAU (TU DRESDEN)

UNIwersYTET EKONOMICZNY WE WROCLAWIU

WYDZIAŁ EKONOMII, ZARZĄDZANIA I TURYSTYKI W JELENIEJ GÓRZE

Indexed in:

INDEX  COPERNICUS
I N T E R N A T I O N A L

Liberec – Zittau/Görlitz – Wrocław/Jelenia Góra

© **Technická univerzita v Liberci 2018**

ISSN 1803-9782 (Print)

ISSN 1803-9790 (CD-ROM)

ISSN 2571-0613 (Online)

ACC JOURNAL je mezinárodní vědecký časopis, jehož vydavatelem je Technická univerzita v Liberci. Na jeho tvorbě se podílí čtyři vysoké školy sdružené v Akademickém koordinačním středisku v Euroregionu Nisa (ACC). Ročně vycházejí zpravidla tři čísla.

ACC JOURNAL je periodikum publikující původní recenzované vědecké práce, vědecké studie, příspěvky ke konferencím a výzkumným projektům. První číslo obsahuje příspěvky zaměřené na oblast přírodních věd a techniky, druhé číslo je zaměřeno na oblast ekonomie, třetí číslo pojednává o tématech ze společenských věd. ACC JOURNAL má charakter recenzovaného časopisu. Jeho vydání navazuje na sborník „Vědecká pojednání“, který vycházel v letech 1995-2008.

ACC JOURNAL is an international scientific journal. It is published by the Technical University of Liberec. Four universities united in the Academic Coordination Centre in the Euroregion Nisa participate in its production. There are usually three issues of the journal annually.

ACC JOURNAL is a periodical publishing original reviewed scientific papers, scientific studies, papers presented at conferences, and findings of research projects. The first issue focuses on natural sciences and technology, the second issue deals with the science of economics, and the third issue contains findings from the area of social sciences. ACC JOURNAL is a reviewed one. It is building upon the tradition of the “Scientific Treatises” published between 1995 and 2008.

Hlavní recenzenti (major reviewers):

Ing. Vojtěch Radolf, Ph.D.

The Czech Academy of Sciences
Institute of Thermomechanics
Czech Republic

Ing. Štěpán Kunc, Ph.D.

Technical University of Liberec
Faculty of Science, Humanities and Education
Czech Republic

Contents

Research Articles

- Identification of Mid-spatial Frequency Error on the Optotech MCG 100 when Grinding Optical Elements 7**
Ing. Jiří Beneš; Ing. Michal Špína; Ing. František Procháska, Ph.D.
- Construction of a Vacuum Ultraviolet Transmission Spectrometer 17**
Ing. Jiří Hlubuček; Ing. Jiří Budasz; Ing. Jan Václavík; RNDr. Karel Žídek, Ph.D.
- Hyperspectral Imaging in Infrared Region Using Compressed Sensing Methods..... 24**
Ing. Jiří Hlubuček; RNDr. Karel Žídek, Ph.D.
- Time Average Scanning Digital Holography 33**
Ing. Pavel Psota, Ph.D.; Ing. Vít Lédl, Ph.D.; Ing. Roman Doleček, Ph.D.; Ing. Ondřej Matoušek; Ing. Jan Kredba
- Objective Evaluation of Upright and Grand Pianos by Measuring Play-Bench..... 43**
Ing. Jana Urbánková

Miscellanea

- Total Run-Out Measurement of the Multistart Worm by the Laser Line Triangulation Sensor..... 53**
Ing. Alexander Prošek
- DiverGrass – A Cross Border Project to Promote Sustainable Management of Grasslands..... 61**
Ing. Jan Titěra; Henning Haase, MSc; Ing. Teowdroes Kassahun Teku;
Ing. Chukwudi Nwaogu, MSc; Ing. Klára Pavlů, Ph.D.; Dr. Matthias Kändler;
Ing. Lenka Pavlů, Ph.D.; Ing. Jan Gaisler, Ph.D.; František Paška; Heike Heidenreich;
Dipl.-Ing (FH) Gerlinde Liepelt; Irena Jonášová; Prof. Dr. Vilém Pavlů
- List of Authors 81**
- Guidelines for Contributors 82**
- Editorial Board 83**

Research Articles

IDENTIFICATION OF MID-SPATIAL FREQUENCY ERROR ON THE OPTOTECH MCG 100 WHEN GRINDING OPTICAL ELEMENTS

Jiří Beněš¹; Michal Špina²; František Procháska³

Institute of Plasma Physics, Academy of Sciences of the Czech Republic,
Regional Centre for Special Optics and Optoelectronic Systems (TOPTEC),
Sobotecká 1660, 511 01 Turnov, Czech Republic
e-mail: benes@ipp.cas.cz; spina@ipp.cas.cz; prochaska@ipp.cas.cz

Abstract

The mid-spatial frequency errors, surface defects arising from the production of optical aspherical surfaces may be a major problem, for example in high-performance systems. At the production of aspherical surfaces on the Optotech MCG100, vibration measurements were performed in various operating modes. The measurement was done with VibXpert II. This device uses piezoelectric sensors to record vibration acceleration. The measurement data were then processed in Matlab software. The aim was to identify frequencies, which may have a negative influence on optical element manufacturing, and also to outline possible causes of their origin.

In the observed spectrum (30-800 Hz), significant frequencies from several basic sources were found. This is the tool spindle rotation, tool rotation, the axes control loop, and the movement of the axes themselves.

Keywords

Vibration; Middle; Frequency; Optical; Aspheric; Surface.

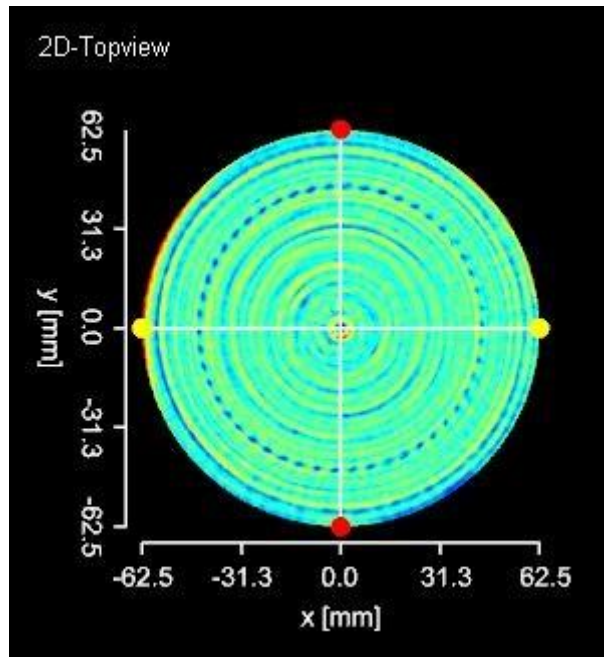
Introduction

Vibrations in CNC machines are a complex phenomenon. They are caused by interactions between the solid and flexible elements constituting the machine. These vibrations may be caused by imbalance of rotating parts, inertia forces of elements performing a direct or circular reciprocating motion, imprecision of transmission mechanisms, or by background interference via the base to the machine.

For optical fine grinding, vibration is a major obstacle to achieving the required quality. Transmission of vibration into process means deformation of the optical surface. This has a negative effect on the transmission of light through the optical element and creates a defect in the image.

1 Research Objectives

The aim of the research is to investigate the occurrence of mid-spatial frequency errors and to propose methods for their suppression. These defects are due to vibrations (Figure 1). These vibrations are transmitted to the optical surface in the form of a regular local shape defect. The defect thus created adverse effects on the entire optical system. So we have tried to find out the causes of the vibrations and tried to design a way to reduce these vibrations.



Source: Own

Fig. 1: An example of mid-spatial frequency error

2 Methods of Research

The basic source of mid-spatial frequency error is the grinding process. During this process, defects occur on the optical surface, which is very difficult to suppress in the later stages of machining. The entire grinding process is performed on an Optotech MCG 100 machine where the occurrence of these defects was observed earlier. The whole process is divided into several basic stages. First, rough and fine grinding. Second, ultra fine grinding, and the last are corrections. Grinding involves the removal of four layers, followed by a profile measurement on the LUPHOScan contactless profilometer. The measured data are then used to correct the optical deflection of the optical surface. This step is performed by removing two layers. The diamond tools are used with 100 mm diameters and grains D91, D38 with a metal bond and D20 with a resin bond. During the grinding process, vibration acceleration is measured with the VibXpert II. The measuring instrument uses a pair of piezoelectric sensors mounted on a magnet. These sensors are mounted on the rotating head of the tool spindles (Figure 2) in the Y direction. From the measured data, FFT frequency analysis is then created in Matlab software.



Source: Own

Fig. 2: Sensors mounted on the rotating head of the tool spindles

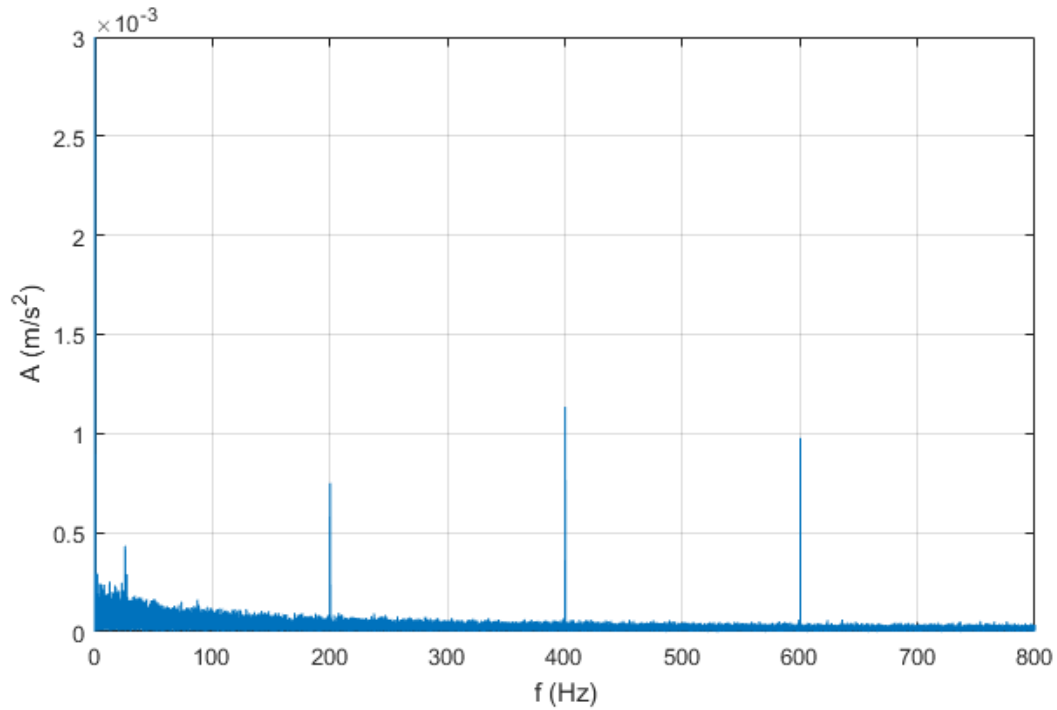
3 Mid-spatial Frequency

Mid-spatial frequency errors include structures with wavelength of 0.46 – 10 mm. The wavelength of the structures in the concentric direction is determined by the circumferential workpiece velocity and the frequency of undesirable vibrations (1). For a circumferential velocity $v_o = 20$ m/min it is approximately 33 - 724 Hz.

$$\lambda = \frac{v_o}{f} \quad (1)$$

4 Identification of Key Frequencies and Potential Vibration Sources

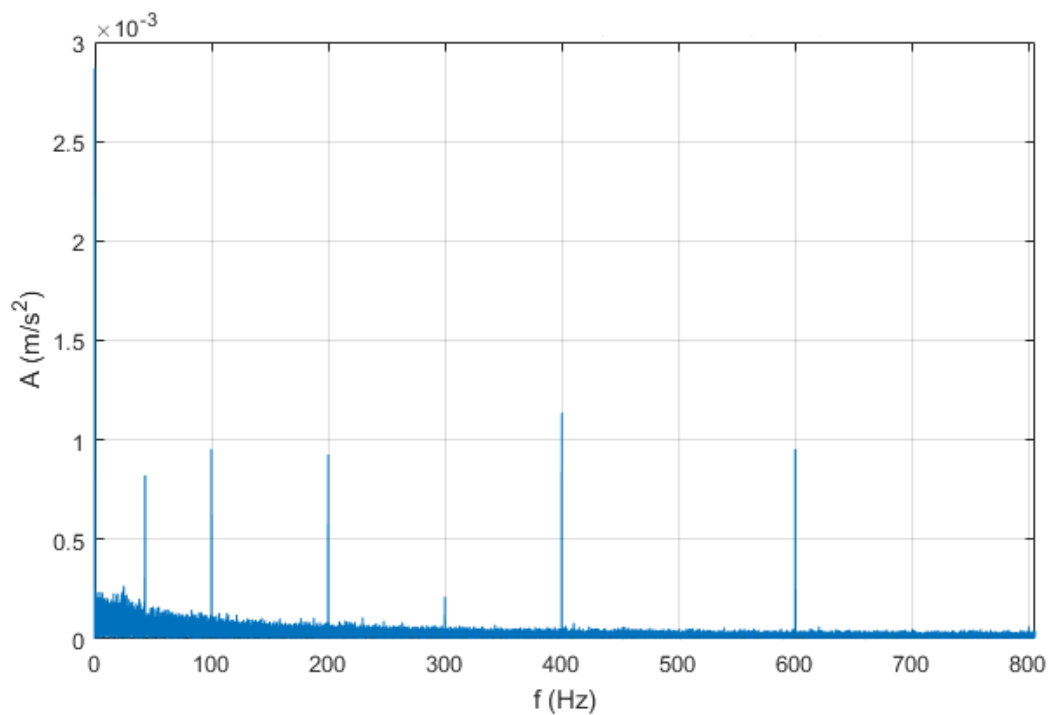
Research into vibration sources in this range revealed several factors. To enable identification of specific vibration sources, the experiment was begun by a measurement of vibrations in different modes of the machine. The first measurement was carried out on a switched-off machine. Thus, we acquired an indication of interference (Figure 3). [1]



Source: Own

Fig. 3: Frequency analysis of vibration acceleration measurement on a switched-off machine

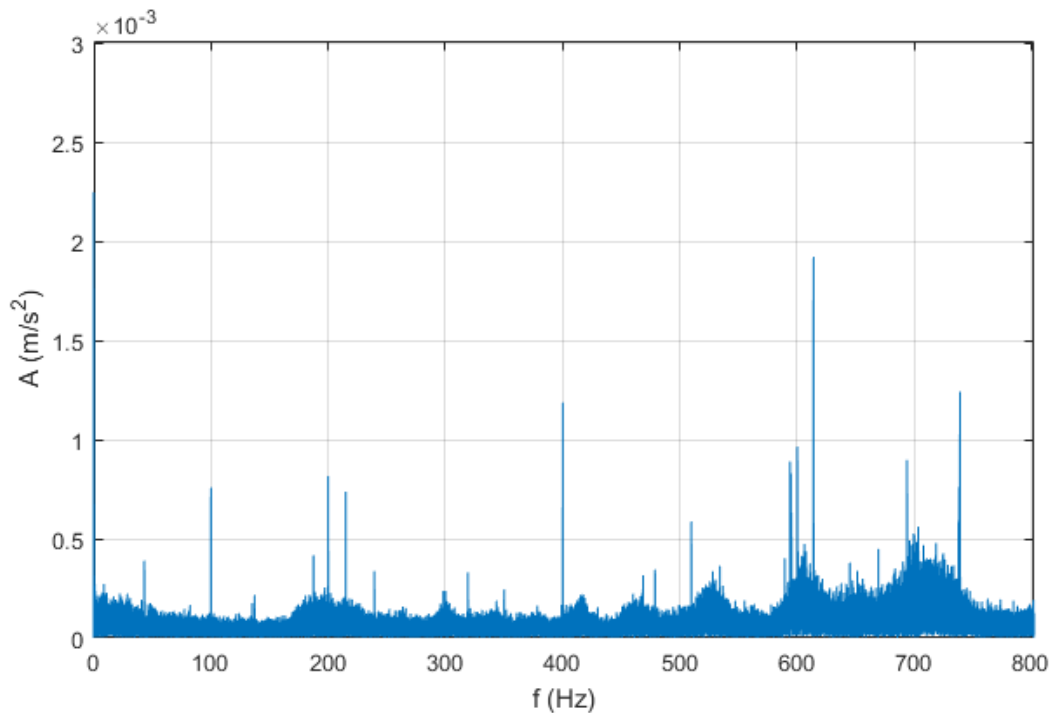
In a resting-state mode, once the machine was switched on (Figure 4), frequencies of 50 and 100 Hz, which are attributed to the operating system of the machine, were revealed in addition to the above-described interferences.



Source: Own

Fig. 4: Frequency analysis of vibration acceleration measurement upon switching on electric current

Next, the measurement was completed during a running process, in which workpiece and tool drives were deactivated, as were linear axes motions (Figure 5). The measurement showed that, in addition to the previously discovered frequencies, this mode generated a number of others. Given the mode of the machine, these frequencies are primarily ascribed to the axes positioning system or more precisely to regenerative loops, which ensure precise positioning of the axes. While these loops operate at a much higher frequency (around 4 kHz), they generate frequencies near 200 and 600 Hz in the mechanical system of the machine. [1][5]

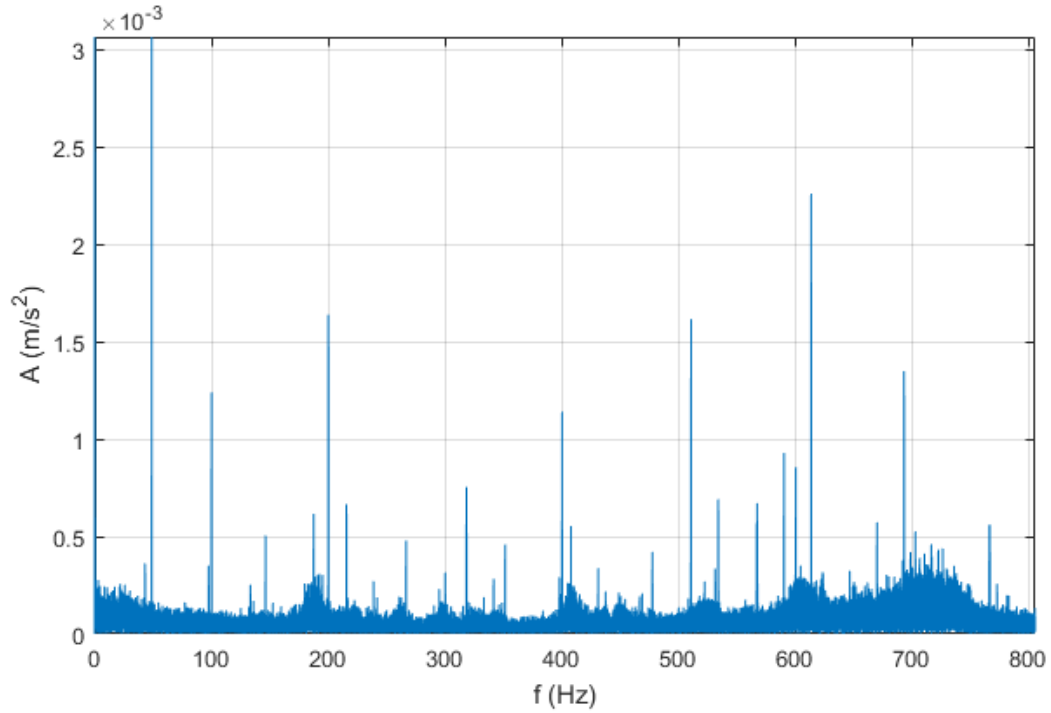


Source: Own

Fig. 5: Frequency analysis of vibration acceleration measurement during a running process, tool rotation and axes motion deactivated

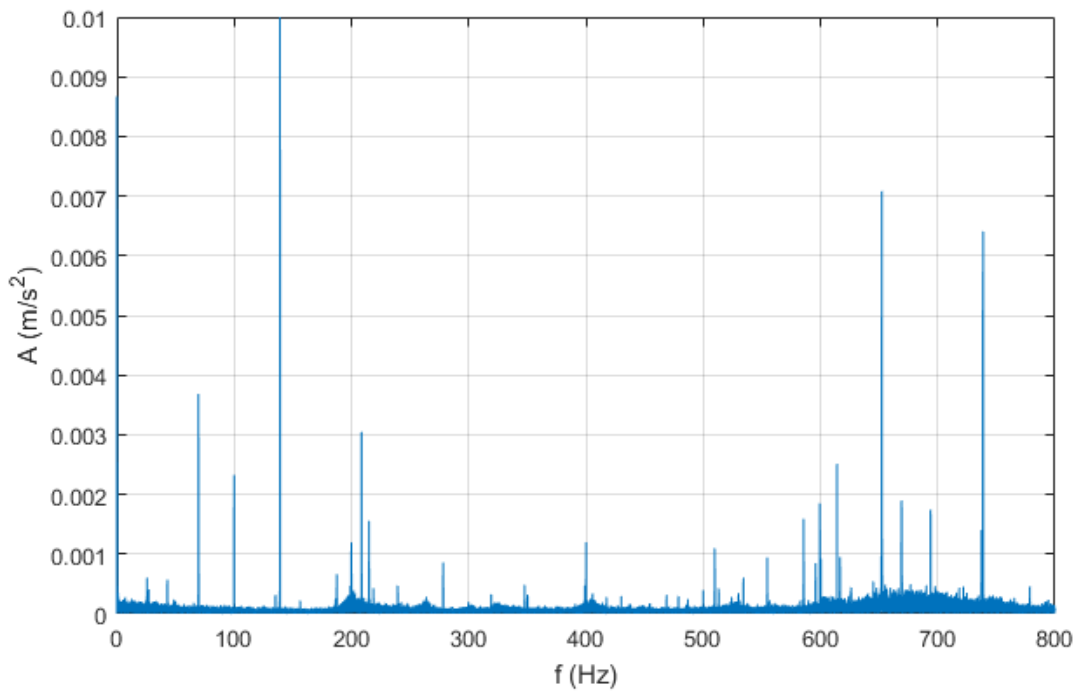
Following activation of axes motion (Figure 6), multiple frequencies in the whole monitored frequency range appear. However, their amplitude remains very low.

In the last two experiments, the influence of the rotation of the tool spindle was tested. First, a measurement was carried out with the tool removed. It became apparent that the spindle itself, or more precisely the driving electric motor and bearings defining the axis, present a significant source of vibrations (Figure 7). Compared to the previous experiments, there is a marked increase in the amplitudes of certain specific frequencies. These are frequencies generated by the rotation itself (main rotation frequency 69.5 Hz and harmonic frequency 139 Hz) and frequencies created on the bearing fit of the axis (652 and 738 Hz). The frequencies observed in the previous measurements have also shown a moderate growth. [1][5]



Source: Own

Fig. 6: Frequency analysis of vibration acceleration measurement following process initiation, tool rotation deactivated, axes motion active

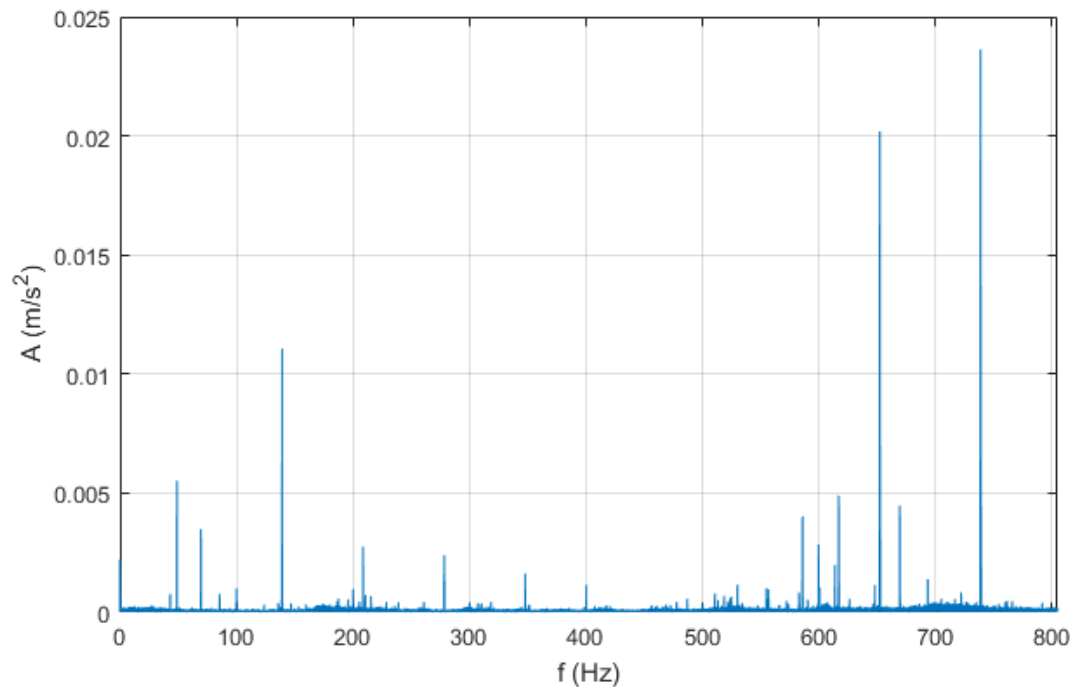


Source: Own

Fig. 7: Frequency analysis of vibration acceleration measurement during the tool spindle rotation (without the tool)

With the tool attached, amplitudes of 69.5 and 139 Hz frequencies rise moderately (most likely due to a slight unbalance of the tool) and amplitudes of 652 and 738 Hz grow almost

threefold. This phenomenon is attributed to the change in weight distribution on the spindle caused by the attachment of the tool (Figure 8).



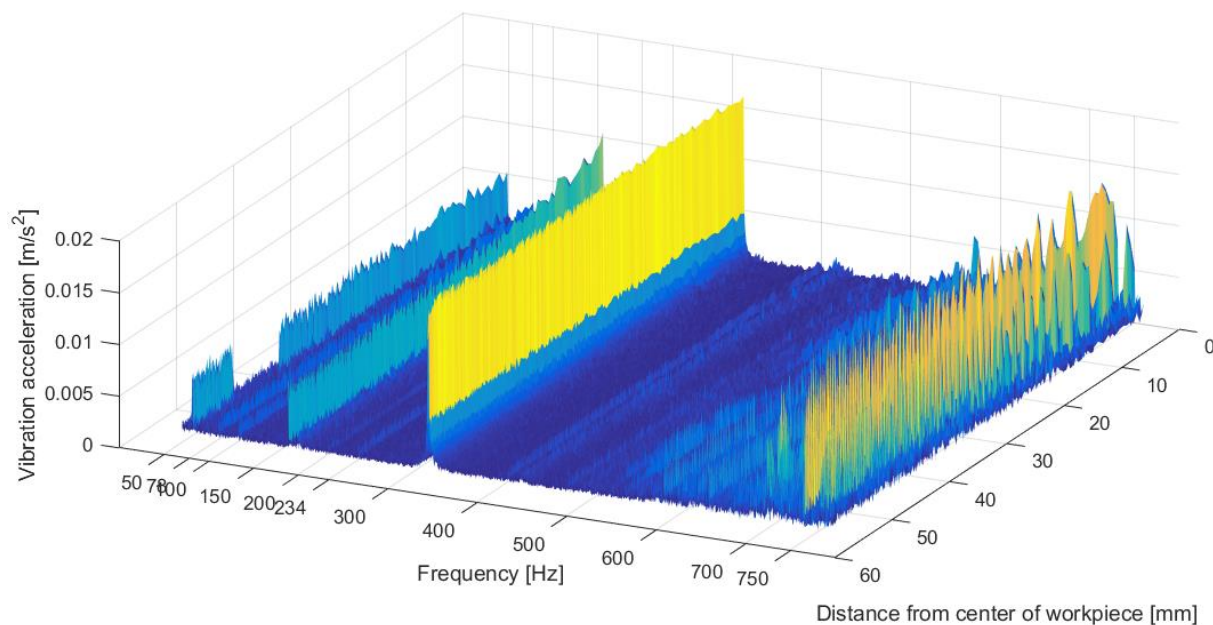
Source: Own

Fig. 8: Frequency analysis of vibration acceleration measurement during the tool spindle rotation (with the tool attached)

5 Vibration Monitoring During Real Grinding Process

In the second phase, experiments were performed on actual grinding processes. Primary experiments were conducted on horizontal planes, where the generated artifacts could be measured and examined more precisely. In these experiments, two different cutting speeds of the tool were tested during otherwise identical processes. It was discovered that a large number of the frequencies detected in the previous experiments are suppressed during the machining itself. This is ascribed to the impact of the tool on the workpiece, i.e. to the rigidity of the axes and to the forces produced during the process.

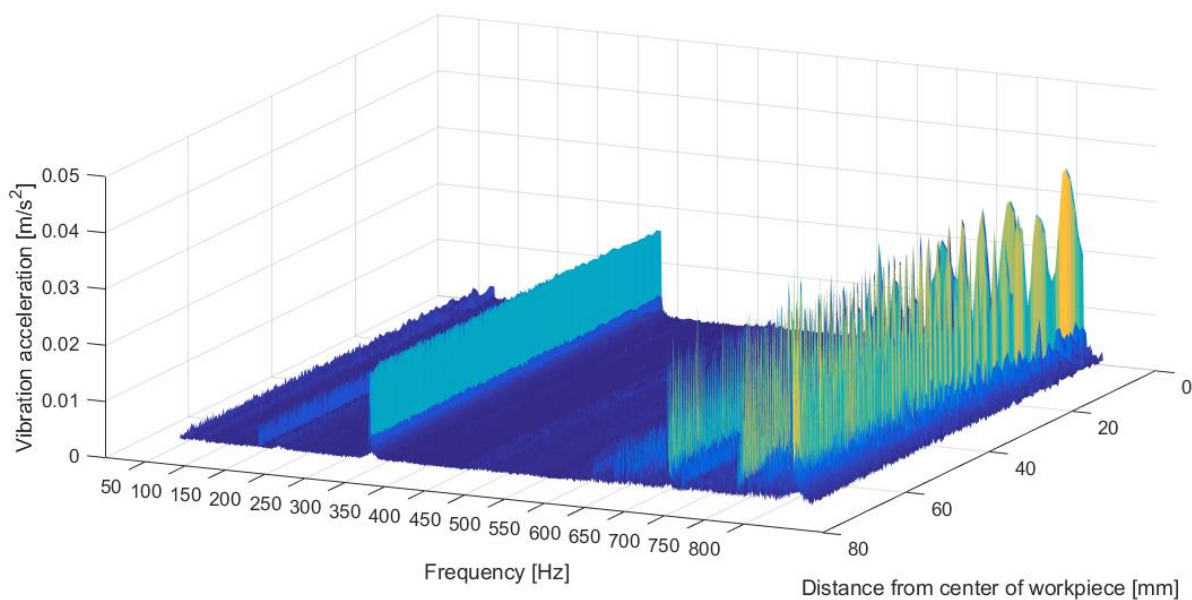
The individual measurements show that in the monitored frequency range there appear frequencies corresponding with the revolutions of the tool (they change with the tool revolutions) as well as frequencies in the 500 – 800 Hz range, which are caused by the mechanical core of the machine (they remain constant despite a change in revolutions). An example of a graph depicting the machining process, i.e. the dependence of individual frequency amplitudes on the medial distance on the machined surface, is shown in Figure 9.



Source: Own

Fig. 9: Frequency analysis of measurement during an actual process of horizontal plane grinding (cutting speed 24 m/s)

The last step was to test if changes in process behavior occur during grinding of non-horizontal planes. Experiments conducted on several types of aspheric surfaces revealed that the processes behave in very similar ways. Figure 10 shows marked amplitude of tool-generated frequencies as well as of frequencies in the aforementioned 500 – 800 Hz range.



Source: Own

Fig. 10: Frequency analysis of measurement during an actual process of aspheric surface grinding (cutting speed 20 m/s)

6 Vibration Suppression Options

Frequencies occurring in the 50-500 Hz range due to the tool speed could be partially suppressed by balancing the tool. This method is useful for tools that have stable properties

over time. Therefore, for metal bonded tools there is no need for frequent maintenance (change of tool properties). For resin-bonded tools, this method is not suitable. [3][4]

Another option to partially suppress frequencies of 50 - 500 Hz is machine maintenance specifically of the bearings on the tool axis. The measured data indicate a certain wear rate on bearings and their service could be used to suppress vibrations generated by tool rotation. This service may also have a positive effect on suppression of frequencies of 500 - 800 Hz. The last proposed solution is adding load to the Y axis. This should change the way the vibration propagates and shifts it out of the critical area.

Conclusion

During the experiments, it was found that vibrations from three basic sources affected the machining process. They are the rotation of the tool spindle, axis positioning system, and axis movement. A great deal of blame for these sources is the wear of the machine tool. Therefore, service was designed to solve these problems, which could greatly help to suppress these unfavorable influences.

Acknowledgements

This work was supported by the Ministry of Education, Youth and Sports of the Czech Republic in the project NPU no. LO1206 and by the Ministry of Industry and Trade in the project "Avoiding and removing mid-spatial frequency errors in asphere and free form fabric" with No. CZ.01.1.02/0.0/0.0/15_019/0004798.

Literature

- [1] JANÍČKOVÁ, P.: *Moderní konstrukční řešení*. [Online] 2010. [accessed 2018-12-04] Available from WWW: <http://www.uh.cz/szegsm/files/sblizovani/pdf/mod-konstr-cnc.pdf>
- [2] MELOUN, M.; MILITKÝ, J.: *Statistická analýza experimentálních dat*. Praha: Academia, 2004. ISBN 80-200-1254-0.
- [3] SUCHNA K.: Jednoduché vyvažování nástrojů. *MM Průmyslové spektrum*. [Online] [accessed 2018-12-04] Available from WWW: <https://www.mmspektrum.com/clanek/jednoduche-vy vazovani-nastroju.html>
- [4] SHAFRIR, S. N.: *Diamond Tool Wear - Observation by Scanning Electron Microscopy (SEM)*. [Online] [accessed 2018-12-04] Available from WWW: <http://www.optics.rochester.edu/workgroups/cml/opt307/spr04/shai/index.html>
- [5] HELEBRANT, F.; ZIEGLER J.: *Technická diagnostika a spolehlivost*. Ostrava: VŠB - Technická univerzita, 2004. ISBN 9788024806501.

IDENTIFIKACE STŘEDNÍCH PROSTOROVÝCH FREKVENCÍ PŘI OBRÁBĚCÍM PROCESU NA OPTOTECH MCG 100

Střední prostorové frekvence, povrchové vady vznikající při výrobě optických asférických ploch, mohou být velkým problémem např. ve vysoce výkonných optických systémech. Při výrobě asférických ploch na stroji Optotech MCG100 bylo proto provedeno měření vibrací v různých režimech chodu měřicím zařízením VibXpert II. Toto zařízení pomocí piezoelektrických snímačů zaznamenává zrychlení vibrací. Data z měření byla následně zpracována v softwaru Matlab. Cílem bylo identifikovat frekvence, které mohou nepříznivě ovlivňovat výrobu optických elementů a dále nastínit možné příčiny jejich vzniku.

Bylo zjištěno, že ve sledovaném spektru 33 – 800 Hz se vyskytují výrazné frekvence z několika základních zdrojů. Jedná se o rotaci nástrojového vřetena, o rotaci nástroje, regulační smyčku pohybu os a samotný pohyb os.

IDENTIFIZIERUNG MITTLERER RÄUMLICHER FREQUENZEN BEIM FRÄSPROZESS MIT DEM OPTOTECH MCG 100

Die mittlere räumliche Frequenz und Oberflächenschäden, welche bei der Produktion optischer asphärischer Flächen entstehen, können ein großes Problem z. B. bei hoch leistungsfähigen optischen Systemen darstellen. Bei der Produktion asphärischer Flächen auf der Maschine Optotech MCG100 wurde daher eine Messung der Vibrationen in verschiedenen Arbeitsabläufen mit Hilfe der Messeinrichtung VibXpert II durchgeführt. Diese Einrichtung zeichnet mit Hilfe piezoelektrischer Sensoren die Beschleunigung der Vibrationen auf. Die Messdaten wurden im Anschluss mit der Software Matlab verarbeitet. Ziel war die Identifizierung der Frequenzen, welche die Produktion optischer Elemente ungünstig beeinflussen und Hinweise auf weitere mögliche Ursachen von deren Entstehung geben können.

Es wurde festgestellt, dass im beobachteten Spektrum 33 – 800 Hz deutliche Frequenzen aus mehreren Quellen auftreten. Es handelt sich um die Rotation der Instrumentenspindel, um die Rotation der Regulationsschleife der Achsenbewegung und die eigentliche Achsenbewegung.

IDENTYFIKACJA ŚREDNICH CZĘSTOTLIWOŚCI PRZESTRZENNYCH W PROCESIE OBRÓBKI NA URZĄDZENIU OPTOTECH MCG 100

Średnie częstotliwości przestrzenne, wady powierzchniowe powstające w procesie produkcji optycznych powierzchni asferycznych mogą stanowić duży problem w bardzo wydajnych systemach optycznych. Podczas produkcji powierzchni asferycznych na maszynie Optotech MCG100 wykonano więc pomiaru wibracji dla różnych trybów pracy urządzenia. Pomiaru wykonano urządzeniem VibXpert II. Przy pomocy czujników piezoelektrycznych urządzenie to odnotowuje przyspieszenie wibracji. Następnie dane z pomiaru opracowano w oprogramowaniu Matlab. Celem było zidentyfikowanie częstotliwości, które mogą mieć niekorzystny wpływ na produkcję elementów optycznych oraz wskazanie możliwych przyczyn ich powstania.

Stwierdzono, że w analizowanym spektrum 33—880 Hz występują wyraźne częstotliwości pochodzące z kilku źródeł podstawowych. To rotacja wrzeciona urządzenia, rotacja urządzenia, pętla regulacyjna ruchu oraz własny ruch osi.

CONSTRUCTION OF A VACUUM ULTRAVIOLET TRANSMISSION SPECTROMETER

Jiří Hlubeček¹; Jiří Budasz²; Jan Václavík³; Karel Židek⁴

Institute of Plasma Physics, Academy of Sciences of the Czech Republic,
Regional Centre for Special Optics and Optoelectronic Systems (TOPTEC),
Za Slovankou 1782/3, 182 00 Prague 8, Czech Republic

e-mail: hлубeček@ipp.cas.cz; budasz@ipp.cas.cz; vaclavik@ipp.cas.cz; zidek@ipp.cas.cz

Abstract

Measuring transmittance in the so-called vacuum ultraviolet (UV) region, namely between 160 and 190 nm, is of interest for a range of materials (UV optical glasses and coatings, diamond, thin polymer films, etc.). However, both the necessity to carry out the measurement in vacuum and the need for specific UV-designed optical elements lead to the fact that the vacuum UV spectrometers are rather rare. Here we present construction of a home-made transmission vacuum UV spectrometer. It is based on a Seya-Namioka monochromator and enables us to determine transmittance of flat optical samples in the spectral range of 160 nm–600 nm with a spectral resolution below 2 nm. We also outline future upgrade of the setup, which will highly improve its parameters.

Keywords

Ultraviolet spectrometer; Transmission spectrometer; Seya-Namioka monochromator.

Introduction

Transmission spectrum of a material or a sample carries immense amount of information about the studied specimen. In the case of thin films, the transmission curve can be used to extract the film thickness [1]. It can also provide information about concentration of a substance, or even reveal microscopic properties of the measured material (e.g. size of quantum dots) [2, 3]. For this reason, a transmission spectroscopy counts among basic pieces of equipment of spectroscopic laboratories.

A number of spectral features of interest are present in the ultraviolet (UV) part of spectra or even in the so-called vacuum UV (VUV) region with wavelengths below 190 nm [4–6]. This term is used due to the necessity to carry out the measurements in vacuum, since air very strongly absorbs the light in this spectral region. In addition, the VUV light needs to be emitted by a distinctive lamp and special imaging optics has to be used. Due to this fact, VUV transmission spectrometers, in spite of being a very useful spectroscopic tool, are rare.

1 Research Objectives

VUV spectral region covers wavelengths which are of interest for two main research applications: (i) development of UV optics for excimer lasers and photolithography [7, 8], (ii) material science (diamond, polymer thin films) [4–6]. Construction of a transmission spectrometer in this spectral range is indispensable for carrying out the research in the two topical directions.

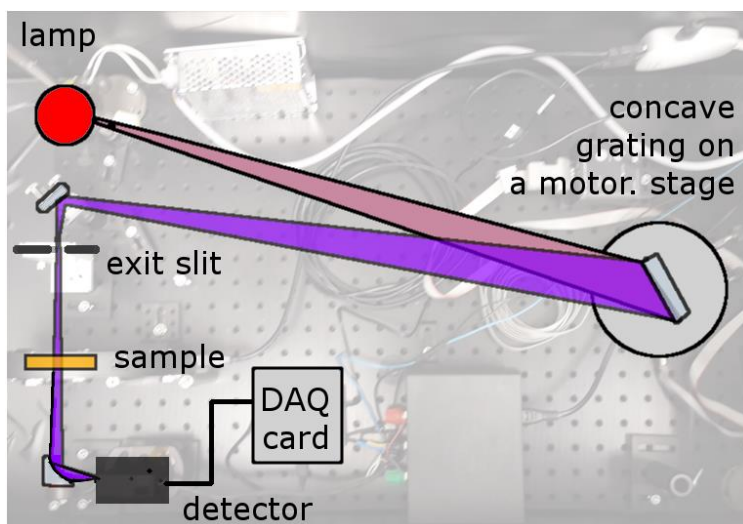
In this article we present construction of such VUV spectrometer together with the testing measurements in the VUV region. The presented spectrometer can be used to carry out

transmittance measurement in the 160-600 nm region and complement a broad range of spectrometers available in the visible spectral region.

2 Experimental Methods

The transmission spectrometer is depicted in Fig. 1. It is based on the so-called Seya-Namioka monochromator construction, where the light source and exit slit are placed on the so-called Rowland circle [9]. The light source (Hamamatsu L7293 VUV lamp) is projected by a concave grating (Richardson Gratings) on a slit, which selects a wavelength for measurement. The selected wavelength is transmitted through a measured sample and refocused by an off-axis parabolic mirror (MgF₂-coated Al mirror, Thorlabs) onto a scintillator (home-made, sodium salicylate layer). The light intensity is detected by using a photomultiplier (PMT) module Hamamatsu HC120.

The signal from the detector is read out via a DAQ card (National Instruments) and processed by a computer. The measured wavelength is scanned by rotating the concave grating via a motorized rotational stage (Thorlabs).



Source: Own

Fig. 1: Photo and an overlaid scheme of the UV spectrometer with removed covers of lamp, measurement and sample compartments

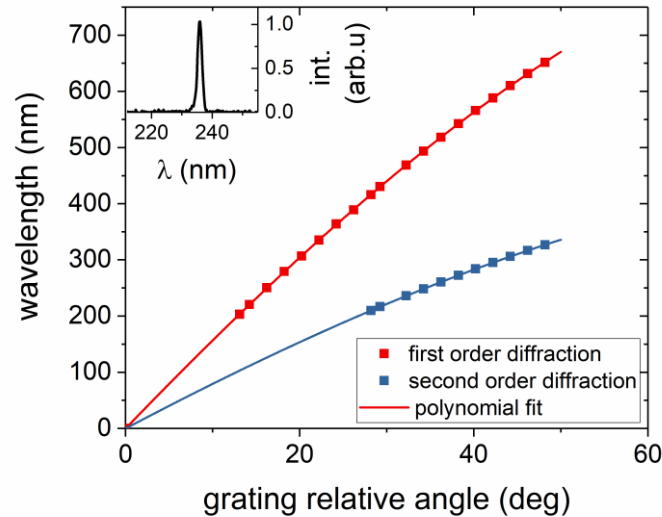
In order to carry out measurements in the VUV spectral region we enclosed the spectrometer in an aluminum box, which can be flushed with pure dry nitrogen and subsequently kept under a constant slight overpressure of the nitrogen inner atmosphere.

A 5-position filter-wheel is placed in the measurement spot and enables to measure background (blocked beam), full intensity (empty slot) and three samples. Future implementation of a separate mechanical shutter will extend the number of sample slots to four.

3 Results and Discussion

Firstly, we used a conventional spectrometer for wavelengths above 190 nm (Ocean Optics Flame) for the monochromator calibration (see Fig. 2). A “zero” position of the grating was found by searching for an intense zero-order peak (note that a decreased PMT gain has to be used in this case). Subsequently, the concave grating was rotated by small steps and for each step we recorded a spectrum of the light transmitted through the monochromator (see Fig. 2 inset). By rotating the concave grating we have tuned the wavelength from 190 nm to 650 nm.

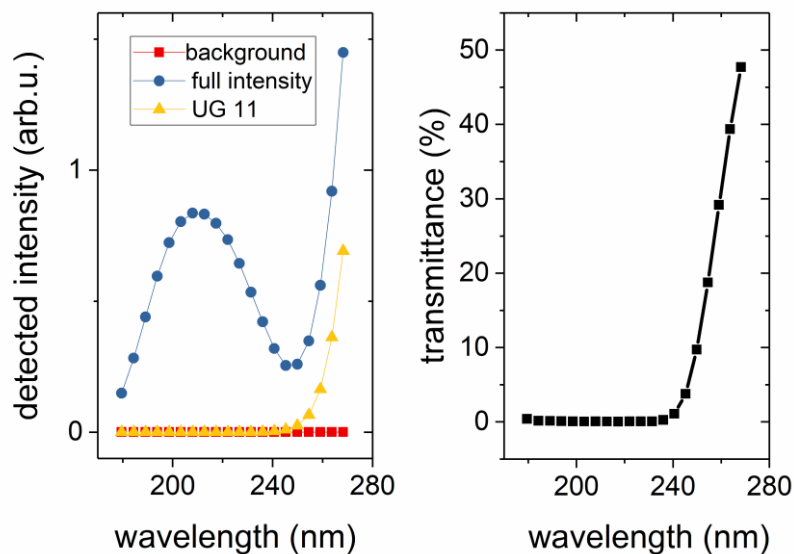
The obtained calibration points can be well described by a third-order polynomial. Finally, it is worth stressing that the monochromator can be used for wavelength above 320 nm only after a proper color filter (e.g. N-WG320 Schott) is inserted, so that the second-order diffraction does not interfere with the measurements.



Source: Own

Fig. 2: Calibration curve of the UV spectrometer showing first- and second-order diffraction peaks (squares) fitted by a polynomial curve (solid lines). Inset: example of a measured spectrum with 1 mm exit slit. FWHM of the measured curves was used to determine resolution of the system.

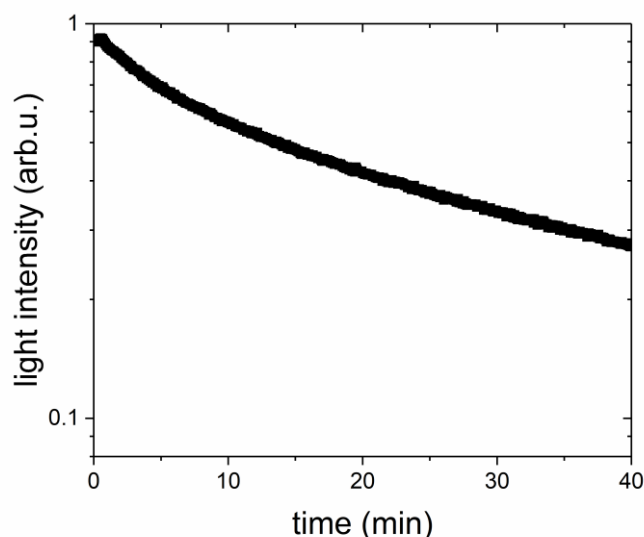
The monochromator output was a narrow spectral line, which featured full-width in half maximum (FWHM) of 3.5 nm for 1 mm wide exit slit. This is in accordance with the grating spectral dispersion. Owing to a high sensitivity of the PMT photodetection, the spectral resolution of our experimental setup can be significantly improved by closing the exit slit.



Source: Own

Fig. 3: Left panel: Example of measured background signal (squares), full-intensity spectrum (circles), and spectrum of light transmitted through a UG-11 Schott filter (triangles). Right panel: calculated transmittance by using the input data.

Transmittance T of the sample can be simply calculated from a measurement of a background signal (B), full-intensity signal (F) and an intensity of light transmitted through a sample (S) as $T = (S - B) / (F - S)$. Such measurement is illustrated in Fig. 3 for a 3 mm thick UG-11 color filter (Schott). The depicted curves were acquired by using a motorized filter holder with three positions: beam block (background), empty slot (full intensity), and sample (UG-11 filter). We obtained a transmission spectrum which is in accordance with specifications of the measured filter.



Source: Own

Fig. 4: Decrease in the detected UV light intensity (182 nm) after the nitrogen flushing was terminated

As we pointed out in the previous section, the experimental setup has to be constantly flushed with nitrogen in order to avoid the VUV light absorption. When the nitrogen flushing of the apparatus is terminated, diffusion of air commences to decrease the light intensity (see Fig. 4). At 182 nm, the light intensity at the PMT detector decreases to 50% in approx. 15 minutes. This confirms the necessity to constantly keep a slight overpressure of the nitrogen in the system.

4 Future Outlook

In spite of being able to clearly measure in the VUV spectral range, the presented spectrometer had a limited precision in the spectral region below 180 nm. This was caused by using a home-made UV scintillator based on sodium salicylate layer. In the upgraded version we will employ a commercially-available scintillator (McPherson).

The signal-to-noise ratio can be highly improved by using a synchronous detection (combining an optical chopper and electronic lock-in readout). This will also be implemented in the system upgrade.

Finally, the spacious aluminum box is very convenient for the setup optimization. However, this leads to an extensive consumption of nitrogen. Therefore, in the later stage the setup will be enclosed in a vacuum chamber to avoid the necessity of nitrogen flushing.

Conclusion

We present construction of a monochromator capable of measuring transmission spectra in the vacuum UV spectral range (above 160 nm). Such monochromator can be used to measure transmission spectra of flat VUV optical elements or materials with absorption features of interest in the region (diamond, thin polymer films, etc). We have demonstrated its function of a standard color filter. Furthermore, we propose several steps, which will improve parameters of our setup, so that the parameters will be comparable to commercially available systems.

Acknowledgements

We gratefully acknowledge the financial support of the Ministry of Education, Youth and Sports of the Czech Republic (Project NPU LO1206).

Literature

- [1] MACLEOD, H. A.: *Thin-film optical filters*. Taylor&Fracis Group, 2010. ISBN 978-1-420-07303-4.
- [2] YU, W. W.; LIANHUA, Q.; WENZHUO, G.; XIAOGANG, P.: Experimental determination of the extinction coefficient of CdTe, CdSe, and CdS nanocrystals. *Chemistry of Materials*. 2003, Vol. 15, Issue 14, pp. 2854–2860. DOI: [10.1021/cm034081k](https://doi.org/10.1021/cm034081k)
- [3] KLIMOV, V. I.: *Nanocrystal quantum dots*. CRC Press, 2010. ISBN 978-1-420-07926-5.
- [4] TROJÁNEK, F.; ŽÍDEK, K.; DZURNÁK, B.; KOZÁK, M.; MALÝ, P.: Nonlinear optical properties of nanocrystalline diamond. *Optics Express*. 2010, Vol. 18, Issue 2, pp. 1349–1357. DOI: [10.1364/OE.18.001349](https://doi.org/10.1364/OE.18.001349)
- [5] ZAITSEV, A. M.: *Optical properties of diamond: a data handbook*. Springer-Verlag, 2013. ISBN 978-3-662-04548-0.

- [6] MORISAWA, Y.; GOTO, T.; IKEHATA, A.; HIGASHI, N.; OZAKI, Y.: Far-Ultraviolet (FUV) Spectroscopy in the Solid and Liquid States, Principle, Instrumentation, and Application of. In: *Encyclopedia of Analytical Chemistry: Applications, Theory and Instrumentation*. Chichester, UK: John Wiley & Sons, Ltd, 2013. DOI: [10.1002/9780470027318.a9279](https://doi.org/10.1002/9780470027318.a9279)
- [7] JACKSON, K. A.; SCHROTER, W.: *Handbook of semiconductor technology*. Wiley-VCH Verlag GmbH, 2000. ISBN 978-3-527-29970-6.
- [8] BASTING, D.; MAROWSKY, G.: *Excimer laser technology*. Springer-Verlag, 2005, ISBN 978-3-540-26667-9.
- [9] NAMIOKA, T.: Theory of the Concave Grating. III. Seya-Namioka Monochromator. *Journal of the Optical Society of America*. 1959, Vol. 49, Issue 10, pp. 951–961. DOI: [10.1364/JOSA.49.000951](https://doi.org/10.1364/JOSA.49.000951)

Ing. Jiří Hlubuček; Ing. Jiří Budasz; Ing. Jan Václavík; RNDr. Karel Židek, Ph.D.

KONSTRUKCE TRANSMISNÍHO SPEKTROMETRU PRO VAKUOVOU ULTRAFIALOVOU SPEKTRÁLNÍ OBLAST

Měření transmise v tzv. vakuové ultrafialové (UV) spektrální oblasti, konkrétně mezi 160 až 190 nm, je důležité pro řadu materiálů (UV optická skla a pokrytí, diamant, tenké polymerní filmy, atd.). Nicméně, nutnost provádět měření ve vakuu a nutnost použití specifických optických elementů určených pro UV záření vede k tomu, že spektrometry pro oblast vakuového UV světla se vyskytují zřídka. Zde prezentujeme konstrukci našeho transmisního spektrometru pro vakuovou UV oblast. Je založen na Seya-Namiokově monochromátoru a umožňuje nám určit transmissi planparalelních optických vzorků ve spektrální oblasti od 160 – 600 nm se spektrálním rozlišením méně než 2 nm. V článku jsou také načrtnuta budoucí vylepšení systému, která výrazně zlepší jeho měřicí parametry.

DIE KONSTRUKTION EINES TRANSMISSIONSSPEKTROMETERS FÜR DEN LUFTLEEREN ULTRAVIOLETTEN SPEKTRALBEREICH

Die Messung der Transmission im so genannten luftleeren ultravioletten Spektralbereich, konkret zwischen 160 bis 190 nm, ist für eine Reihe von Materialien wichtig (UV-optische Gläser und Abdeckungen, Diamanten, dünne polymere Filme usw.). Nichtsdestoweniger führt die Notwendigkeit der Durchführung von Messungen im Vakuum und der Nutzung spezifischer, für die UV-Strahlung bestimmter optischer Elemente dazu, dass Spektrometer für den Bereich des UV-Lichts im Vakuum nur selten vorkommen. Hier präsentieren wir die Konstruktion unseres Transmissionsspektrometers für den luftleeren UV-Bereich. Er basiert auf Seva-Namioks Monochromator und ermöglicht uns die Bestimmung einer planparallelen Transmission optischer Muster in einem Spektralbereich von 160 bis 600 nm mit einer spektralen Unterscheidung, die weniger als 2 nm beträgt. Im Artikel werden auch künftige Verbesserungen des Systems skizziert, welche seine Messparameter bedeutend heraufsetzen.

KONSTRUKCJA SPETROMETRU TRANSMISYJNEGO DLA PRÓŻNIOWEGO ULTRAFIOLETOWEGO ZAKRESU SPEKTRALNEGO

Pomiar transmisji w tzw. próżniowym ultrafioletowym zakresie spektralnym, ściślej pomiędzy 160 a 190 nm, jest ważny dla wielu materiałów (szkła optyczne UV, diament, cienkie warstwy polimerowe itd.). Konieczność dokonywania pomiarów w próżni a także niezbędne zastosowanie specyficznych elementów optycznych przeznaczonych do promieniowania UV skutkuje tym, że spektrometry dla zakresu próżniowego promieniowania ultrafioletowego są rzadkością. Prezentujemy konstrukcję naszego spektrometru transmisyjnego dla próżniowego zakresu UV. Oparty jest on na monochromatorze Seya-Namioka. Umożliwia nam określenie w płaszczyznach równoległych transmisji wzorów optycznych w zakresie spektralnym od 160 do 600 nm z rozdzielczością spektralną poniżej 2 nm. W artykule zasygnalizowano także przyszłe udoskonalenie systemu, które w znacznym stopniu poprawi jego właściwości pomiarowe.

HYPERSPECTRAL IMAGING IN INFRARED REGION USING COMPRESSED SENSING METHODS

Jiří Hlubeček¹; Karel Židek²

Institute of Plasma Physics, Academy of Sciences of the Czech Republic,
Regional Centre for Special Optics and Optoelectronic Systems (TOPTEC),
Za Slovankou 1782/3, 182 00 Prague 8, Czech Republic
e-mail: hlubucek@ipp.cas.cz; zidek@ipp.cas.cz

Abstract

We provide a review of hyperspectral imaging in infrared region as well as simulation of measurements and reconstructions of test datacubes using the compressed sensing method CASSI (Coded Aperture Snapshot Spectral Imaging). We simulate the presence of the chemical compounds on parts of the image and then we reconstruct its absorption spectrum and localization back from a single snapshot. In other words, we prove that in principle it is possible to reconstruct a sparse 3D datacube from a single 2D dataset. Furthermore, we discuss the quality of the reconstructed data and limitations of the chosen simulation method.

Keywords

Hyperspectral imaging; Infrared spectrum; Spectroscopy; Compressed sensing.

Introduction

Hyperspectral imaging (HSI) refers to all methods where, besides image information, we obtain also the spectrum of light at each point of the image. Hyperspectral imaging in infrared (IR) region is important because it could give us an enormous amount of information of the scene of our interest which we are not able to acquire in any other mean, e.g. remote sensing of the chemical composition. For this reason, the field of HSI has been very lively in the past decades.

A specific task of HSI is to carry out imaging in the IR region. It is worth noting that this article focuses on the IR region which is beyond the scope of conventional optics and detectors, i.e. we consider the so-called middle and far infrared ($\lambda > 2.5 \mu\text{m}$). HSI in the IR is not widespread due to the need of using unusual optical materials and detectors.

A possible solution to this problem is using compressed sensing methods. Compressed sensing denotes a signal processing technique which exploits the essence of natural signals that is not obvious at the first sight. The natural signals are sparse which means you can recover them from far fewer measurements than it is required by the Shannon-Nyquist theorem. Basically, you acquire and reconstruct the signals by finding solutions to underdetermined linear systems. More details can be found in [1].

1 Research Objective

This article comprehensively deals with the possibility of using compressed sensing in HSI in the IR region, which would allow a simpler construction of HSI devices. An overview of the published results on this topic is supplemented by samples of reconstructions of artificial data (hyperspectral scenes) where we simulate the presence of the chemical compounds on parts of the image and then we reconstruct its absorption spectrum back. We simulate spectrally

constant irradiation of the studied scene, as well as the radiation of the black body. The main goal of this article is to evaluate feasibility of using the CASSI method in the IR HSI.

2 Experimental Methods

Data simulations and reconstructions were performed using Matlab. Two types of scenes were selected for the reconstruction – a simple and a more complex scene. The simple one was a scene with constant intensity in every pixel, while the one more complex was an image of a real scene captured by an infrared camera. For every type of scene a few different variants were evaluated. The variables were size of the scene (32x32, 64x64, 128x128, ...), the number of wavelengths (117, 235, 470, ...) and concentration of the chemical substance.

As a chemical substance we used isopropyl alcohol. The results shown in this article are for path concentration of 500 ppm m. The IR spectrum for isopropyl alcohol was obtained from The National Institute of Standards and Technology (NIST), the data were compiled by: P.M. Chu, F.R. Guenther, G.C. Rhoderick, and W.J. Lafferty with parameters IFS66V (Bruker); 3-Term B-H Apodization and resolution of 0.4820 cm⁻¹.

For simulation of compressed sensing we focused on the so-called method CASSI (Coded Aperture Snapshot Spectral Imaging), which is described in more detail below or in literature [1]. This method is one of the standard methods of compressed scanning.

We used the TwIST (Two-Step Iterative Shrinkage/Thresholding) algorithm for image restoration during the reconstruction to minimize expression (1)

$$f(x) = \frac{1}{2} \|y - Kx\|^2 + \lambda\Phi(x), \quad (1)$$

where K is the linear direct operator, Φ is a regularizer, and λ is a regularization parameter [2].

2.1 Hyperspectral Imaging in IR

Infrared (IR) electromagnetic spectrum can be divided into three regions:

- Near IR – 13,500 – 4000 cm⁻¹
- Mid IR – 4000-400 cm⁻¹
- Far IR – 400-10 cm⁻¹

Definition of these regions can slightly differ through scientific literature.

Each chemical compound has a characteristic absorption spectrum in the IR region. This is due to the changes in vibrational and rotational energy of the chemical bonds of the molecules while they interact with the IR radiation and also because quantum mechanics allows only a few energy levels [3, 4].

Hyperspectral imaging (HSI), also known as chemical or spectroscopic imaging, is a technique that combines conventional imaging with spectroscopic systems in order to obtain both spatial and spectral information. IR spectroscopy, which is the core of the IR-HSI, is based on the interaction of IR light with molecules of the sample examined. The result of this interaction can be characterized by absorption, reflection and emission. Absorption in the near-IR region is relatively shallow [4], therefore in this article we focus on the mid- and far-IR region. Fundamentals and development of IR spectroscopy can be found in publications [5, 6, 7].

In classical spectroscopy, a spectrum is integral spectral information about the sample surface, which is dependent on the size of the irradiated spot, i.e. we obtain only a single spectrum. In hyperspectral imaging, the measurement results in a three-dimensional data array called

“datacube” – each pixel is assigned to one spectrum. We can also imagine the datacube as a stack of papers where each sheet of paper denotes the sample at different wavelength.

For a better idea of how this datacube is obtained, here are examples of the basic types of configurations of devices for obtaining hyperspectral information.

1. **Point mapping** – The sample is scanned point by point, and for each such point one spectrum is acquired.
2. **Line Scan** – The detector records the spectral information for the entire line of pixels of the image simultaneously; the light passes through the slit on the detector, so it is possible to record the spectral information along the entire line depending on the location from which the light comes; in this way a two-dimensional array is obtained which has one spectral dimension and one spatial dimension; for the second spatial dimension of the datacube, we need to scan the sample in a direction perpendicular to the imaging line.
3. **Plane scan** – This type of configuration does not require any movement of the sample (or spatial scanning), so it is also referred to as “staring configuration”; the incoming light is recorded on the detector as a two-dimensional spatial array for each wavelength separately; this is achieved by means of filters (band-pass filters [8] or adjustable acousto-optic filters [9]) which can be placed on a revolving disc or change the passing wavelength respectively [1].

Two basic configurations listed above that use the translational motion of the sample are whisker-broom and push-broom scans. These methods have excellent spatial and spectral resolution; however, from the principle it implies that the acquisition time is very long, in the order of tens of minutes to hours, depending on the size of the scanned area, the wavelength range and the number of scans per pixel [3]. On the contrary, when using a plane scan we are able to record a complete datacube in a matter of seconds or minutes, depending on the number of scanned wavelengths. This can be especially used to explore processes that are unstable in time.

Hyperspectral camera contains: the light source (or uses a scattered ambient light), beam splitters (tunable filters, diffraction gratings, Fourier transformation spectrometers [10]), imaging lenses, detector, motion control / motion sensing devices to obtain very accurate spatial information.

HSI is used in many different fields, e.g. medical applications [11], quality control and food analysis [12, 13], forensic sciences [14, 15], art conservation [16], etc.

2.2 Compressed Sensing

Recording, “storing”, and processing a datacube are very demanding with respect to time, computing power, data storage and what is more, in conventional signal processing, we are limited by the so-called Shannon-Nyquist theorem, which tells us that for the correct reconstruction of the signal the sampling frequency must be at least twice as high as the highest frequency present in the signal. However, this is very inconvenient in accordance to capture very fast processes (e.g. quantum dots) or in the IR region, where we are very limited by the structural elements of IR cameras and their high purchase price.

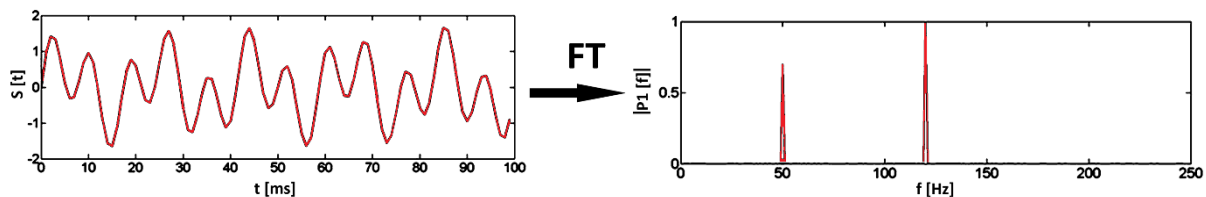
Shannon-Nyquist theorem and processing very large datasets can be bypassed by the method called compressed sensing (CS), which uses two assumptions – sparsity of a signal and incoherence.

2.2.1 Sparsity of a Signal

If a signal contains only a small percentage of important information, the signal is denoted to be sparse – it can be written very concisely in the correctly chosen base ψ . For example, a conventional camera captures the scene, pixel by pixel, and consequently from the knowledge of “important points”, it compresses the scene into a JPEG format that is many times smaller than the RAW data, all without apparent loss of image quality.

2.2.2 Incoherence

A signal having a sparse representation in ψ must be spread out in the domain in which it was recorded. For example, the peak in the time domain is spread out in the frequency domain [1].



Source: Own

Fig. 1: Fourier transform of the signal from time domain to frequency domain

In Fig. 1 we see that the relatively complex signal displayed in the time domain has a very sparse representation in the frequency domain, which similarly works for the video signal. Speaking about the JPEG compression example above, typically, a 1Mpx image can be compressed to 2.5% of the original size without apparent loss of the image quality by using 25000 strongest Fourier transform coefficients. The problem is that we are not able to compress the scene until we capture it because we generally do not know which pixels will carry the important information about the image.

If we capture the scene pixel by pixel, we are very limited by the acquisition time for recording very fast processes. Conversely, compressed sensing is able to encode the whole scene in a single instant using a random mask, and then to reconstruct the image exploiting its knowledge. This makes it possible to capture events taking place in the order of dozens of ps [17].

The so-called CASSI (Coded Aperture Snapshot Spectral Imaging) method exploits a coded aperture and dispersive element(s) to modulate the optical field from the scene, which is captured in one instance on the detector into the two-dimensional snapshot. As a coded aperture a random mask (i.e. random binary pattern) can be used. An example of the random mask can be seen in Fig. 2 (middle). The random mask blocks or passes the light coming inside the aperture depending on the binary value of the pixel. The random mask blocks approximately $\frac{1}{2}$ of the incoming light and the pixel columns in the mask should be independent.

It is worth nothing that by CASSI we capture 3D information onto 2D detector. However, we can retrieve the 3D information back because we know the structure of the pattern (random mask) we used to encode the scene and we presume that the signal is sparse. Hence, we are able to reconstruct the scene by an algorithm calculating equation (1) [1].

2.3 Using Compressed Sensing in IR Hyperspectral Imaging

Absorption in the mid-IR corresponds to the fundamental vibrational states of the chemical bonds. When the molecule interacts with IR light, chemical bonds begin to vibrate more

energetically, and thus affect absorption at certain wavelengths in the spectrum that is characteristic for each chemical bond.

On contrary, the ability to absorb near-IR is relatively small and depends on the harmonic and anharmonic movement of molecules, which is due to electronic transitions. Therefore, this technique is also called electronic or vibrational spectroscopy [4].

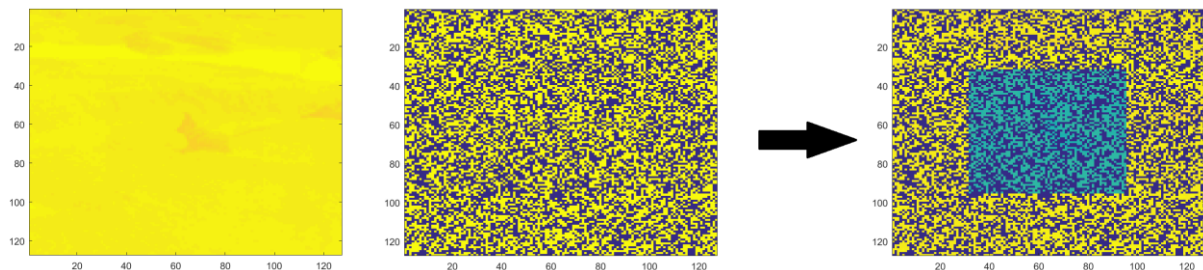
There are only few articles dealing with application of CS in mid- and far-IR HSI, e.g. [18, 19, 20]. The lack of publications could be attributed to the difficulties connected to the need of special optic elements and detectors in IR region.

3 Simulation of Hyperspectral Datacubes and their Reconstruction

We used a plain scene as well as a more complicated one, see Fig. 2 (left). In the terms of the plain scene, we used the same intensity in each pixel, i.e. in real situation (capturing the IR image) it would mean that we detected constant temperature through the whole scene.

3.1 Synthetic Data Preparation

For simulation of capturing the scene through CASSI method, we placed a chemical substance on part of the scene, which caused distinguishable difference in image intensity at specific slices of a datacube in accordance with the absorption spectrum of the chemical substance. In terms of computation, we have to multiply our scene (2D) with the transmission spectrum (1D) of the chemical compound. That is how we obtain the 3D datacube. Then (optionally) we add nonlinear Planck's law, i.e. black body radiation which is wavelength dependent. After that we apply a random mask to every slice of the datacube, see Fig. 2 (right).



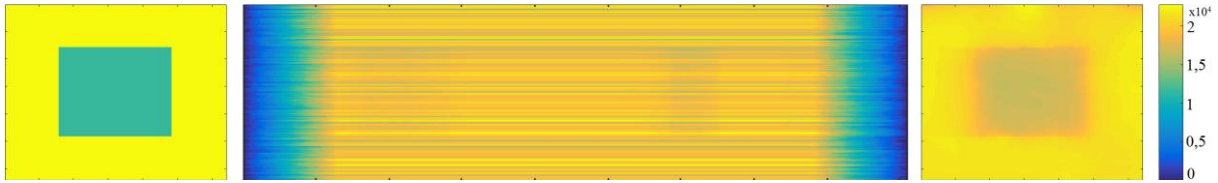
Source: Own

Fig. 2: Example of the scene 128x128 (left), random mask (middle), slice of the datacube with applied chemical substance on the scene (right)

3.2 Detector Signal

Detecting the 3D information on 2D detector could seem illogical, however, as mentioned above, we can retrieve the 3D information back from the knowledge of the random mask pattern and knowing the captured signal is sparse.

During detection of the signal, the IR spectrum coming to the IR optics of a hyperspectral camera would be refracted to different positions on the detector depending on the wavelength. In our simulation, when we work with an image size of 64x64 pixels and using 200 wavelengths, every wavelength (i.e. every slice) would be shifted by one pixel to the right on the detector, i.e. the image is spectrally sheared. The first slice would be in position 1-64, the second slice 2-65 and so on; hence the detector has to be 64x263 pixels to capture the whole datacube. The intensities of the slices are summed up in according positions creating the shear pattern on the detector, see Fig. 3 (middle).



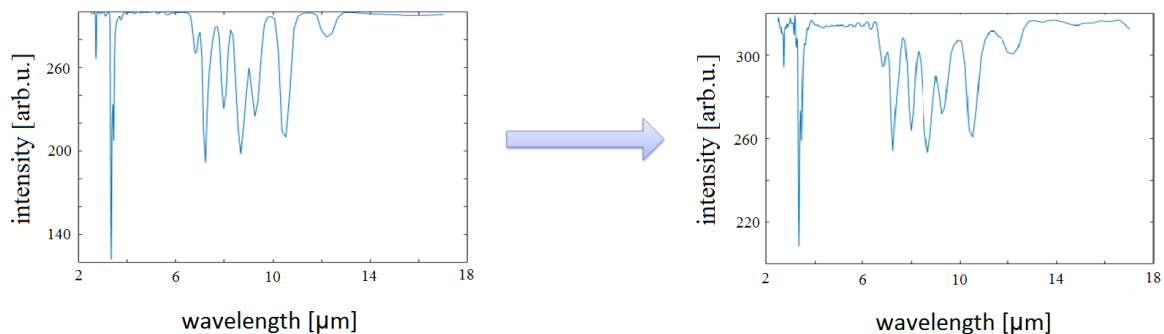
Source: Own

Fig. 3: Reconstruction of the plain scene. Original scene (left), detected image at the detector (middle), reconstructed scene (right).

In Fig. 3 (left) we can see the example of one slice of the datacube. For the sake of demonstration, we selected the wavelength in which the absorption was most significant. We show only one wavelength for the original and reconstructed scene, but in fact there are many different wavelengths which are altogether composing the datacube (every wavelength denotes one slice in the datacube).

3.3 Reconstructing Data

For reconstruction of the data we used TwIST (Two-Step Iterative Shrinkage/Thresholding) algorithm, which is an improved version of standard IST algorithm [20]. For each slice of the original datacube, we obtain one slice of the reconstructed datacube. From the reconstructed slices we take the sum of the area of where was the chemical compound applied in the original image and put it into a graph depending on wavelength to obtain the reconstructed intensity spectrum as can be seen in Fig. 4 (right).



Source: Own

Fig. 4: Original spectrum (left) vs. reconstructed spectrum (right) of plain scene

In Fig. 4, we can see that the total intensities of the reconstructed spectrum are not the same as in the original one, but the position of the peaks/dips and their relative intensity to each other are particularly important in order to successfully distinguish the type and volume of the chemical compound measured.

The reconstructed spectrum can be used for recognition of the chemical compound. Simulations with the plain scene granted better results over the usage of the more complex one. The reconstructed complex scene lacks details, therefore the results (from visual point of view) look very similar to the plain scene. As can be seen in Fig. 3 (right), the area where the chemical compound was, is authentically depicted. However, when we include the Planck's law (black body radiation) into the simulation, the quality of the reconstructed spectrum and the resolution of the slices of the datacube reduce greatly (results not shown).

Conclusion

In this article, we have provided an overview of IR hyperspectral imaging, with particular attention to using compressed sensing. We also created testing hyperspectral datacubes, in

which we simulated their measurements by the CASSI method. The simulated measurements were subsequently reconstructed by the TwIST algorithm.

We have found that we are able to obtain good results only with simulations of a plain scene. When we simulate a measurement of a more complex scene, we do not achieve a sufficient reconstruction quality and in the case of using black body radiation the CASSI method cannot be directly applied in this particular layout. One of the possible issues could be the reconstruction algorithm and the aim of the further research will be the use of, for example, several measurements of different random masks or rotation of spectral sweeping.

Acknowledgements

We gratefully acknowledge the financial support of the Ministry of Education, Youth and Sports of the Czech Republic (Project NPU LO1206).

Literature

- [1] ARCE, G. R.; BRADY, D. J.; CARIN, L.; ARGUELLO, H.; KITTLE, D. S.: Compressive Coded Aperture Spectral Imaging: An Introduction. *IEEE Signal Processing Magazine*. 2014, 31(1), pp. 105–115. Available from WWW: <https://ieeexplore.ieee.org/document/6678264/>. DOI: [10.1109/MSP.2013.2278763](https://doi.org/10.1109/MSP.2013.2278763)
- [2] BIOUCAS-DIAS, J. M.; FIGUEIREDO, M. A. T.: A New TwIST: Two-Step Iterative Shrinkage/Thresholding Algorithms for Image Restoration. *IEEE Transactions on Image Processing*. 2007, 16(12), pp. 2992–3004. Available from WWW: <https://ieeexplore.ieee.org/document/4358846/>. DOI: [10.1109/TIP.2007.909319](https://doi.org/10.1109/TIP.2007.909319)
- [3] GENDRIN, C.; ROGGO, Y.; COLLET, C.: Pharmaceutical applications of vibrational chemical imaging and chemometrics: A review. *Journal of Pharmaceutical and Biomedical Analysis*. 2008, 48(3), pp. 533–553. DOI: [10.1016/j.jpba.2008.08.014](https://doi.org/10.1016/j.jpba.2008.08.014)
- [4] STUART, B. H.: *Infrared Spectroscopy: Fundamentals and Applications*. Wiley Press: London, UK, 2004, pp. 29–36. ISBN 978-0-470-85428-0.
- [5] MANLEY, M.: Near-infrared spectroscopy and hyperspectral imaging: Non-destructive analysis of biological materials. *Chemical Society Reviews*. 2014, 43(24), pp. 8200–8214. DOI: [10.1039/C4CS00062E](https://doi.org/10.1039/C4CS00062E)
- [6] HUCK, Ch. W.; OZAKI, Y.; VERENA, A.; HUCK-PEZZEI, V. A.: Critical Review Upon the Role and Potential of Fluorescence and Near-Infrared Imaging and Absorption Spectroscopy in Cancer Related Cells, Serum, Saliva, Urine and Tissue Analysis. *Current Medicinal Chemistry*. 2016, 23(27), pp. 3052–3077. DOI: [10.2174/0929867323666160607110507](https://doi.org/10.2174/0929867323666160607110507)
- [7] TÜRKER-KAYA, S.; HUCK, Ch. W.: A Review of Mid-Infrared and Near-Infrared Imaging: Principles, Concepts and Applications in Plant Tissue Analysis. *Molecules*. 2017, 22(1), p. 168. DOI: [10.3390/molecules22010168](https://doi.org/10.3390/molecules22010168)
- [8] JUNKERMANN, W.; BURGER, J. M.: A New Portable Instrument for Continuous Measurement of Formaldehyde in Ambient Air. *Journal of Atmospheric and Oceanic Technology*. 2006, 23(1), pp. 38–45. DOI: [10.1175/JTECH1831.1](https://doi.org/10.1175/JTECH1831.1)
- [9] KATRAŠNIK, J.; BÜRMEIN, M.; PERNUŠ, F.; LIKAR, B.: Spectral characterization and calibration of AOTF spectrometers and hyper-spectral imaging systems. *Chemometrics and Intelligent Laboratory Systems*. 2010, 101(1), pp. 23–29. DOI: [10.1016/j.chemolab.2009.11.012](https://doi.org/10.1016/j.chemolab.2009.11.012)

- [10] HAMMOND, S. V.; CLARKE, F. C.: *The handbook of vibrational spectroscopy, sampling techniques, microscopy*. In: Chalmers J. M.; Griffiths P. R. (eds), Wiley, Hoboken, 2002, pp. 1405–1431.
- [11] CARRASCO, O.; GOMEZ, R. B.; CHAINANI, A.; ROPER, W. E.: Hyperspectral imaging applied to medical diagnoses and food safety. In: *Proc. SPIE 5097, Geo-Spatial and Temporal Image and Data Exploitation III*. (14 August 2003). DOI: [10.1117/12.502589](https://doi.org/10.1117/12.502589)
- [12] MAHESH, S.; JAYAS, D. S.; PALIWAL, J.; WHITE, N. D. G.: Hyperspectral imaging to classify and monitor quality of agricultural materials. *Journal of Stored Products Research*. 2015, Vol. 61, pp. 17–26. DOI: [10.1016/j.jspr.2015.01.006](https://doi.org/10.1016/j.jspr.2015.01.006)
- [13] FENG, Y.-Z.; SUN, D.-W.: Application of hyperspectral imaging in food safety inspection and control: a review. *Critical Reviews in Food Science and Nutrition*. 2012, 52(11), pp. 1039–1058. DOI: [10.1080/10408398.2011.651542](https://doi.org/10.1080/10408398.2011.651542)
- [14] SCHULER, R. L.; KISH, P. E.; PLESE, C. A.: Preliminary observations on the ability of hyperspectral imaging to provide detection and visualization of bloodstain patterns on black fabrics. *Journal of Forensic Sciences*. 2012, 57(6), 1562–1569. DOI: [10.1111/j.1556-4029.2012.02171.x](https://doi.org/10.1111/j.1556-4029.2012.02171.x)
- [15] EDELMAN, G. J.; GASTON, E.; van LEEUWEN, T. G.; CULLEN, P. J.; AALDERS, M. C. G.: Hyperspectral imaging for non-contact analysis of forensic traces. *Forensic Science International*. 2012, 223(1–3), pp. 28–39. DOI: [10.1016/j.forsciint.2012.09.012](https://doi.org/10.1016/j.forsciint.2012.09.012)
- [16] BALAS, C.; EPITROPOU, G.; TSAPRAS, A.; HADJINICOLAOU, N.: Hyperspectral imaging and spectral classification for pigment identification and mapping in paintings by El Greco and his workshop. *Multimedia Tools and Applications*. 2018, 77(8), pp. 9737–9751. DOI: [10.1007/s11042-017-5564-2](https://doi.org/10.1007/s11042-017-5564-2)
- [17] GAO, L.; LIANG, J.; LI, Ch.; WANG, L. V.: Single-shot compressed ultrafast photography at one hundred billion frames per second. *Nature*. 2014, Vol. 516, pp. 74–77. DOI: [10.1038/nature14005](https://doi.org/10.1038/nature14005)
- [18] FERNANDEZ, Ch. A.; GUENTHER, B. D.; GEHM, M. E.; BRADY, D. J.; SULLIVAN, M. E.: Longwave infrared (LWIR) coded aperture dispersive spectrometer. *Frontiers in Optics*. 2006, OSA Technical Digest (CD) (Optical Society of America, 2006), paper JSuA10. DOI: [10.1364/FIO.2006.JSuA10](https://doi.org/10.1364/FIO.2006.JSuA10)
- [19] RUSSELL, T. A.; McMACKIN, L.; BRIDGE, B.; BARANIUK, R.: Compressive hyperspectral sensor for LWIR gas detection. *Proc. SPIE 8365, Compressive Sensing*. 2012, 83650C. DOI: [10.1117/12.919522](https://doi.org/10.1117/12.919522)
- [20] DUPUIS, J. R.; KIRBY, M.; COSOFRET, B. R.: Longwave infrared compressive hyperspectral imager. *Proc. SPIE 9482, Next-Generation Spectroscopic Technologies VIII*. 2015, 94820Z. DOI: [10.1117/12.2177893](https://doi.org/10.1117/12.2177893)

HYPERSPEKTRÁLNÍ ZOBRAZOVÁNÍ V INFRAČERVENÉ OBLASTI VYUŽÍVAJÍCÍ KOMPRIMOVANÉ SNÍMÁNÍ

Tento článek se zabývá hyperspektrálním zobrazováním v infračervené oblasti, simulacemi měření a rekonstrukcemi testovacích datakrychlí za použití metody komprimovaného snímání CASSI (Coded Aperture Snapshot Spectral Imaging). Provedli jsme simulace přítomnosti chemické látky na části obrazu a poté jsme zrekonstruovali její absorpční spektrum a lokalizovali ji z jediného snímku detektoru. Jinými slovy, ukázali jsme, že v podstatě je možné rekonstruovat řídkou 3D datakrychli z jediného 2D obrazu. Dále diskutujeme kvalitu rekonstruovaných dat a limity zvolených metod simulace.

HYPERSPEKTRALES ABBILDEN IM INFRAROTEN BEREICH ZUR ANWENDUNG KOMPRIMIERTEN SCANNENS

Dieser Artikel befasst sich mit dem hyperspektralen Abbilden im infraroten Bereich, mit Simulationen des Messens und mit Rekonstruktionen von Testdatenwürfeln unter Verwendung der Methode des komprimierten Scannens, genannt CASSI (Coded Aperture Snapshot Spectral Imaging). Wir haben Simulationen der Gegenwart eines chemischen Stoffes auf einem Teil des Bildes durchgeführt. Danach haben wir dessen Absorptionsspektrum rekonstruiert und es auf einer einzigen Aufnahme des Detektors lokalisiert. Mit anderen Worten haben wir gezeigt, dass es im Grunde möglich ist, den seltenen 3D-Datenwürfel auf einem einzigen 2D-Bild zu rekonstruieren. Weiter diskutieren wir die Qualität der rekonstruierten Daten und die Grenzen der gewählten Methoden der Simulation.

OBRAZOWANIE WIELOSPEKTRALNE W ZAKRESIE PODCZERWIENI PRZY WYKORZYSTANIU TECHNIKI COMPRESSED SENSING

Niniejszy artykuł poświęcony jest obrazowaniu wielospektralnemu w zakresie podczerwieni, symulacjom pomiaru i odtwarzaniu testowych kostek danych przy wykorzystaniu metody compressed sensing CASSI (Coded Aperture Snapshot Spectral Imaging). Przeprowadziliśmy symulację obecności substancji chemicznej na części obrazu, po czym odtworzyliśmy jej widmo absorpcyjne i zlokalizowaliśmy ją z jednego obrazu zarejestrowanego przez czujnik. Innymi słowy, pokazaliśmy, że w zasadzie można odtworzyć niezbyt gęstą kostkę danych 3D z jednego tylko obrazu 2D. Ponadto omawiamy jakoś odtworzonych danych oraz ograniczenia wybranych metod symulacyjnych.

TIME AVERAGE SCANNING DIGITAL HOLOGRAPHY

Pavel Psota¹; Vít Lédl²; Roman Doleček³; Ondřej Matoušek⁴; Jan Kredba⁵

^{1,2,3}Institute of Plasma Physics, Academy of Sciences of the Czech Republic,
Regional Centre for Special Optics and Optoelectronic Systems (TOPTEC),
Za Slovankou 1782/3, 182 00 Prague 8, Czech Republic

^{4,5}Institute of New Technologies and Applied Informatics (NTI)
Faculty of Mechatronics, Informatics and Interdisciplinary Studies,
Technical University of Liberec

Studentská 2, 461 17 Liberec 1, Czech Republic

e-mail: ¹psota@ipp.cas.cz; ²ledl@ipp.cas.cz; ³dolecek@ipp.cas.cz;
⁴ondrej.matousek@tul.cz; ⁵jan.kredba@tul.cz

Abstract

This paper presents a novel method for amplitude distribution measurement of harmonically oscillating objects called time average scanning digital holography (TASDH). Reconstructed intensity image from time averaged digital hologram has the form of a set of fringes that follow a zero-order Bessel function of the first kind. When the phase of light beam in the interferometer is modulated, the bright zero-order fringe shifts with respect to the modulation depth. The method is based on continuous shift of the zero-order fringe over the object surface and the value of vibration amplitude is evaluated independently in every single pixel. An advantageous feature of the proposed technique with respect to other digital holographic vibrometry methods is the ability to measure amplitudes of vibration without the risk of interference fringe order, or 2π , errors. On that account, the method allows to measure high slopes amplitudes distribution or discontinuous/partially shaded objects. The correctness of the method was experimentally verified by measuring the bending piezo actuator.

Keywords

Digital holography; Time-average holography; Scanning holography; Vibrations; Phase modulation.

Introduction

Vibrometry is an integral part of various technical and scientific disciplines. There is a broad portfolio of vibration measurement devices, which are usually based on the Doppler phenomenon [1], correlation analysis [2], speckle ESPI (Electronic Speckle Pattern Interferometry) [3], and others. These methods are mostly single-point methods or their measuring capabilities in terms of maximal amplitudes or frequency range are limited. Thus, an extra care must be taken to parameters of a device when choosing one for a certain application. Another suitable tool for analyzing vibrations in the whole surface are digital holography based methods.

The holographic approach to measurement of vibration depends mainly on the frequency of the measured phenomena. For very low frequencies (much lower than FPS of the digital camera) it is possible to use “classical” digital holographic interferometry [4]. The first hologram is captured at steady-state without object oscillation while other holograms are captured at different phases of the movements. The measured interference phase between the reference and the hologram at a certain phase of the movement is proportional to vibration

amplitude of the object. This approach can be used unless the hologram within the exposure time is blurred by the object movement. High-speed cameras allowing very short exposure time together with the use of high-power laser can push the limits [5]. Similar approach for high frequencies is called the stroboscopic method [6]. The method requires using of a coherent pulse laser synchronized with digital camera. Short light pulses “freeze” the oscillating movement of the object at certain phase of the movement and therefore the hologram is not blurred. The interference phase between steady-state hologram and hologram at certain phase of the movement is measured and converted to vibration amplitude and phase.

The above mentioned methods were conditioned by short exposure time when compared to the period of the object oscillation. However, much longer exposure time than the period of the oscillation leads to so called time average digital holography (TADH). The intensity image reconstructed from such digital hologram exhibits a system of interference fringes described by Bessel function, which map contours of constant vibration amplitude. On that account high frequencies can be holographically measured without need of any special equipment. A lot of work has been done in order to modify the method for very low [7-9] or large [10, 11] amplitudes.

One of the most challenging tasks in TADH is to qualitatively determine the amplitude distribution from the fringe pattern modulated by Bessel function. Numerical analysis of cosine fringes (exhibiting in other interferometric techniques) by phase-shifting techniques [12] allows the determination of interference phases even between the fringe intensity maxima and minima with high accuracy. Phase-shifting technique was also developed for TADH employing phase modulation by mirror mounted on piezoelectric transducer [13] or acousto-optical modulator [14] in order to shift the Bessel fringes similarly to phase stepping in case of cosine fringes. This resulted in relative quantitative measurement of amplitudes of vibrations independently in every single pixel. Such methods, however, have some limitations. On the one hand, it is necessary to correct the result due to the difference between cosine and Bessel functions. Further, a spatial unwrapping algorithm is needed to demodulate the wrapped phase field and determine the “zero point” (oscillation node) from where other pixels are relatively measured. Naturally, the methods fail when it comes to vibration modes with high slopes leading to very dense fringe patterns. Moreover, for the correct amplitude distribution evaluation the nodal line is supposed to be within the field of view and simultaneously the FOV should be a continuous area without shading effects, etc.

We propose scanning time average scanning digital holography (TASDH) tackling the aforementioned drawbacks. It is also based on the phase modulation of the reference or object wave. The alter phase is now continuously scanned and using non-harmonic properties of zero-order first kind Bessel function we can determine the amplitude of vibration absolutely in every single pixel. Therefore, no spatial unwrapping or Cosine-Bessel correction is required. Although the principle is different, TASDH can be qualitatively compared to coherence scanning interferometry or white light. In comparison to phase-shifting methods, TASDH needs more data to be acquired, which is no problem for today’s computers. This paper introduces the basic principle of TASDH and its experimental verification.

1 Aim of Research

At the highest level, the research focuses on environmental noise management. More specifically, the focus is on sounds that people prefer to hear, and the acoustic environment is considered as a resource. The absolute elimination of all sounds is not natural, and the strategy of general noise suppression has been overcome by the possibilities of new technologies. Such a novel approach within soundscape planning allows elimination of just particular unwanted sounds and purifies the acoustic environment within the controlled space.

Implementation of the soundscape planning principles requires the research and development of efficient tools for a delicate control of sound wave propagation in an open space. Within this research project, our attention is focused on so called acoustic metasurfaces (AMS). Such research must cover several areas. Besides the development of AMS, it is mainly methods for measuring of specific acoustic impedance that control the transmission of sound waves through interfaces between two different media. Holographic methods allow fast and precise measurements of vibration amplitudes over the whole inspected area with high lateral resolution and are therefore one of the pillars of the whole research aim.

2 Time Average Scanning Digital Holography

2.1 Digital Holography

Digital holography (DH) involves the recording and reconstruction of optical waves. The recording is based on the superposition of a wave scattered from the object surface (called the object wave) O with a known reference wave R and recording their interference pattern. This interference pattern is called a digital hologram and can be described by the interference formula [4]:

$$H = |O + R|^2 = |R|^2 + |O|^2 + O^* R + OR^* . \quad (1)$$

The hologram H carries information about the intensity and phase of the waves and is stored in computer as an array of numbers U_o .

The reconstruction retrieves the information of the amplitude and phase from the digital hologram. The digital hologram H is multiplied with a numerical representation of conjugated reference wave $R^* U_r^*$, which results in a complex wave field in the hologram plane (with coordinates notation ξ, η). This wave field is then numerically propagated in a free space according to the laws of diffraction and the resulting complex field is calculated in a certain reconstruction distance d called the image plane (coordinates notations x, y). The free space propagation can be computed by Fresnel approximation [4]:

$$U(x, y) = \mathfrak{F}^{-1} \left\{ H(\xi, \eta) R^*(\xi, \eta) \exp \left[-\frac{j\pi}{\lambda d} (\xi^2 + \eta^2) \right] \right\}, \quad (2)$$

where \mathfrak{F}^{-1} denotes the inverse discrete Fourier transform and λ is the wavelength of the laser. Both hologram and image plane are sampled by $N \times M$ pixels. Pixel extension in the hologram plane $\Delta\xi \times \Delta\eta$ is naturally defined by real pixel extension of the sensor. The image plane pixel dimensions $\Delta x, \Delta y$ are given by parameters of the reconstruction [4]:

$$x = \frac{\lambda d}{N \Delta\xi} \quad \text{and} \quad \Delta y = \frac{\lambda d}{M \Delta\eta} . \quad (3)$$

The result of the reconstruction process $U(n\Delta x, m\Delta y)$ is a complex wave field in the image plane $U(x, y)$ from which the intensity $I(n\Delta x, m\Delta y)$ and phase distributions can be computed as [4]:

$$I(x, y) = |U(x, y)| \quad \text{and} \quad \varphi(x, y) = \arg(U(x, y)) . \quad (4)$$

2.2 Principle of the Method

Holographical recording of a harmonically oscillating object with an exposure time much longer when compared to the period of the object vibrations results in so called time average holography. Considering amplitude distribution $d^v(x, y, t) = d^v(x, y) \sin(\omega t)$ oscillating in time t , where d^v is the amplitude of vibration and ω stands for the angular frequency, the intensity of the reconstructed image is proportional to magnitude of the first kind zero-order Bessel function J_0 [4]:

$$I(x, y) = |J_0(\varphi(x, y))|. \quad (5)$$

In equation (5) the argument of the Bessel function (further called interference phase) $\varphi(x, y) = d^v(x, y) e^p(x, y)$ is proportional to amplitude of the vibration and sensitivity vector e^p , which is given by the geometrical properties of the holographic arrangement. We can assume only out-of-plane vibrations $d^v = [0, 0, D]$ and perpendicular illumination and observation of the object $e^p = 2\pi/\lambda [0, 0, 2]$ yielding in [4]:

$$\varphi(x, y) = D(x, y) 4\pi/\lambda. \quad (6)$$

The TASDH requires the phase modulation of the reference R or the object O beam with the same frequency ω as the oscillating object and with a modulation depth Ω :

$$O(t) = O \exp(jB \sin(\omega t)). \quad (7)$$

Putting the phase modulated object wave (7) into interference equation (1) modifies equation (5) into:

$$I(x, y, \Omega) = |J_0(\varphi(x, y) - \Omega)|. \quad (8)$$

Now, the reconstructed intensity image involves the modulation depth Ω . The loci of bright zero fringes appear where

$$\varphi(x, y) = \Omega \quad (9)$$

and can be unambiguously determined. Scanning of the modulation depth Ω provides an intensity signal for each image pixel as a function of the modulation depth (6). The modulation depth is not exactly known since it is defined by the transfer function between user controllable electronic device and the real phase modulation of the light beam. Therefore the interference phase φ is computed as the envelope shift between steady-state ($\varphi = 0, \Omega = 0$) with intensity:

$$I(x, y, 0) = |J_0(0)| \quad (10)$$

and the oscillating state defined in equation (6). Although there are several strategies how to search for the envelope shift, due to noise resistance we decided for cross-correlation (operator denoted by $*$) based searching using formula:

$$C(\hat{\Omega}) = I_0 * I = \int I_0(\Omega) I(\Omega + \hat{\Omega}) d\Omega, \quad (11)$$

where the lag of the cross-correlation function $\hat{\Omega}$ has the physical meaning of the modulation depth Ω . The maximum of the cross-correlation function $C(\hat{\Omega})$ indicates the lag where the signals are best aligned and $\hat{\Omega} \approx \varphi$. The interference phase can be therefore computed as:

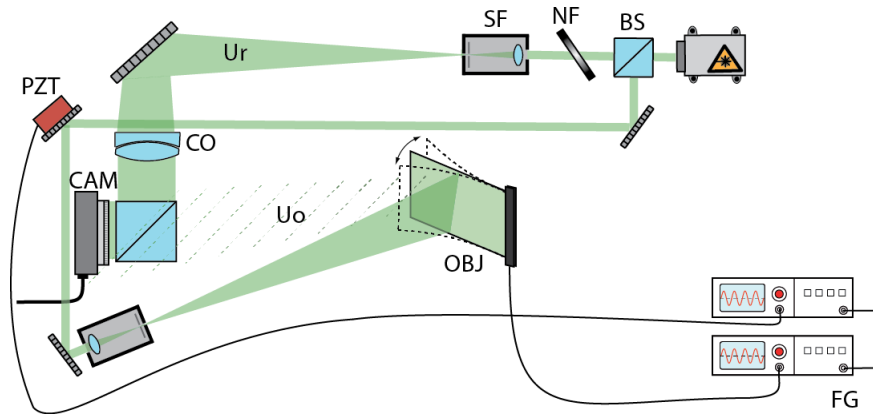
$$\varphi = \arg \max(I_0 * I). \quad (12)$$

Hence, the out-of-plane amplitude $D(x, y)$ is computed as simple inversion of (6):

$$D(x, y) = \varphi(x, y) \lambda / 4\pi. \quad (13)$$

3 Experiment and Results

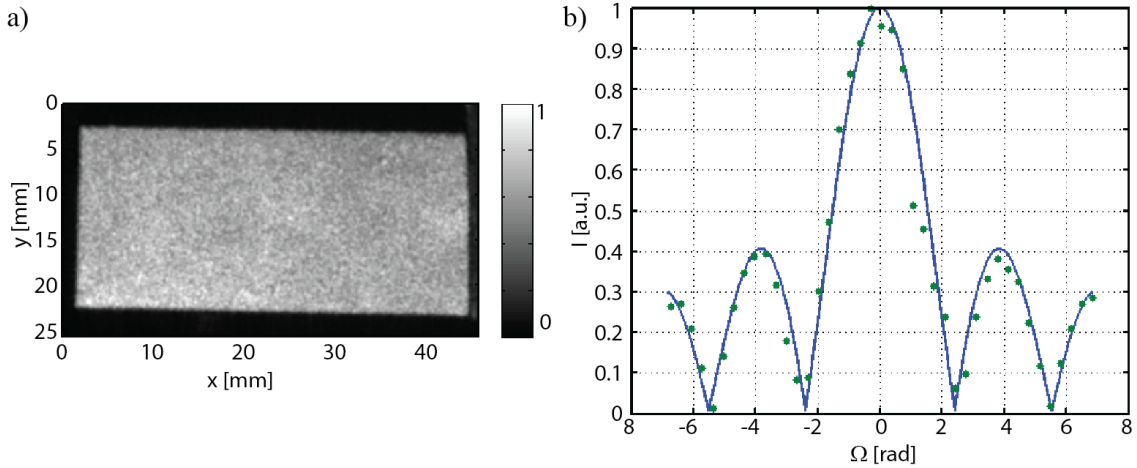
The experimental arrangement used for verification of TASDH principles is introduced in Fig. 1. The Nd:YAG laser emits coherent light with the wavelength of 532 nm that is split into the reference and the object arm. Both arms of the holographic interferometer are spatially filtered and impinging the sensor of a digital camera having 2048×2048 pixels each of size $3.45 \mu\text{m} \times 3.45 \mu\text{m}$. Superposition of the reference and the object wave generates an interference structure that is captured by the digital camera and creates a digital hologram. The phase of the object wave is on the one hand modulated by the object vibrations and on the other hand by the oscillating mirror mounted on an electronically controlled piezoelectric transducer (PZT). Naturally, the PZT mirror can also be placed in the reference arm.



Source: Own

Fig. 1: Principal scheme of a holographic interferometer for TASDH employing components: BS – beam splitter, NF - neutral density filter, SF – spatial filter, CO – collimating objective, OBJ – object, FG – arbitrary waveform generator, CAM – digital camera, M – mirror, PZT – piezoelectric transducer, Ur denotes reference wave while Uo stands for object wave.

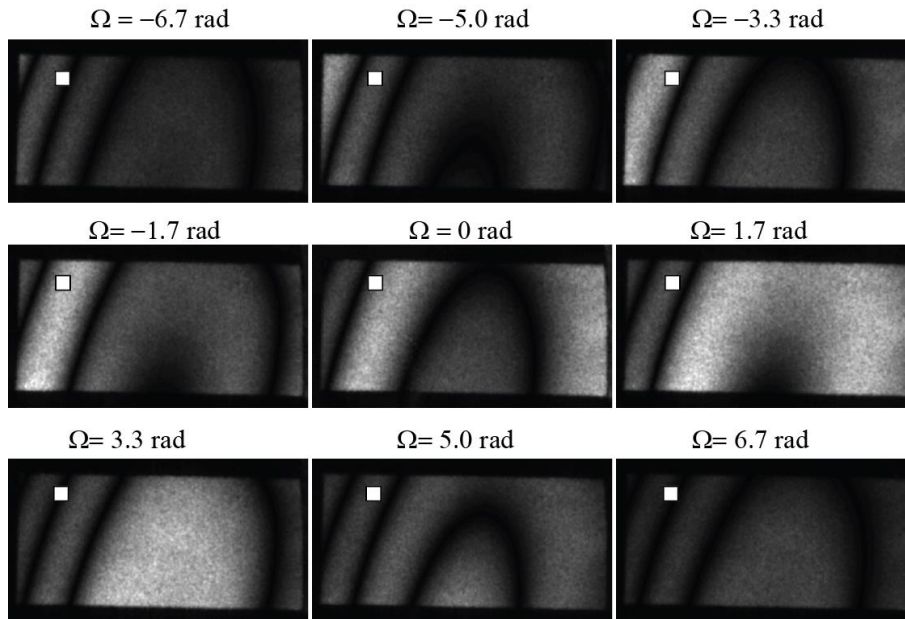
The investigated object is a bending piezoelectric actuator driven by a two channel waveform generator. One channel of the waveform generator sets the frequency and amplitude of the harmonic object vibrations, while the second channel controls the PZT mirror.



Source: Own

Fig. 2: a) Reconstructed intensity image of steady-state object with no phase modulation $\Omega = 0$; b) measured (green) and fitted (blue) intensity values at $x = 25$ mm and $y = 13$ mm as a function of the modulation depth

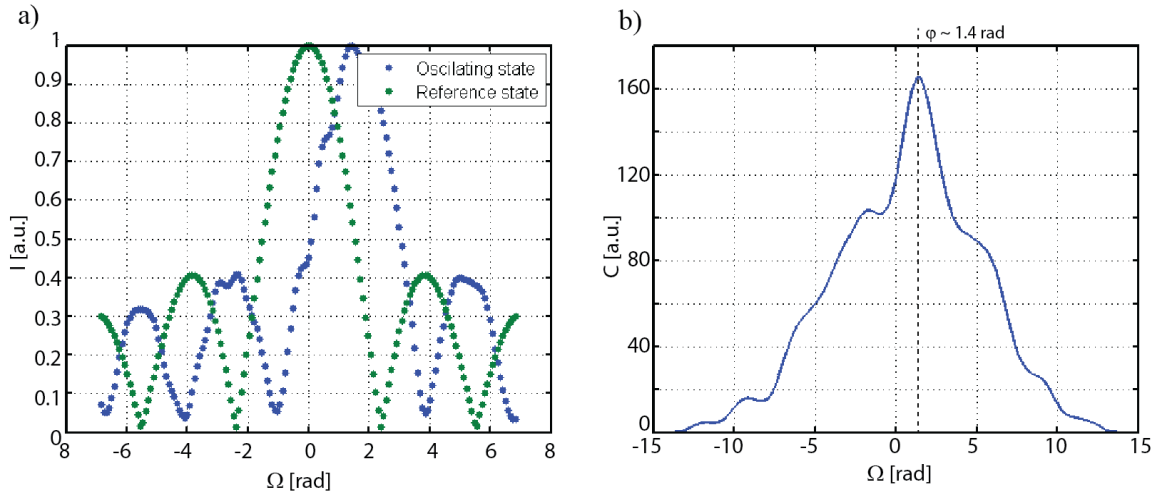
In the first step, the object is in steady-state and the PZT is oscillating with a frequency of 700 Hz. The driven amplitude of PZT was scanned in the range from -20 VPP (peak-to-peak) to 20 VPP with the step of 1 VPP. The reconstructed intensity image of steady-state object with no phase modulation $\Omega = 0$ is shown in Fig. 2a. As expected, the intensity at any object point (in our case $x = 25$ mm, $y = 13$ mm) is a function of the phase modulation depth and in every pixel follows equation (8) with $\varphi = 0$, see Fig. 2b.



Source: Own

Fig. 3: Sequence of intensity images of oscillating object with different phase modulation depths. The white square denotes pixel used for analysis in Fig. 4.

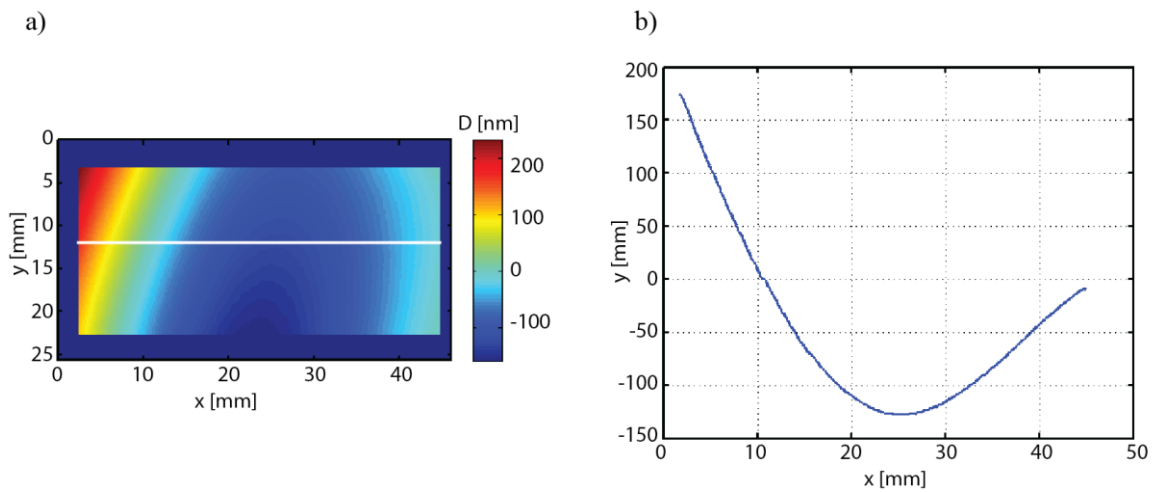
The green markers are measured values and the blue line is fitted magnitude of Bessel function. The results of the Bessel function fitting provide also the transfer function between the electronic output signal (PZT driven amplitude) from the waveform generator and the phase modulation depth of the light wave: 1 VPP \sim 0.34 rad. The measured or fitted result can be used as reference for the following measurement.



Source: Own

Fig. 4: Interference phase evaluation in the “white square” pixel (see Fig. 3): a) plot of steady-state (reference) Bessel function and measured intensity values as a function of phase modulation depth that form shifted Bessel function; b) cross-correlation of green and blue functions in a) with highlighted lag corresponding to the value of interference phase.

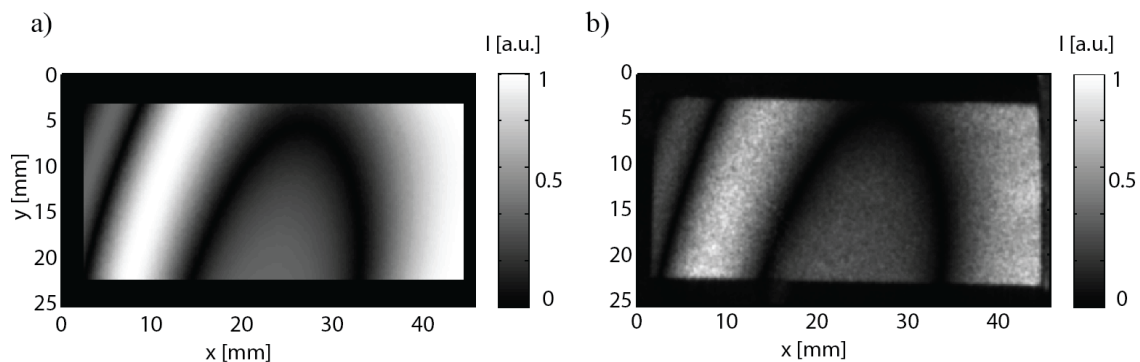
In the second step, we set the object frequency to 700 Hz with 1 VPP driven amplitude. The frequency of the PZT remains 700 Hz, the start phase of the PZT is aligned with the object vibration phase and the modulation depth (driven amplitude) is scanned from -20 VPP to +20 VPP with the step of 1 VPP. The sequence of some intensity images for different phase modulation in Fig. 3 illustrates how the bright fringe shifts over the object surface. Further, one pixel (at position of the white square) is chosen for detailed analysis. Green markers in Fig. 4a plots reference (steady-state) Bessel function analogously to Fig. 2b and the measured values in the “white square” pixel - blue markers - are represented by the shifted Bessel function. Maximum of cross-correlation function between the green and blue functions (plotted in Fig. 4b) indicates the lag corresponding to the interference phase $\hat{\Omega} \approx \varphi$ as discussed in equation (12). This procedure is realized independently in every single pixel and using formula (13) the interference phase is converted to amplitude distribution, see Fig. 5.



Source: Own

Fig. 5: Amplitude distribution measured by TADSH: a) false color image, where different colors represent different values of out-of-plane vibration amplitudes; b) vibration amplitude values along white line in a).

To verify the correctness of the result, we substitute the measured interference phase φ into equation (5). The resulting intensity map (Fig. 6a) should correspond to the reconstructed intensity image with no modulation (Fig. 6b). Both images are in very good agreement.



Source: Own

Fig. 6: Verification of the results: a) intensity image computed from evaluated interference phase by TASDH; b) measured intensity image; the both images are in very good agreement.

Conclusion

This paper presents basic principles and experimental verification of novel time average scanning digital holography (TASDH). This method is applied to the measurement of harmonic vibration amplitudes. The reconstructed intensity image from the time averaged digital hologram consists a fringe pattern structure (described by Bessel function) reflecting contours of vibration amplitudes. The principle of the TASDH method is based on phase modulation of light beam in the object or reference arm of the holographic interferometer. As the phase modulation depth varies, the fringes in the reconstructed intensity image continuously shift over the object surface and the brightest zero order fringe can be easily located. The interference phase value corresponding to this zero order fringe is ambiguously known and therefore can be easily linked to the certain surface point. This procedure is done independently in every single pixel and thus no spatial unwrapping is needed. An advantageous feature of the TASDH technique with respect to other quantification methods within TADH is the ability to measure amplitudes of vibration without the risk of interference fringe order, or 2π , errors. On that account the method allows to measure high slopes amplitudes distribution or discontinuous/partially shaded objects. The correctness of the method was experimentally verified by measuring the bending piezo actuator.

Acknowledgements

This work was supported by the Ministry of Education, Youth and Sports of the Czech Republic in the Project No. NPU LO1206. This work was also supported by the Czech Science Foundation Project No.: GACR GA 16-11965S.

Literature

- [1] McCONNELL, K. G.; VAROTO, P. S.: *Vibration testing: theory and practice*. John Wiley & Sons, 1995. ISBN: 978-0-471-66651-6.
- [2] BUTTERS, J. N.; LEENDERTZ, J. A.: Holographic and Video Techniques Applied to Engineering Measurement. *Measurement and Control*. 1971, Vol. 4, Issue 12, pp. 349–354. DOI: [10.1177/002029407100401201](https://doi.org/10.1177/002029407100401201)

- [3] MACOVSKI, A; RAMSEY, S. D.; SCHAEFER, L. F.: Time-Lapse Interferometry and Contouring Using Television Systems. *Applied Optics*. 1971, Vol. 10, Issue 12, pp. 2722–2727. DOI: [10.1364/AO.10.002722](https://doi.org/10.1364/AO.10.002722)
- [4] KREIS, T.: *Handbook of holographic interferometry: optical and digital methods*. Wiley-VCH, 2005. DOI: [10.1002/3527604154](https://doi.org/10.1002/3527604154)
- [5] PEDRINI, G.; OSTEN, W.; GUSEV, M. E.: High-speed digital holographic interferometry for vibration measurement. *Applied Optics*. 2006, Vol. 45, Issue 15, pp. 3456–3462. DOI: [10.1364/AO.45.003456](https://doi.org/10.1364/AO.45.003456)
- [6] De GREEF, D.; SOONS, J.; DIRCKX, J. J. J.: Digital stroboscopic holography setup for deformation measurement at both quasi-static and acoustic frequencies. *International Journal of Optomechatronics*. DOI: [10.1080/15599612.2014.942928](https://doi.org/10.1080/15599612.2014.942928)
- [7] PSOTA, P.; LÉDL, V.; DOLEČEK, R.; ERHART, J.; KOPECKÝ, V.: Measurement of piezoelectric transformer vibrations by digital holography. *IEEE Transactions on Ultrasonics, Ferroelectrics, and Frequency Control*. 2012, Vol. 59, Issue 9, pp. 1962–1968. DOI: [10.1109/TUFFC.2012.2414](https://doi.org/10.1109/TUFFC.2012.2414)
- [8] PSOTA, P.; LÉDL, V.; DOLEČEK, R.: High Dynamic Range Digital Holographic Method for Very Small Amplitude Measurement. *Fringe 2013*. pp. 635–640. DOI: [10.1007/978-3-642-36359-7_117](https://doi.org/10.1007/978-3-642-36359-7_117)
- [9] VERRIER, N.; ATLAN, M.: Absolute measurement of small-amplitude vibrations by time-averaged heterodyne holography with a dual local oscillator. *Optics Letters*. 2013, Vol. 38, Issue 5, pp. 739–741. DOI: [10.1364/OL.38.000739](https://doi.org/10.1364/OL.38.000739)
- [10] JOUD, F.; LALOË, F.; ATLAN, M.; HARE, J.; GROSS, M.: Imaging a vibrating object by Sideband Digital Holography. *Optics Express*. 2009, Vol. 17, Issue 4, pp. 2774–2779. DOI: [10.1364/OE.17.002774](https://doi.org/10.1364/OE.17.002774)
- [11] PSOTA, P.; LÉDL, V.; DOLEČEK, R.; VÁCLAVÍK, J.; KOPECKÝ, V.: Improved holographic method for vibration amplitude measurement from nano to microscale. In: AIP Conference Proceedings. 2014, Vol. 1600, Issue 1, pp. 228–236. DOI: [10.1063/1.4879587](https://doi.org/10.1063/1.4879587)
- [12] CREATH, K.: Phase-shifting holographic interferometry. In: Rastogi P. K. (eds) *Holographic Interferometry*. Springer Series in Optical Sciences. 1994, Vol. 68, pp. 109–150. Springer, Berlin, Heidelberg. DOI: [10.1007/978-3-540-48078-5_5](https://doi.org/10.1007/978-3-540-48078-5_5)
- [13] STETSON, K. A.; BROHINSKY, W. R.: Fringe-shifting technique for numerical analysis of time-average holograms of vibrating objects. *Journal of the Optical Society of America A*. 1988, Vol. 5, Issue 9, pp. 1472–1476. DOI: [10.1007/978-3-540-48078-5_5](https://doi.org/10.1007/978-3-540-48078-5_5)
- [14] PSOTA, P.; LÉDL, V.; DOLEČEK, R.; MOKRÝ, P.; VOJTÍŠEK, P.; VÁCLAVÍK, J.: Comprehensive time average digital holographic vibrometry. *Optical Engineering*. 2016, Vol. 55, Issue 12. DOI: [10.1117/1.OE.55.12.121726](https://doi.org/10.1117/1.OE.55.12.121726)

ČASOVĚ STŘEDOVANÁ SKENOVACÍ DIGITÁLNÍ HOLOGRAFIE

Tento článek představuje novou metodu pro měření amplitud harmonických oscilací nazvanou časově středovaná skenovací digitální holografie. Rekonstruovaný intenzitní obraz z časově středovaného digitálního hologramu vytváří interferenční strukturu, která je popsána Besselovou funkcí prvního typu nultého řádu. Je-li fáze laserového svazku v interferometru modulována, interferenční proužek odpovídající nultému řádu se v závislosti na hloubce modulace posune. Metoda je založena na skenování proužku nultého řádu přes celý povrch objektu. Amplituda vibrací je nezávisle a absolutně vyhodnocena v každém pixelu. Výhodou navrhované techniky ve srovnání s dalšími metodami digitální holografické vibrometrie je schopnost měřit amplitudu vibrací bez rizika správnosti určení interferenčního řádu. Z tohoto důvodu metoda umožňuje měření amplitud vibrací s velkou strmostí či nespojitých / částečně zastíněných objektů. Správnost metody byla experimentálně ověřena měřením ohybového piezoelektrického aktuátoru.

ZEITDURCHSCHNITT DER SCAN-DIGITAL-HOLOGRAPHIE

Diese Arbeit stellt ein neuartiges Verfahren zur Amplitudenverteilung harmonisch oszillierender Objekte vor, das als zeitgemittelte digitale Holographie bezeichnet wird. Das rekonstruierte Bild des zeitgemittelten digitalen Hologramms hat die Form eines Satzes von Streifen, die einer Bessel-Funktion nullter Ordnung des ersten Typs folgen. Wenn die Phase des Lichtstrahls in dem Interferometer moduliert wird, verschiebt sich der helle Streifen nullter Ordnung in Bezug auf die Modulationstiefe. Das Verfahren basiert auf der kontinuierlichen Verschiebung des Streifens nullter Ordnung über die Objektoberfläche und der Wert der Schwingungsamplitude wird unabhängig in jedem Pixel bewertet. Ein vorteilhaftes Merkmal der vorgeschlagenen Technik in Bezug auf andere digitale holographische Vibrometrieverfahren ist die Fähigkeit, die Schwingungsamplitude ohne Risiko von Interferenzstreifenordnungen oder 2π -Fehlern zu messen. Aus diesem Grund erlaubt das Verfahren die Messung großer Amplitudenverteilungen oder diskontinuierlicher / teilweise schattierter Objekte. Die Richtigkeit der Methode wurde experimentell durch die Messung des Biegepiezoaktors überprüft.

CZASOWO WYŚRODKOWANA CYFROWA HOLOGRAFIA SKANINGOWA

W artykule przedstawiono nowatorską metodę pomiaru amplitud oscylacji harmoniczných nazwaną czasowo wyśrodkowaną cyfrową holografia skaningową. Obraz odtworzony z czasowo wyśrodkowanego cyfrowego hologramu tworzy strukturę interferencyjną, opisaną funkcją Bessela pierwszego rodzaju zerowego rzędu. Jeżeli faza wiązki laserowej w interferometrze jest modulowana, pasek interferencyjny odpowiadający rzędowi zerowemu w zależności od głębokości modulacji przesuwa się. Metoda oparta jest na skanowaniu paska rzędu zerowego na całej powierzchni obiektu. Amplitudę drgań oceniano niezależnie i absolutnie dla każdego piksela. Zaletą proponowanej techniki w porównaniu z innymi metodami cyfrowej wibrometrii holograficznej jest zdolność pomiaru amplitudy drgań bez ryzyka dla prawidłowego określenia rzędu interferencyjnego. Z tego powodu metoda pozwala na pomiar amplitud wibracji o dużej strmości lub niespójnych/częściowo zacienionych obiektów. Prawidłowość metody została zweryfikowana eksperymentalnie poprzez pomiar giętego piezoelektrycznego aktuatora.

OBJECTIVE EVALUATION OF UPRIGHT AND GRAND PIANOS BY MEASURING PLAY-BENCH

Jana Urbánková

VÚTS, a.s., Measurement Department,
Svárovská 619, Liberec XI - Růžodol I, 460 01 Liberec, Czech Republic
e-mail: jana.urbankova@vuts.cz

Abstract

This article describes the measuring equipment which is used in the objective evaluation of pianos. This equipment in the form of a play-bench replays each key of the piano keyboard separately, making it possible to measure the acoustics such as sound pressure level and tone reverberation length. Objective evaluation of such a complicated instrument as the piano is a very complex task. An integral part of evaluation is the psychoacoustic dimension and the conversion of subjective perceptions into objective acoustical values.

Keywords

Piano; Play-bench; Striking pins; Acoustics; Psychoacoustics.

Introduction

The piano is a very complicated musical instrument and it is relatively new, first introduced in the 18th century and evolving to the current appearance of the grand piano in 19th century [3]. In comparison with other musical instruments, the piano offers huge possibilities of playing. The enormous range of loudness consists the name itself – “pianoforte” (piano = quietly, forte = loud).

The traditional manufacture of musical instruments is a highly prestigious handcraft, and famous producers base their reputation on precise handmade work. So when they are assessed, it cannot be practically circumvented without a subjective evaluation. Simply the evaluation of the musical sound itself is very narrow specialization [1] and [2]. If the manufacturer wants to find out the quality of their instrument, they are practically always dependent on professional players’ opinion. This form of feedback is lengthy and uneconomical in many ways. For the manufacturer it is very complicated to round up more players together, ensure equal conditions for everyone and compare their answers, which are often very specific. Next problem is the fact that players (especially pianists) are often unable to separate the perception of the sound from the perception of running the mechanics; it is said that “they hear with their hands”. It is therefore increasingly necessary for manufacturers to evaluate their instruments in an objective way so that they can compare each other and go forward with their own development.

The branch of science called psychoacoustics deals with the subjective percept transfer into objective data and use the knowledge of human perception [6].

1 Research Objective

In the first place, the research objective is to modernize and rebuild the original play-bench for new measurement requirements and finding a suitable measurement methodology.

2 Measuring Equipment

Big advantages of objective measurement are specifications of clearly and repeatable measurement conditions and results presented by a single value. The evaluation and comparison of single instruments becomes much easier.

At the end of the 1960s, measuring equipment [5] was developed in the State School of Music in Warsaw for Czechoslovak musical instruments. This device consisted mainly of a bench used in Petrof company for research and development [4] in the 1990s. In the last two years, the play-bench was renovated and upgraded to offer greater possibilities for measuring pianos.

2.1 The Original Play-Bench of Petrof

The original play-bench (shown in Fig. 1) was composed of aluminium rail on which two striking pins were moved - one for the white keys and the second for the black ones. A system of metallic contacts on the rail allowed the pin to stop above the particular key. Then the key was excited by the striking pin with a defined power. The pins consisted of a pair of electromagnets and a set of two artificial fingers. The artificial fingers were conical in shape and were made of teflon. The keystroke was performed by the free fall of the pin on the key. The movement of the pins and the measurement was realized by the control system (Fig. 2) remotely.



Source: Own

Fig. 1: Original equipment constructed in 1960s



Source: Own

Fig. 2: The control system for measurement settings of the original play-bench

Because of obsolete system, long time inactivity and need of wider setting of play-bench, the measuring equipment was rebuilt for the need of the Petrof company, involving modernizing the control system and adapting it for easier programming.

2.2 Rebuilding and Modernization of the Play-Bench

Only the set of electromagnets and both pins were used from the original device and they were also partially modified. The aluminium rail was replaced by a steel girder and universal clamping brackets which hold the equipment onto the piano. The pins are transported along a circular slide way and move using a toothed belt and a stepper motor. The new play-bench is shown in Fig. 3. An industrial computer (PLC) is used to control and set the measurement (shown in Fig. 4). This allows us to change the setting of the measured range and the play mode, the time of the keystroke and the time between the pins movement and the keystroke.

The entire device was modified in particular to measure the full dynamic range of the instrument. The keystroke is performed by free fall, so it is possible to control and vary its impact force only by additional weights and adjustment of the height of the artificial fingers. Compared to the original adjustment of the pins height, when it was necessary to change the internal structure of the pins, the height (2-20 mm above the keyboard, including the possibility of adding weight) is set directly by the artificial fingers.



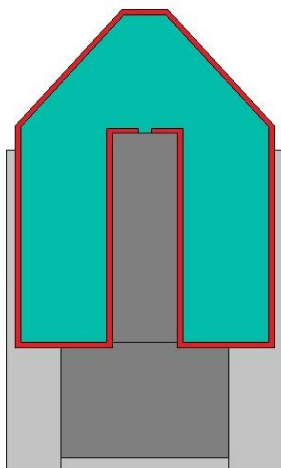
Source: Own

Fig. 3: The rebuilt and modernized play-bench



Source: Own

Fig. 4: The industrial computer for control and measurement setting



Source: Own

Fig. 5: Scheme of the artificial finger structure:
 red – teflon tape,
 turquoise – silicone head,
 dark gray – reinforcing screw



Source: Own

Fig. 6: The development of artificial fingers
 to the far left: original artificial
 finger made of teflon, to the far
 right: the final form of artificial
 finger made of addition silicone and
 teflon tapes

2.3 The Striking Pins

As has been said, one of the important claims of the modernization was the ability to play the keys in the full dynamic range of the instrument. This is mainly influenced by the appearance of the artificial fingers. Many shapes and materials were tested in the past, particularly because of the durability of the material and the ability to easily slip over the key surface. Original fingers were constructed with the bevelled cylindrical pins from teflon. This solution had lots of advantages - there was no deformation after repeated use, the location of striking on the key was sufficiently defined, and friction was minimized. But it was unusable for the lowest dynamics because of the hard material that made a lot of noise by the keystroke.

Therefore, new artificial fingers were made of soft addition silicone, which is very close to the silicones used in orthopaedics and prosthetics. A thin teflon foil is also attached to the surface of the silicone finger to ensure easy slipping on the key. A simple diagram of a silicone artificial finger is shown in Fig. 5 and the development of the artificial fingers themselves is illustrated in Fig. 6.

3 The Methods of Research

Methods of research represent mainly measurements of instruments themselves, verification of these measurements and subsequent comparison of achieved results.

4 The Measurement

After the final adjustment and modification of the measuring play-bench, three pianos were measured – two upright pianos and one grand piano. All instruments were measured in semi-anechoic chamber with two microphones positions – objective and “psychoacoustics”. The first (objective) position is different for upright pianos and for grand pianos. For the upright piano, the microphone is placed 1 m high at a distance of 1 m on the axis perpendicular to the surface of the soundboard and in case of the grand piano; the microphone is positioned in the extension of the right edge of the instrument, 160 cm high and parallel to the opened main lid. The position of the microphone for the psychoacoustic measurement is in the location of the player.

4.1 Measurement Settings

Five specifications of dynamics for the measurement were determined. These specifications differed in the height and weight of the striking pins with the same step. It was found that the maximum weight of the striking pin for the black keys was lower than for the white keys because of different inner stroke mechanism and treatment of the key surface itself. While the maximum weight of the additional weights is given by the play-bench options, or by the electromagnets options, the minimum weight is given by the possibilities of individual instruments and must be determined for each instrument individually.

Replaying of keys was done in the “All” play-mode, so that all 88 keys on the keyboard were replayed sequentially.

4.2 Evaluation

For objective comparison of each instrument, it is necessary to reduce a large amount of data (88 keys) to a single number that evaluates the entire range of the instrument or (better) to three values corresponding to distribution of the range according to Tab. 1.

Tab. 1: Dividing the keyboard range into approximately three equal groups

Distribution	Tone range (German notation)	Order of tones on the play-bench
bass	A2 – d	88 – 59
alto	dis – gis2	58 – 29
descant	a2 – c5	28 – 1

Source: Own

The range of piano dynamics is according to the literature from 40 dB to 100 dB. Tab. 2 shows a more detailed distribution.

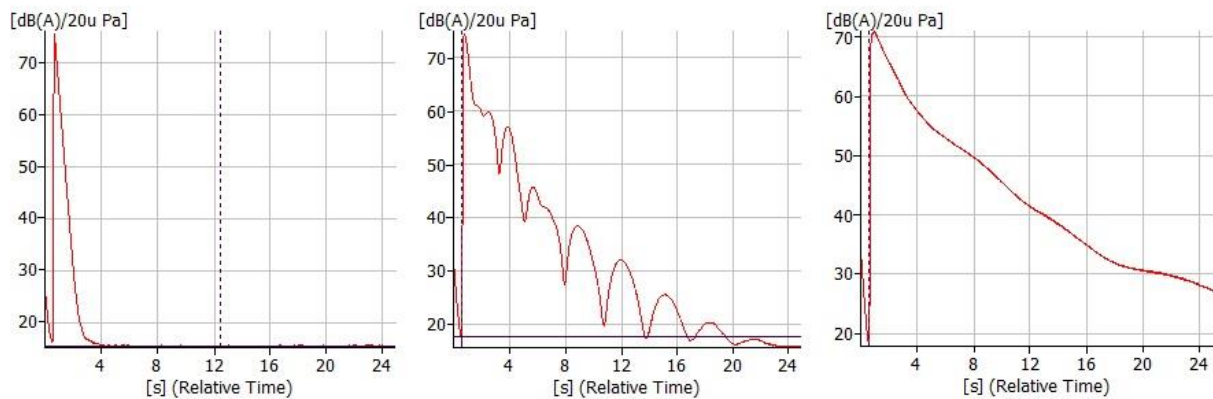
Tab. 2: Theoretical range of piano dynamics

Dynamics	Sound pressure level [dB]	Tolerance [dB]
ppp (piano pianissimo)	40	± 5
pp (pianissimo)	50	± 5
p (piano)	60	± 2.5
mp (mezzopiano)	65	± 2.5
mf (mezzoforte)	70	± 2.5
f (forte)	80	± 5
ff (fortissimo)	90	± 5
fff (forte fortissimo)	100	± 5

Source: [7]

The time records of the sound pressure signals were obtained by the measuring system. From these time records, the waveforms of sound pressure levels were evaluated, weighted by the filter A and exponentially averaged with a time constant of $\tau = 1/8$ s. This setting represents the acoustic emission as perceived by the human ear. After that, the maxima of sound pressure levels for each key were found in different dynamics and the overall "loudness" of individual pianos was evaluated. The term of loudness is not defined here by psychoacoustic metric but for the comparison of instruments it is sufficient to define the maximum sound pressure level.

Together with the waveforms of tones, the tone reverberation length of the individual keys and the whole instrument were determined. An example of the tone reverberation length of tones a4 (descant), a1 (alto) and A1 (bass) is shown in Fig. 7.



Source: Own

Fig. 7: The sound pressure level depending on time, tones a4 (descant), a1 (alto) and A1 (bass) (left to right) in German notation

Tab. 3 to 5 show the results of the total sound pressure level L_p (A) and tone reverberation length t_r for different dynamics over the entire instruments range. The "D1" represents the lowest dynamic and "D5" the loudest one.

Tab. 3: Total sound pressure level and tone reverberation length for different dynamics over the entire range of upright piano 1

Upright piano 1	Microphone 1 (objective)		Microphone 2 (psychoacoustic)	
Dynamics	$L_p(A)$ [dB]	t_r [s]	$L_p(A)$ [dB]	t_r [s]
D1	64.52	4.57	61.38	3.94
D2	76.76	8.28	70.32	6.01
D3	82.02	9.91	74.82	7.51
D4	84.81	10.79	77.48	8.05
D5	86.42	11.13	79.02	8.36

Source: Own

Tab. 4: Total sound pressure level and tone reverberation length for different dynamics over the entire range of upright piano 2

Upright piano	Microphone 1 (objective)		Microphone 2 (psychoacoustic)	
Dynamics	$L_p(A)$ [dB]	t_r [s]	$L_p(A)$ [dB]	t_r [s]
D1	63.79	4.71	57.40	3.37
D2	77.03	8.38	67.31	5.51
D3	81.19	9.57	73.76	7.67
D4	83.87	10.22	76.34	8.39
D5	85.83	10.90	78.26	8.92

Source: Own

Tab. 5: Total sound pressure level and tone reverberation length for different dynamics over the entire range of grand piano

Grand piano	Microphone 1 (objective)		Microphone 2 (psychoacoustic)	
Dynamics	$L_p(A)$ [dB]	t_r [s]	$L_p(A)$ [dB]	t_r [s]
D1	65.60	5.93	61.38	3.94
D2	78.17	9.45	72.44	7.15
D3	83.87	11.57	78.21	8.88
D4	86.88	12.52	81.17	9.50
D5	88.64	12.93	82.80	9.94

Source: Own

Conclusion

The improved and upgraded play-bench allows us to reliably replay each key of the piano keyboard with a defined and standardized keystroke in the dynamic range from *piano* (*p*) to *fortissimo* (*ff*), which is sufficient for general piano ratings. Limitations of the lowest dynamics are mainly due to the instruments themselves and their inner mechanisms. The play-bench is also universally applicable to any type of upright or grand piano thanks to the universally adjustable construction.

Two upright pianos and one grand piano were measured and evaluated using the play-bench. Based on the sound pressure measurement, the overall sound pressure level (overall “loudness”) of the individual instruments and the tone reverberation length were evaluated for five defined dynamics. The correct functionality and limits of the play-bench were verified during the measurement.

Acknowledgements

This project has been supported by the CTU research project SGS16/221/OHK3/3T/13 Measurement, modelling and evaluation methods in acoustics and by the Czech Ministry of Education, project LO1213.

The author would also like to thank the company Petrof.

Literature

- [1] TERHARDT, E.: Psychoacoustic evaluation of musical sounds. *Perception & Psychophysics*. 1978, 23(6), pp. 483–492. ISSN 0031-5117. DOI: [10.3758/BF03199523](https://doi.org/10.3758/BF03199523)
- [2] SYROVÝ, V.: *Hudební akustika*. 3. doplněné vydání. Praha: Akademie múzických umění, 2013. Akustická knihovna Zvukového studia Hudební fakulty AMU. ISBN 978-80-7331-297-8.
- [3] GIORDANO, N. J.: *Physics of the piano*. Oxford: Oxford University Press, 2010. ISBN 0199546029.
- [4] NOSEK, J.; RAFFAJ, A.: *Objektivní měření akustických vlastností pian*. Výzkumně-vývojové středisko s. p. Petrof, 1991.
- [5] BOBILEWICZ, Z.: *Universalna LAWA Pomiarowa do Poloautomatycznej Kontroly Pianin*. Warszawa: AM Chopina, 1970.
- [6] MELKA, A.: *Základy experimentální psychoakustiky*. 1. vyd. Praha: Akademie múzických umění v Praze, 2005. ISBN 80-7331-043-0.
- [7] KURFÜRST, P.: *Základy hudební akustiky*. Brno: Masarykova univerzita, 2000. ISBN 80-210-2333-3.

OBJEKTIVNÍ HODNOCENÍ PIANIN A KLAVÍRU POMOCÍ PŘEHRÁVACÍ LAVICE

Tento článek popisuje měřicí zařízení používané při objektivním hodnocení pian. Zařízení v podobě přehrávací lavice samostatně přehraje každou klávesu na klaviatuře a umožní tak změření akustických vlastností, jako je hladina akustického tlaku a délka doznívání tónu. Objektivní hodnocení tak složitého nástroje, jako je klavír, je velmi komplexní úkol. Nedílnou součástí hodnocení je psychoakustický rozsah a přeměna subjektivního vnímání na objektivní akustické hodnoty.

OBJEKTIVE BEWERTUNG DER PIANINOS UND KLAVIERE MIT DER MESSBANK

Dieser Artikel beschreibt ein Messgerät, das bei der objektiven Bewertung von Klavieren verwendet wird. Dieses Gerät in Form einer Messbank überspielt unabhängig jede Taste der Klaviertastatur und ermöglicht die Messung akustischer Eigenschaften wie Schalldruckpegel und Tonausklanglänge. Die objektive Beurteilung eines so komplizierten Instruments wie des Klaviers eine sehr komplexe Aufgabe. Ein wesentlicher Bestandteil der Bewertung ist die psychoakustische Dimension und die Umwandlung subjektiver Wahrnehmungen in objektive akustische Werte.

OBIEKTYWNA OCENA PIANIN I FORTEPIANÓW ZA POMOCĄ ŁAWKI ODTWARZAJĄCEJ

W niniejszym artykule opisano urządzenie pomiarowe używane do obiektywnej oceny pianin. Urządzenie w postaci ławki odtwarzającej odtwarza oddzielnie każdy klawisz klawiatury, umożliwiając pomiar cech akustycznych takich jak poziom ciśnienia akustycznego i długość rezonansu dźwięku. Obiektywna ocena tak skomplikowanego instrumentu, jakim jest fortepian, jest bardzo kompleksowym zadaniem. Integralną częścią oceny jest zakres psychoakustyczny i konwersja subiektywnego odbioru na obiektywne wartości akustyczne.

Miscellanea

TOTAL RUN-OUT MEASUREMENT OF THE MULTISTART WORM BY THE LASER LINE TRIANGULATION SENSOR

Alexander Prošek

VÚTS, a.s., Measurement Department,
Svárovská 619, Liberec XI - Růžodol I, 460 01 Liberec, Czech Republic
e-mail: alexander.prosek@vuts.cz

Abstract

This article describes a total run-out measurement of a multistart worm which is pressed on a rotor shaft of an electric motor. The measurement is realized by a laser line triangulation sensor during the motor's running. The total run-out evaluation is executed for each spiral of the worm on its addendum circle along the whole length of the worm.

Keywords

Total run-out; Laser line triangulation sensor; Multistart worm.

Introduction

Measuring total run-out by a mechanical gauge is difficult because the addendum cylinder of the worm is not continuous and this approach requires tracing the worm outer surface during its rotation. Moreover, it is not possible to maintain a constant speed of the rotor in our case. On the other hand, the optical measurement by laser triangulation is simple to apply.

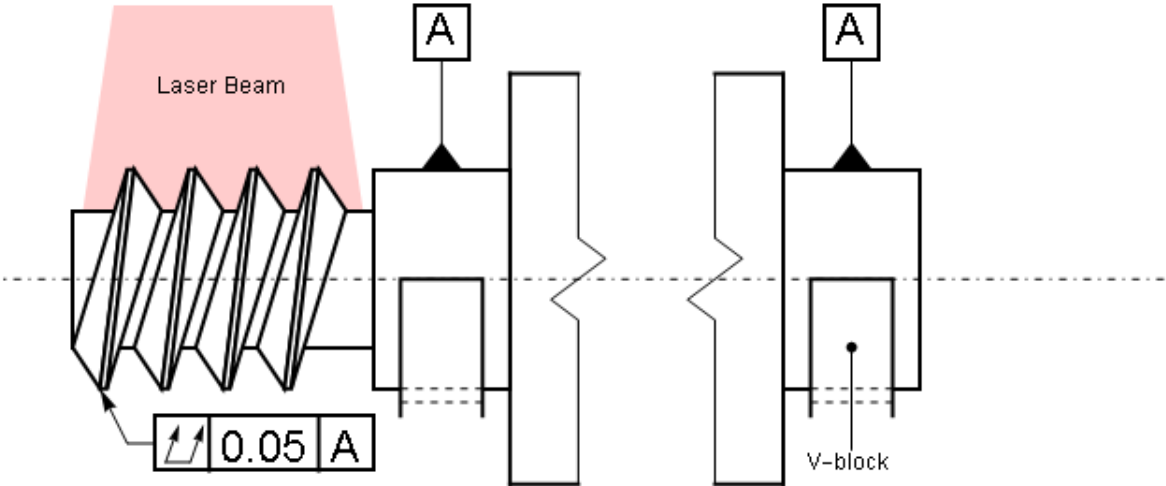
It is supposed that the rotor shaft rotation axis is identical to the motor housing axis. The datum is on the housing mounting region cylindrical surface (Figure 1). If this assumption is violated, then the whole shaft can lie out of the tolerance range related to the datum surface due to axes misalignment but the rotor does not run-out relative to its rotation axis. The rotor position is variable relative to the motor body and the previous condition ensures the axis symmetry with respect to datum axis. This condition is justified for any other measurement method and it is caused by the fact that the rotor is movable relative to the datum.

Another advantage of the optical method is the absence of a contact between the measured part and the gauge, and thus the measured part is protected from damage. On the other hand, this method is sensitive to optical conditions; these issues are discussed later.

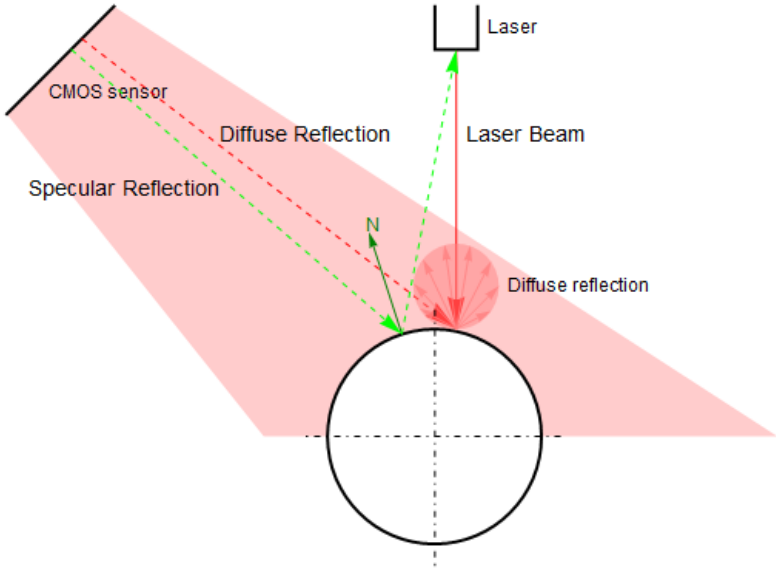
1 Measurement Equipment

The motor is set in a V-block which ensures an accurate motor positioning relative to the sensor. The motor is mounted by prism on the datum surfaces which are defined by the geometrical tolerance. The profilometer is set in the accurately defined position relative to the supposed axis of the reference cylinder surface. The sensor is not set directly against the supposed shaft axis but it is slightly shifted in order to eliminate the specular reflection of the laser light that can reach the profilometer CMOS sensor. A precise calibration specimen with the same geometry on the significant surfaces as the real motor was manufactured. This calibration specimen should be a tool for finding a trend in data which is caused by the inaccurate assembly of the measurement equipment. This trend is used for the data calibration during the measurement. A scheme of the measurement geometrical conditions is shown in Figure 1.

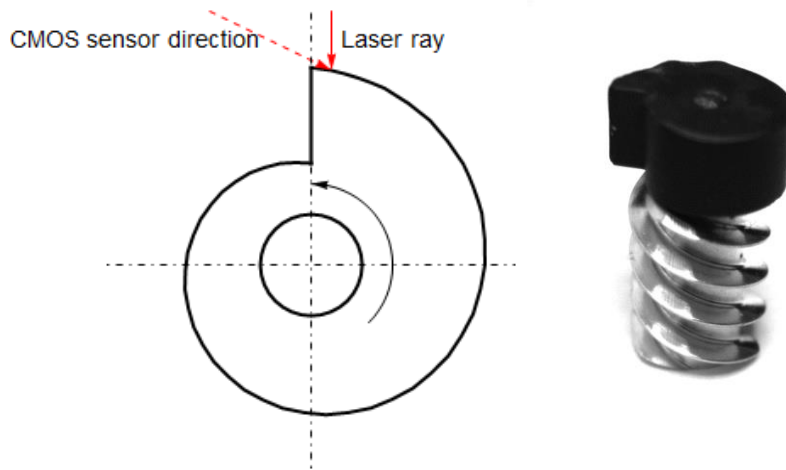
The profilometer measures the distance of the worm profile from its reference surface. One sample of profile data is a vector of the 2D points of coordinates which are related to reference surfaces of the sensor. These coordinates are measured directly in micrometres. The sensor is used in a stream mode, i.e. the profiles are acquired continuously one by one. A profilometer TLE1 with measurement range 35 - 65 mm produced by the Metralight company was selected for the measurement.



Source: Own
Fig. 1: Measurement scheme



Source: Own
Fig. 2: Laser line triangulation sensor principle – The image shows both types of reflections which are visible on the shiny cylinder surface (diffuse reflection and unwanted specular reflection, N is the surface normal).



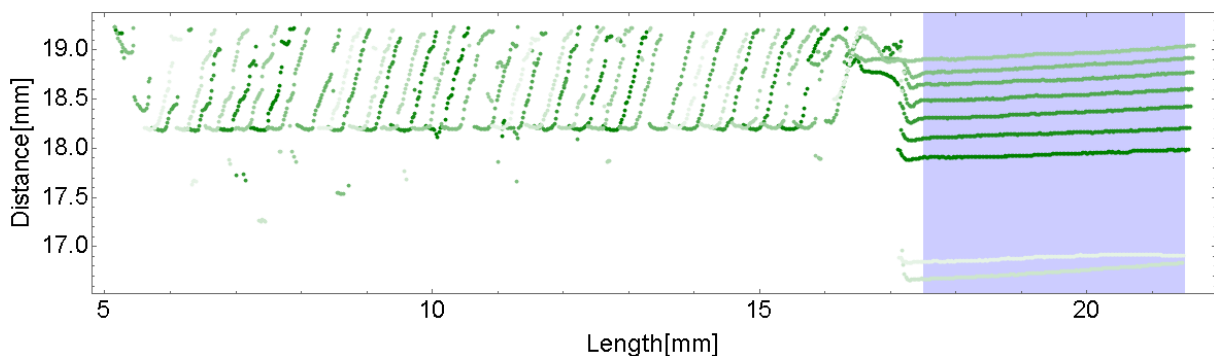
Source: Own

Fig. 3: Spiral part – The part placement on the worm is shown on the right.

2 Measurement

The motor with a worm (pressed on the rotor shaft) is connected to power supply, and rotor revolutions are controlled by voltage level. The voltage is set to a value that ensures as a stable and low speed as possible. It is necessary to detect the rotor shaft rotation angle during the measurement. A special plastic part, which is attached on the shaft end by a magnet, is used for this purpose. This part has a variable radial displacement along the rotation angle so there is a unique value of displacement for each shaft rotation angle (see Figure 3).

Whole angle range (0, 360) degrees are split into disjointed circular sectors with an angle of 5 degrees. The length range along the shaft axis was split into sectors of 0.5 mm width (these parameters are variable). This division creates a 2D bins array of the measurement area. The measurement is executed for several revolutions. The spiral part displacement is detected for each profile. This value is intended for the profiles sorting by the rotation angle into angle bins. When the measurement is finished, each profile set relative to specified circular sector is evaluated by statistical methods. This is discussed later in section 2.2.



Source: Own

Fig. 4: Record of ten successive profiles –attached spiral part is in the light blue region

2.1 Measurement Settings

Maximum frame rate of the used sensor is about 30 frames per second (depending on exposure time, but the readout time of the used CMOS chip is 33.34 ms). The lowest motor revolutions that can be used are about 4 revolutions per second so it is not possible to obtain more than nine frames per revolution with the full frame readout. The selected profilometer TLE1 supports quite a variable region of interest (ROI) settings that allows setting ROI close to the watched edge neighborhood. It is necessary to set short exposure time to achieve the

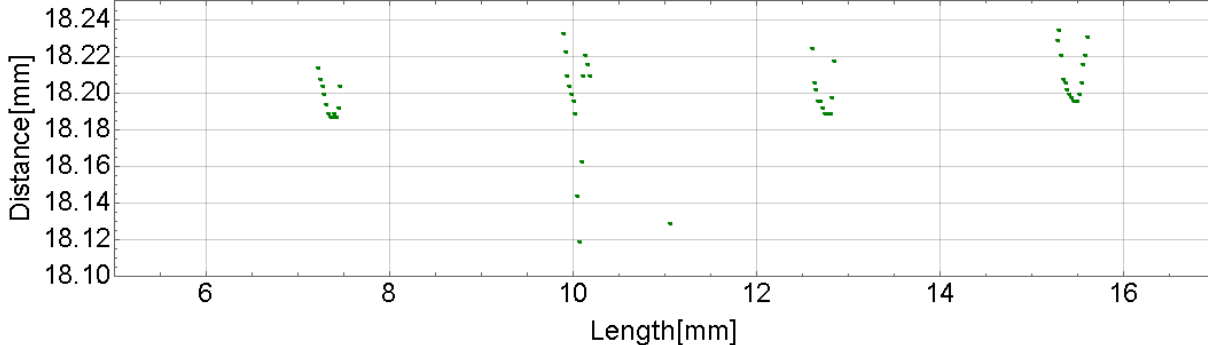
maximum frame rate. Additionally, it is necessary to set high laser power and CMOS sensor gain due to low light diffusion of the shiny metal surface.

It is necessary to repeat the measurement for several revolutions because of the low frame rate per one revolution. However, a case when a ratio of the frame rate and revolutions number is integer can occur. Then, the same places are observed and the other places are skipped during two successive revolutions. Some angle bins remain empty in this case. This problem is solved by checking points count in the bins array. This can be simply solved by changing the sensor frame rate which can be achieved by enlarging ROI over more CMOS sensor rows. This causes the CMOS sensor readout time increase.

The first step of the measurement is the spiral part mapping. The sensor ROI is set to the possible smallest region that covers the decreasing surface of this part. This allows us to scan the surface with approximately a two degrees' step. This map is used to detect the shaft rotation angle. Linear interpolation over this map is used for the shaft angle detection during the measurement.

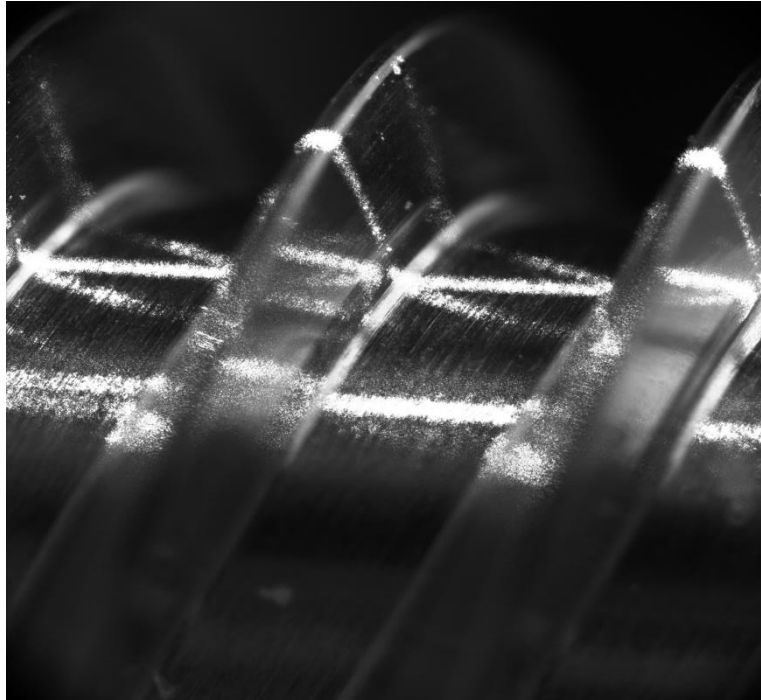
There are several other issues with optical properties of the observed surface which influence setting of the measurement. As mentioned above, the sensor is not placed against the shaft axis directly but it is slightly shifted behind the axis (shown in Figure 2). The measurement principle of the laser line triangulation sensor is based on capturing an image of the laser light diffused on the target surface. The worm is made of a ground metal and the biggest part of the laser light is specular reflected. The first problem is to avoid the laser light reflection into the CMOS sensor. This is partially solved by the sensor shift out of the shaft axis plane. However, two reflection lines on the shaft surface still exist (see Figure 2). The first is diffused light on the surface and the second is specular reflection. Specular reflection in the sensor direction is caused by the fact that there is always a point on the shaft cylindrical surface where the laser light is reflected into sensor according the Snell's law. It is necessary to choose a geometrical arrangement of the measurement equipment so that these two phenomena remain separated.

The evaluation is also complicated by secondary specular reflections between the thread faces (see Figure 6). Although these reflections are not visible on the addendum cylindrical surface of the profilometer, which evaluates light intensity over the each CMOS sensor row separately, the secondary reflection on the face can be chosen instead of the diffuse reflection on the addendum. This sensor behavior cannot be simply eliminated so it is necessary to carefully select those parts of the profile which really represent the thread addendum during the data processing.



Source: Own

Fig. 5: Worm profile detail – several outlying points caused by dirt on thread surface visible on second thread from left



Source: Own

Fig. 6: Detail of the worm with visible multiple reflections of the laser beam between thread faces. The thickest horizontal line is specular reflection which is drawn in Figure 2 by green arrows (image was acquired by camera with macro lens – it is not an image acquired by used profilometer).

Moreover, the measurement data can be influenced by the CMOS rolling shutter effect. This effect is more significant for higher rotation speed. The CMOS chip rows are exposed with a short time delay. The rotor is slightly turned about its axis during this delay so the profile scan does not correspond with the unique angle. The profile continuously crosses the short angle range which is determined by the time delay between the first and the last exposed row. It was possible to reach a sufficiently low speed in our case so this effect can be ignored. Generally, this effect can be totally eliminated by using a chip with a global shutter.

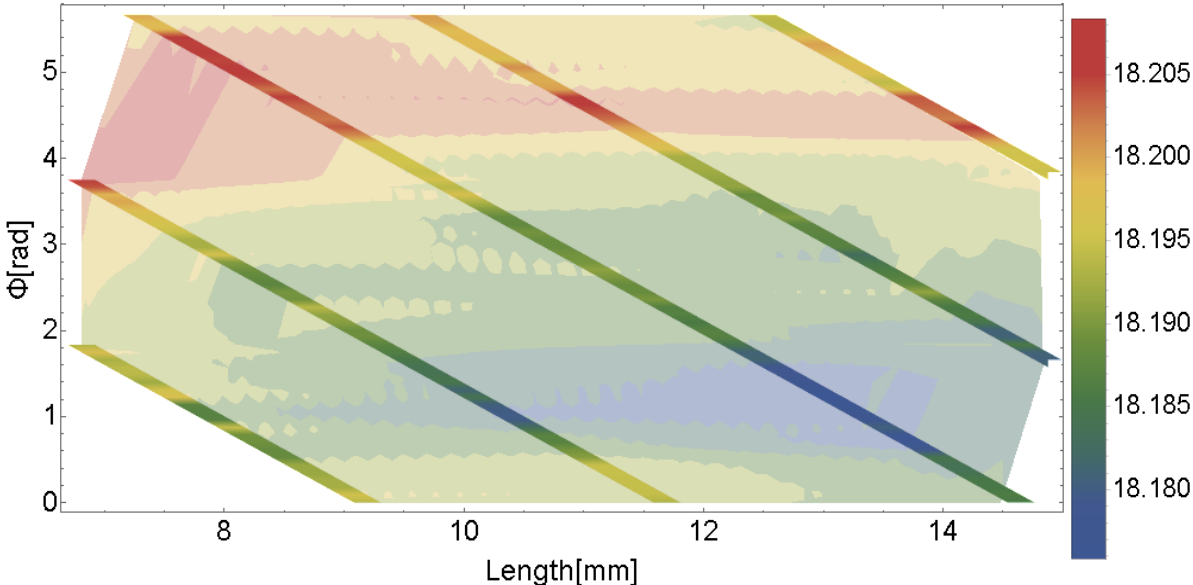
2.2 Evaluation

A rotation angle is determined for each obtained profile. Points on the addendum circle are found then. Each upper thread edge is replaced by one delegate point. These points are sorted into a 2D bin array according to its angle and x -coordinate.

Precise data processing is necessary due to high sensitivity of the measurement method on the optical conditions which were described in the previous section. Under specific conditions, which cannot be surely eliminated, problematic places (e.g. scratches, grease or other dirt) are scanned periodically. These faulty values undesirably influence the used statistics. Hence, if the data condition for the expected shape or continuity were violated, then the point was rather dropped.

Values from each bin are replaced by median and these values are considered as a distance map result. This result is shown in Figure 7. Diagonal strips represent the real measured data and the transparent part of the plot is only an interpolation for better visualization. In Figure 8, the same result is mapped on a 3D cylindrical surface.

The total run-out is approximately equal to a difference between the global maximum and minimum on this distance map. A real total run-out is slightly different due to geometrical conditions of the measurement since the profile is observed from behind the worm axis (Figure 2).



Source: Own

Fig. 7: Distance map – Strips represent the real measured points, an area between the strips is interpolated for better visualization of the distance layout over the outer cylinder.



Source: Own

Fig. 8: Distance map mapped on the outer cylinder of the worm

Conclusion

The total run-out measurement based on laser triangulation is simply applicable. The measurement is executed during the motor operation and there is no need for any other measurement equipment than the laser profilometer. In our case, it was not possible to run a motor with a low enough speed that allowed us to capture enough profiles for just one revolution. Hence, a special spiral part was used to observe the shaft rotation angle and the results were evaluated for several successive revolutions.

Although the measurement by the laser profilometer can be simply realized, there are some issues based on the optical conditions. These problems were solved by precise setting of the profilometer and careful data processing. The used method provides stable and repeatable results.

Part of the data processing is executed by the sensor itself. This approach can be restrictive because the image information obtained by the CMOS sensor is lost. An alternative approach that can provide a more flexible evaluation is processing the whole image data. For example, specular reflection can be detected from the knowledge of geometry and erased from the image. But the selected sensor does not provide sufficient data transfer for the image data streaming.

Alternatively, the measurement can be executed without the spiral part because the worm thread can also be used for the rotation detection. But the spiral part is more convenient because the worm can contain more helices and it is necessary to distinguish them for the correct angle detection.

Literature

- [1] *TLE1 Sensor*. Technical specification (rev. G), sensor firmware: 111 3v2 [online], available from: http://www.metrалight.com/products/doc/tle1/tle1_ug_g.pdf
- [2] CHEN, F; BROWN, G. M.; SONG, M.: Overview of 3-D shape measurement using optical methods. *Optical Engineering*. 2000, Vol. 39, Issue 1. DOI: [10.1117/1.602438](https://doi.org/10.1117/1.602438)
- [3] VÁRADY, T.; MARTIN, R. R.; COX, J.: Reverse engineering of geometric models – an introduction. *Computer-Aided Design*. 1997, Vol. 29, Issue 4, pp. 255–268. DOI: [10.1016/S0010-4485\(96\)00054-1](https://doi.org/10.1016/S0010-4485(96)00054-1)
- [4] MIKULSKI, S.: Laser triangulation in three-dimensional scanners. *Computer Application in Electrical Engineering*. 2013, Vol. 11, pp. 485–491. All volumes are available from WWW: <http://www.iee.put.poznan.pl/wydawnictwa>

MĚŘENÍ CELKOVÉHO HÁZENÍ VÍCECHODÉHO ŠNEKOVÉHO PASTORKU POMOCÍ LASEROVÉHO TRIANGULAČNÍHO SNÍMAČE

Tento článek popisuje měření vícechodého šnekového pastorku nalisovaného na hřídeli rotoru elektrického motoru. Měření realizováno pomocí laserového triangulačního snímače za běhu motoru. Vyhodnocení celkového házení je provedeno pro každý závit šneku na jeho vnější kružnici po celé délce šneku.

MESSUNG DER GESAMTEN LAUFABWEICHUNG DES MEHRGÄNGIGEN SCHNECKENRITZELS MIT HILFE EINES LASERTRIANGULATIONSSENSORS

Dieser Artikel beschreibt die Messung des mehrgängigen Schneckenritzels, welche auf die Rotorwelle eines Elektromotors gepresst ist. Die Messung wurde mit Hilfe eines Lasertriangulationssensors durchgeführt, während der Motor lief. Die Auswertung der Laufabweichung wird für jede Windung der Schnecke auf ihrer äußeren Kreisbahn über die gesamte Länge der Schnecke durchgeführt.

POMIAR OGÓLNYCH DRGAŃ ŚLIMAKOWEGO KOŁA ZĘBATEGO PRZY POMOCY LASEROWEGO CZUJNIKA TRIANGULACYJNEGO

W niniejszym artykule opisano pomiar ślimakowego koła zębatego umieszczonego na wale wirnika silnika elektrycznego. Pomiaru dokonywano przy pomocy laserowego czujnika triangulacyjnego w czasie pracy silnika. Ogólne drgania badano dla każdego gwintu ślimaka na jego zewnętrznym kole na całej długości ślimaka.

DIVERGRASS – A CROSS BORDER PROJECT TO PROMOTE SUSTAINABLE MANAGEMENT OF GRASSLANDS

Jan Titěra¹; Henning Haase²; Teowdroes Kassahun Teka³; Chukwudi Nwaogu⁴;
Klára Pavlu⁵; Matthias Kändler⁶; Lenka Pavlu⁷; Jan Gaisler⁸; František Paška⁹;
Heike Heidenreich¹⁰; Gerlinde Liepelt¹¹; Irena Jonášová¹²; Vilem Pavlu¹³

^{1, 3, 4, 5, 7} Česká zemědělská univerzita v Praze, Faculty of Environmental Sciences,
Department of Ecology, Laboratory of Agroecosystems Study
Rolnická 85/6, 46011 Liberec, Czech Republic

^{2, 6, 10, 11} Technische Universität Dresden, International Institute Zittau,
Chair of Biotechnology,
Markt 23, 02763 Zittau, Germany

^{1, 8, 9, 12, 13} Výzkumný ústav rostlinné výroby, v.v.i.,
Department of Weeds and Vegetation of Agroecosystems,
Grassland Research Station Liberec,
Rolnická 85/6, 46011 Liberec, Czech Republic

e-mail: ¹titeraj@fzp.czu.cz; ²henning.haase@tu-dresden.de; ³teka@fzp.czu.cz;
⁴cnwaogu@gmail.cz; ⁵kpavlu@fzp.czu.cz; ⁶matthias.kaendler@tu-dresden.de;

⁷pavlu@fzp.czu.cz; ⁸gaisler@vurv.cz; ⁹paska@vurv.cz; ¹⁰heike.heidenreich@tu-dresden.de;
¹¹gerlinde.liepelt@tu-dresden.de; ¹²jonasova@vurv.cz; ¹³pavlu@vurv.cz

Abstract

Most temperate European meadows and pastures belong to semi-natural and temporarily sown intensive grasslands. Semi-natural, mostly rich grasslands species have been maintained by agriculture activities for centuries. However, intensive grasslands are a more modern but widespread phenomenon nowadays. Livestock grazing is the key management for pastures and regular cutting for meadows. A combination of grazing and cutting is typical for grazed meadows. The absence of grassland defoliation, extensification and too intensive management can lead to a decline in plant species diversity resulting in disappearance of endangered plant species. Decreasing of grassland diversity in natural habitats is one of key problems in present nature protection on both sides of Czech (CZ) / German (D) border. In the transboundary region comprising the Jizerské hory Mts (CZ), the Lužické hory Mts (CZ) and the Zittauer Gebirge Mts and foreland (D), twelve manipulative management experiments were established in DiverGrass project on different types of grasslands in order to find optimal measures for stopping declining or increasing of plant species diversity in grasslands habitats.

Keywords

Grassland; Management; Grazing; Cutting; Biodiversity; Nature protection.

Introduction

A high decline in biodiversity has been reported in different habitats by many international and national studies, e.g. [1, 2, 3]. The recent monitoring report on the Natura 2000 habitats in Saxony showed a clear negative trend for grassland biotopes [4]. A large decrease in rare and protected plant species on valuable grassland habitats and a broad loss of conservation quality has been observed by the nature conservation authorities of the Liberec Region and Görlitz District.

General species depletion was found in grassland habitats, although these areas were cultivated as prescribed and with conservation funding. To identify possible reasons for the decline and to reverse the trend by developing and promoting measures for a sustainable management of the valuable habitats, the project 'DiverGrass' was established.

1 Theoretical Background

1.1 Importance of Temperate Central European Grassland

In temperate regions of Europe, grasslands are major components of the landscapes because for centuries they have been playing a vital role in the economic activity including animal production. Grassland is one of the biomes that have a well-developed equilibrium mechanism and stability even in absence of additional input of energy [5, 6]. Although there are large variations in soil condition, climate and history, grasslands across Europe can be distinguished as permanent and temporary grasslands, with the latter consisting of some proportion of forage legumes. Most of the grasslands found in Central European conditions do not represent climax communities as they were largely created after large-scale deforestation and maintained by agricultural activities. In general, grazing and mowing have been the most widely used management strategy for centuries, in some areas possibly as far back as in Neolithic or Bronze ages. These grasslands possess not only natural values, but have also huge cultural historical value, as they have been under the influence of humans for several generations [7, 8].

A review by Hejcman et al. [9] divides grasslands in Central Europe into three broad categories based on their origin: i) *Natural grasslands* are differentiated by the climatic conditions such as limitation of soil moisture, which is common for a steppe region on the eastern border of Central Europe and low temperature with shorter growing season for higher mountains above the upper tree limit; ii) *Semi-natural grasslands* were mostly linked to human interaction starting from the beginning of agricultural practices during the Mesolithic-Neolithic transition; iii) *Intensive grasslands* are the result of intensive agriculture, which includes sowing of highly productive forage grasses and legumes. Semi-natural and intensive grasslands can be further divided based on the management system they belong to, including pastures, meadows, and grazed meadows. They have a wide range of species richness of vascular plants ranging from 1 to 67 species and herbage production from 1 to 10-ton dry matter per hectare. Livestock grazing is the key management for pastures, regular cutting for meadows and cutting in summer and grazing in spring/autumn for grazed meadows.

The countries in Central Europe are comparatively high yield zones, with annual production between 4 to 6 t ha⁻¹. Overall, the variation in productivity between years could be significantly different and this could be related to variability in climate [10].

The existence of temperate grasslands could be attributed to moderate disturbances such as grazing, mowing or fire incidences. Most of them are sub-climax communities; hence they require periodic defoliation to avoid succession that could lead to being converted into shrubs and woodlands [11]. During the last millennia, temperate European grasslands have been largely managed by grazing of domestic animals or by hay making activities. This is one of the main reasons why this ecosystem is mostly described as semi-natural. It just implies the importance of grazing by wild or domestic animals. In general, they are dependent on a form of disturbance that inhibits dominance of woody plant species [12].

The decline in grassland diversity and overall biological diversity has been ongoing for the last hundred years [3, 6]. Among several reasons, changes of agricultural management such as intensive milk husbandry in cowsheds are top on the list leaving only a few portions of

grassland to be used extensively and the vast amount of former semi-natural grassland to be abandoned [6]. Recently, the situation is much more serious in less accessible areas such as mountainous areas that have low productivity, where semi-natural grassland is common. However, the lowland meadows were nearly completely destroyed as they were ploughed in the last fifty years [3, 6]. ‘Extensification’ in terms of avoiding or minimizing the intensive application of fertilizers as well as a change in the frequency and timing of defoliation can be beneficial. But in reality, it can be challenging as it can bring various risks due to the temporary or total abandonment of the grasslands. The absence of grassland defoliation leads to a decline in plant species diversity [13], and abundance of tall species as more litter on the ground promotes the nutrient availability and restricting seedling emergence [14]. As more intensification of livestock production with larger and more specialized farm units continue to develop, the more the role of grasslands in livestock production diminishes [15]. This trend will probably continue as an intensification of cattle production with highly digestible forages from arable lands and concentrates is applied [16, 17].

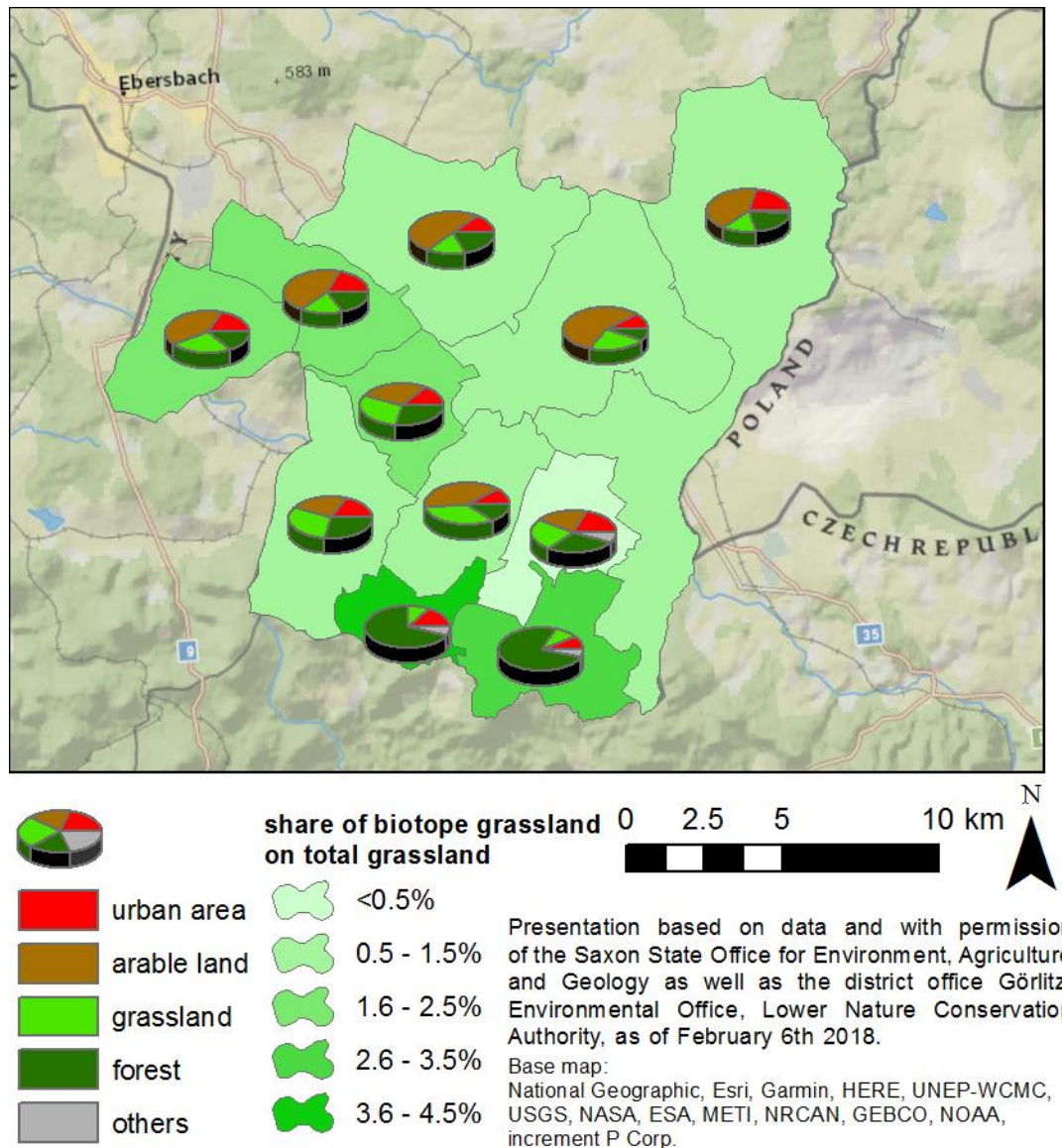
1.2 Characteristics of the Project Area with Focus on Grasslands

1.2.1 The Zittauer Gebirge Mts and Foreland

The German part of the project area is confined by the extent of the former administrative district of Zittau with approximate landmass of 252 km². It contains the municipalities of Oybin, Jonsdorf, Großschönau, Zittau, Olbersdorf, Bertsdorf-Hörnitz, Mittelherwigsdorf, Hainewalde, Leutersdorf, Oderwitz and Seifhennersdorf. Physiogeographically it is divided into the two natural regions “Zittauer Gebirge” (Zittauer Gebirge Mountains) and the southern part of the “Östliche Oberlausitz” (Eastern Upper Lusatia) [18]. Geographically, it is bordered in the west and south by the Czech Republic and in the east by Poland. Nearly two-thirds of the land use in the project area is agriculture (Fig. 1) [19]. The overall proportion of grassland is about 21%. Only a tiny fraction of the grassland (1.4%) is protected grassland in the sense of §21 Saxony Law on Nature protection (SächsNatSchG) [20] and could therefore be addressed as semi-natural grassland according to [9], and this is only 0.3% of the total area.

The Zittauer Gebirge Mts as German part of the Lusatian Mountains (see also 1.2.3) are characterized by cretaceous deposited sandstone sediments with various features (such as hardness). Erosion and tectonic movements because of the Lusatian disturbance led to the recent landscape structure with diverse rock formations and deep valleys. The bedrock of the mountains is granodiorite. As a special feature, volcanic activity formed several numbers of hills made by basalt and phonolite. The most famous one is the Lausche (Luž, 793 m a.s.l.), which is the highest mountain east of the river Elbe (Labe) in Germany. Although most soils are acidic and nutrient-poor due to geology, there has been higher percentage of base saturation near the basalt and phonolite hills [18]. The mean annual amount of precipitations is 828 mm (Jonsdorf) [21]. The Zittauer Gebirge Mts are protected as landscape conservation area “Zittauer Gebirge” and are part of the nature park “Naturpark Zittauer Gebirge”. Furthermore, the region includes two nature reserves “Lausche” and “Jonsdorfer Felsenstadt” and several natural monuments. It is partly protected as Natura 2000 habitat site (SCI) “Hochlagen des Zittauer Gebirges” [uplands of the Zittauer Gebirge Mts] and Natura 2000 bird protection site (SPA) “Zittauer Gebirge” [22]. The area is mostly covered by forest, whereby afforestation with spruce is dominant. Approximately, only 10% of the Zittauer Gebirge Mts is grassland [20]. Extensively used fresh lowland meadows with sub-montane characteristics such *Bistorta officinalis* and *Trisetum flavescens* are common. Most of them were former arable land [23] and are now predominantly classified as *Festuca rubra*-*Agrostis capillaris* meadows with high dominance of different grasses. There are some very small patches with *Nardus* grassland and wet meadows apparent with *Dactylorhiza majalis* or

Listera ovata. Rare species are *Arnica montana* and the two previously mentioned orchids. Remarkably, *Arnica* was lost in many habitats during the last decades [24] as a result; only one site is recently known for this plant. The Zittauer Gebirge Mts have suffered extinction of many communities of typical grassland species such as *Cirsium canum*, *C. rivulare*, *Coeloglossum viride*, *Dactylorhiza incarnata*, *D. sambucina*, *Dianthus superbus*, *Epipactis palustris*, *Eriophorum latifolium*, *Gymnadenia conopsea*, *Orchis mascula*, *O. morio*, *O. ustulata*, *Platanthera bifolia*, and *Traunsteinera globosa* [24].



Source: [19, 20], base map: ESRI

Fig. 1: Distribution of land use and proportion of biotope grassland on total grassland in the German part (at municipality level) of the project area (source [19, 20], base map: ESRI)

The Eastern Upper Lusatia as part of the Saxon Loess-area is a very heterogeneous landscape. It shares land borders with Poland in the east, the Zittauer Gebirge Mts in the south, the Upper Lusatian Heath and Pond Landscape in the north and the Upper Lusatian Mountain Landscape in the west. Southwards, there is found the project area comprising of basins which are often covered with a loess-loam layer relatively enriched by fertile soils [18], thus promoting intensively high agricultural practices (Fig. 1) [19]. Other peculiar physical features are the intermingled basalt and phonolith hills, which structure the landscape in a distinct way as well

as various rivers such as Mandau and Landwasser, which are tributaries of the Neiße (Nisa) [18]. The mean annual temperature is 7.9°C and the mean annual amount of precipitation is 630 mm (Olbersdorf) [21]. There are two landscape protection areas in this part of the project site. The region has four Natura 2000 habitat sites: “Mandautal” [valley of the river Mandau], “Eichgrabener Feuchtgebiet” [wetlands around the village of Eichgraben], “Separate Fledermausquartiere und -habitate in der Lausitz” (separate quarters and habitats of bats in Lusatia) and parts of “Basalt- und Phonolithkuppen der östlichen Oberlausitz” (basalt and phonolite hills in Eastern Upper Lusatia) [22]. The present grasslands are often intensively used for anthropogenic activities and species-poor *Lolium*-meadows dominate. Remnants of wet and dry meadows are found along small rivers and on the basalt hills respectively. On the wet sites there are found rare and typical plant species such as *Dactylorhiza majalis*, *D. fuchsii*, *Sanguisorba officinalis*, *Laserpitium prutenicum* and *Succisa pratensis*, though many of their communities became extinct during the last decades [24]. The semi-arid grasslands are characterized by *Carex caryophylla*, *Potentilla neumanniana*, *Rhinanthus minor*, *Carlina acaulis*, and *Orchis mascula*.

1.2.2 The Jizerské Hory Mts

The Jizerské hory Mts, according to the geomorphological division of the Czech Republic, belong to the province Česká vysočina, Krkonošsko-jesenický system, and Krkonošský sub-system [25]. The relief of the territory was formed by tertiary tectonics and intensive weathering processes. The central part of the Jizerské hory Mts is flat with moderately high ridges and isolated hills. Flat surfaces with shallow drops, peat bogs and the edges of the mountains are cut by deep valleys of watercourses [26]. The central part of the Jizerské hory Mts is bed-rocked by granite. Based on lithology, cambisol is the dominant soil type, though cryptopodzoles, podzoles as well as peat bogs could be found in higher parts of the mountains [27]. In terms of climate, Jizera Mountains are slightly colder and richer with high precipitation. They have the mean annual temperature of 4.6°C and 10.3°C during the vegetation growing season. The mean annual amount of precipitations varies between 800 mm in the uplands and 1700 mm at the altitudes of 900 m [28].

The Protected Landscape Area (PLA) Jizerské hory Mts was established in 1968 with an area of 368 km² [29]. Forest landscape predominantly forms this area. The most widespread forest biotopes are acidophilous beech forests, montane *Calamagrostis* spruce forests, bog and waterlogged spruce forests [30]. The peat bogs communities are the most valuable ones. Mesic *Arrhenatherum* meadows and montane *Trisetum* meadows are the most common grassland communities. However, there are also patches of sub-montane and montane *Nardus* grasslands, *Cynosurus* pastures, wet *Cirsium* meadows and wet *Filipendula* grasslands. At present, there are 3 national nature reserves in the Jizerské hory Mts [30]. Several rare plant species grow on non-forest biotopes in the territory of the PLA, and these include *Gentianella campestris subsp. baltica*, *Botrychium matricariifolium*, *Erica tetralix*, *Scheuchzeria palustris*, *Andromeda polifolia*, *Lycopodiella inundata*, as well as *Trollius altissimus* and *Swertia perennis* [31].

1.2.3 The Lužické Hory Mts

The Lužické hory Mts are located in northwest part of the Krkonošsko-jesenický system. The Lužické hory Mts were formed by tertiary volcanic activity. Another process, which formed the landscape, was due to a continental glacier. The glacier caused deposits of gravels, sands and created rubble areas. The oldest rocks of the Lužické hory Mts are granites. Majority of the territory is formed by chalk sandstones, which are tectonically bounded against granites.

The mean annual temperature is around 7°C and the mean annual amount of precipitation is about 800 mm [32].

PLA Lužické hory Mts was established in 1976 with the area of 265 km² [33]. This area is determined to protect the diverse landscape of sandstone rock towns and single, trachyte and basalt cones [34]. Natural forest remnants accompanying these remarkable geomorphological formations stand in the top parts (herb-rich beech forests and ravine forests), wet mountain and sub-mountain meadows with the occurrence of rare plant species. A large part of the area includes predominantly man-made habitats. Similar to the Jizerské hory Mts, the most spread communities include mesic *Arrhenatherum* meadows, sub-montane and montane *Nardus* grasslands, *Cynosurus* pastures, wet *Cirsium* meadows and wet *Filipendula* grasslands. A few rare plant species are growing on grasslands in the PLA Lužické hory Mts, and they include *Epipactis palustris*, *Gymnadenia conopsea*, *Drosera rotundifolia*, *Carex davalliana*, *Potamogeton alpinus*, and *Pedicularis sylvatica*.

1.3 History of Grassland Management in the Project Area

Up to late Middle Age, when scythe was invented, the main grassland management had been grazing applied from early spring to late autumn. The main critical period was winter when animals were grazing in the forest, grazing woody part of shrubs and trees (shoots, bark). Additionally, the branches with dry leaves after coppicing were a source of winter forage. Consequently, since the 16th century the creation of meadows has been associated with the use of scythes as tools for grassland cutting as it was more efficient for biomass collection than branches with leaves. This was especially practiced in wet meadows, as it was more efficient to get additional dry matter biomass. Consequently, cutting of grasslands as a source of winter forage and creating meadows started from the 17th century. In the 18th century a significant expansion of meadows occurred, leading to a serious deforestation in the landscape [6, 35, 36, 37, 38].

Wide spread hay making was associated with enlargement of arable fields connected with improved three field crops system introduction. It was forced by three factors: i) increased demand for forage as cattle was used as draught animal for ploughing; ii) demand for manure as a fertilizer; iii) a suitable tool for mowing - scythe. Till the 19th century cattle were kept in the barn during winter and grazing was applied during the whole vegetation season. In the 19th century alternating crop management was introduced; hence instead of applying fallow grasslands were sown and used to grow fodder. This resulted in: i) closing cattle in the barn because of an increased demand for manure for field-fodder; ii) less grazing activities supported dominance of tall oat-grass (*Arrhenatherum elatius*); iii) municipal meadows were incorporated in crop rotations and areas of grasslands were reduced. This continued till the middle of the 20th century and predominant land use was arable land [6, 35, 36, 37, 38]. For example, between 1845 and 1948, the percentage of grassland on agricultural land in the Jizerské hory Mts and the Lužické hory Mts was less than 30% and 40% respectively; currently they have increased drastically to about 73% and 69% respectively [39]. On the contrary, the total area of arable land shows a decreasing trend from 18% and 24% in 1845 to the current 4% and 9% for the Jizerské hory Mts and the Lužické hory Mts respectively. Similar could be said for German regions as visibly seen on historical maps [23]. Most of the grasslands were ploughed in the '70s and '80s and the productive clover-grass mixtures were reseeded. Intensification of agriculture led to the application of industrial fertilizers on grasslands and consequently several wet meadows were drained [36, 40]. The intensification process introduced weeds and invasive plants which are presently threats to grasslands. In the 1990s, most of these intensively managed meadows were either less intensively managed or abandoned due to a reduction in cattle heads and consequently a reduced demand for forage

from these areas [17]. A lot of abandoned arable lands in the uplands were converted to unmanaged grasslands. Later, a considerable part of these unmanaged grasslands was managed because of the State subsidies. However, grassland management in the Czech Republic often consisted of mulching or late mowing where the harvested and packaged biomass remained at the margins of the plots to be deposited and hidden under the trees. This type of management caused a rapid decline in biodiversity in the countryside, thus valuable semi-natural meadows and pastures have become rare.

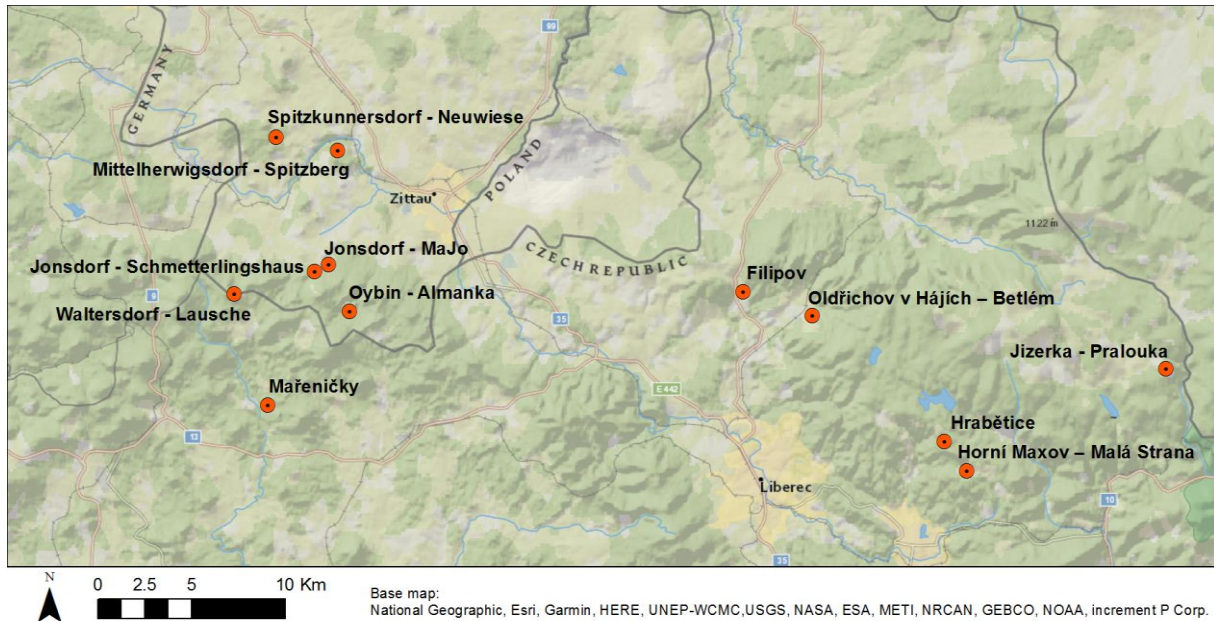
1.4 Grasslands Status and Main Challenges in Relation to Nature Conservation in the Project Area

On the German side of the project area the most valuable grasslands are recently managed by mini-professional nature conservation institutes with funding by the European Union within the guideline “Agrarumwelt- und Klimamaßnahmen (AUK 2015)” overseen by the Saxon State Ministry of the Environment and Agriculture [41]. Even though there were several detailed management plans for most of the top valuable sites [42, 43, 44, 45], the semi-natural grasslands are often cut only once per year in late summer without any additional management, which is sufficient to fulfill the requirements of the guideline and to receive the funding. Although the species diversity could be preserved in mid-term, this more or less rigid regime leads to a convincing support of fallow indicators like dominance of various grasses or an increase of litter layer [44, 46]. On wet sites, tall species like *Filipendula ulmaria* and *Lysimachia vulgaris* form dense dominant communities. Both effects lead to thick vegetation landscape and fewer possibilities for low competitive species to establish. According to [47], a one-cut regime is only useful for meadows with a biomass production of less than $35 \text{ dt} \cdot \text{ha}^{-2}$ if the aim of conservation is to promote herbaceous species. Against the background of eutrophication by air, it is problematic that nitrogen is not removed effectively by cutting late in the year, as most of the plants would have already absorbed their nutrient-resources [48]. There is often no usage of the harvested material since the agricultural demand is not feasible. On valuable grassland, which is often characterized by ecological extremes such as high soil moisture or steep slopes, performing early grazing is prohibited. Aftermath grazing is just allowed with permission from the relevant authority, but without any funding [41].

On the Czech side, nature conservation in the Jizerské hory Mts and the Lužické hory Mts is currently done according to the valid care plans for these areas [30, 33]. Four zones of graduated nature conservation are defined in PLAs and different management is applied on their basis [33, 49]. It is encompassed with a network of biocentres of Territorial System of Landscape Ecological Stability connected by the bio-corridors. Maintenance mandate of PLAs is focused on the protection of their preserved natural, cultural and historical features and on the restoration of the natural functions of the landscape according to the principles of sustainable development. For the non-forest biotopes preservation, nature conservation tasks include: monitoring of sites with rare and endangered plant species and the implementation of measures to support them. It is necessary to provide appropriate care for meadow stands to preserve their maximum diversity and richness of nature communities [30]. However, it is difficult to find using for forage from species rich low-productive areas in the uplands and mountains – these areas become suitable only for afforestation or for speculation and attempts to convert them into building parcels [50]. In the protection of individual rare plant and animal species, active targeted management must be taken, selected with respect to the optimum conditions of the specific species. The care expended on the small-scale protected areas, notwithstanding, the total biodiversity of plant species is declining, and some target species either become extinct or their abundance decreases on these areas. To ameliorate this process and to increase the biodiversity of grasslands, the most suitable management methods and the best principles of conservation and restoration are needed for these habitats.

2 Design of Experiments, Site Characteristics, and Ecological Objectives

Within the DiverGrass project, twelve experimental sites were studied. An overview of these sites is given by Fig. 2. Eight of these sites were established in 2017, in contrast the oldest site has been studied since 1998. The sites have a different history according to the land use. Nevertheless, they can serve as a model for a sustainable grassland management, which will enhance species diversity. On the sites the composition of the vegetation (summer) and the amount of above biomass (before cutting/grazing) will be recorded as well as soil samples (autumn) will be taken each year. Later it is intended to transform the sites into a long term monitoring program.



Source: Own data, base map: ESRI

Fig. 2: Location of the experimental sites of the DiverGrass project

2.1 Horní Maxov – Malá Strana

The experiment was established in nature reserve Malá Strana in 2005 in a wet meadow, which belonged to *Calthion* alliance [51], and was degraded by the expansion of *Typha latifolia*. The experimental treatments are no cutting, one cut per year with the removal of cut biomass in June, one cut per year with the cut biomass-litter in June, two cuts per year with the removal of cut biomass in June and August, two cuts per year with the cut biomass-litter in June and August. The study is aimed at controlling of *Typha latifolia* and changes in plant species composition under different cutting regimes.

2.2 Hrabětice

The experiment was established in 2017 in a mesophytic mountain meadow with *Festuca rubra*, *Agrostis capillaris*, *Bistorta major*, *Cirsium heterophyllum*, and *Hypericum maculatum* as dominant species. The meadow was annually cut in July or August with biomass removal. Oligotrophisation was remarkably found with an average number of plant species of about 20 per a 4 m² plot. The experimental treatments are one cut early in June, one cut late in the end of August, twice cutting per year, twice cutting per year with fertilization and unmanaged grassland. The aim of the study is to compare changes in plant species composition, biomass production and functional traits under different cutting regimes and nutrients application.

2.3 Filipov

The long-term mulching experiment (Fig. 3) was established in the year 2000 in the past sown meadow. Ten years before establishment of the experiment the meadow was drained, fertilized with limed and reseeded with a grass/clover of high productive mixture based on the following species: *Dactylis glomerata*, *Festuca pratensis*, *Phleum pratense*, *Trifolium pratense*, and *Trifolium repens*. After that it was cut twice and occasionally grazed by cattle. The plant community of the study area was classified as *Arrhenatherion* alliance [51] and *D. glomerata*, *F. pratensis*, *P. pratense*, *Galium album*, and *Veronica chamaedrys* were the dominant vascular plant species before the start of the study. The total number of vascular plant species was about 30 per plot (24 m²) in all treatments. The following treatments were applied: unmanaged control, two cuts per year with biomass removal in June and August, mulching performed once per year in July, mulching twice per year in June and August and mulching three times per year in May, July and September. This experiment is aimed at evaluating the effect of different mulching and cutting management regimes on plant species composition in a formerly improved upland meadow.



Source: Jan Gaisler

Fig. 3: Overview of the “Filipov” mulching experiment

2.4 Mařeničky

The experiment was established in 2017 in marginal part of natural reserve Rašeliniště Mařeničky in a mesophytic semi-natural meadow with *Festuca rubra*, *Holcus mollis*, and *Agrostis capillaris* as dominant species. The meadow had been unmanaged for a few years and there was visible total predominance of grasses in comparison with sporadic occurrence of dicotyledonous species. The meadow was relatively degraded and the average number of plant species was about 14 per a 4 m² plot at the beginning of the research. The experimental

treatments are one cut early in June, one cut late in the end of August, twice cutting per year, cutting once per two-year with fertilization and unmanaged grassland. The study is aimed at finding suitable management to enhance the increase of plant species biodiversity and support of dicotyledonous species.

2.5 Oldřichov v Hájích – Betlém

The long-term management experiment was established in the year 1998 on mesophytic upland grassland with dominant species such as *Festuca rubra*, *Agrostis capillaris*, and *Alopecurus pratensis*. The meadow was occasionally grazed a few years before the start of the experiment. On this site, the effect of heifers grazing, cutting twice per year, and abandonment on botanical composition, biomass production and structure of sward is studied (Fig. 4). Presently, an average number of plant species is about 23 on the cut, 20 on grazed and only 8 species on unmanaged plots with a size of 9 m² each. The main aim of this experiment focused on the long-term comparison between different grassland managements and their effect on plant species composition, biomass production and soil properties.



Source: Vilém Pavlů

Fig. 4: Intensively grazed pasture in “Oldřichov Grazing Experiment”

2.6 Jizerka – Pralouka

The experiment was established in the year 1999 in a mountain hay meadow in the Bukovec nature reserve in the north-eastern part of the Jizerské hory Mts. According to the phytosociological nomenclature [51], the vegetation of the experimental site belonged to the alliance *Polygono bistortae-Trisetion flavescens*. At the beginning of the experiment, the dominant species were *Festuca rubra*, *Agrostis capillaris*, *Trisetum flavescens*, *Cirsium heterophyllum*, and *Geranium sylvaticum*. In 1999, the mean number of all plant species per a 25 m² plot was about 34. The experimental treatments are one cut per year with the removal of cut biomass in mid-July, no cutting, one cut per two years and one cut per four years

(Fig. 5). The aim of the study is to compare long-term changes in plant species composition and functional traits under different cutting regimes.



Source: Lenka Pavlů

Fig. 5: One cut (on the left) and no management (on the right) treatment in “Pralouka”

2.7 Oybin – Almanka

The experiment was established in 2017 in a mesophytic and relatively oligotrophic upland meadow with *Festuca rubra*, *Agrostis capillaris*, *Hypochaeris radicata*, and *Anemone nemorosa* as dominant species. The meadow is cut twice annually at the end of May and in October. At present, four management treatments were established: two cuts with biomass removal, two cuts with biomass removal and liming, two cuts with biomass removal, and wood ash fertilization, two cuts with biomass removal, and with sheep dung fertilization. The average number of plant species was about 20 per a 4 m² plot. The aim of the study is to discover suitable management to enable the increase of plant species biodiversity.

2.8 Jonsdorf – Majo

The experiment was established in 2017 in a species poor mesophytic and relatively oligotrophic upland meadow with *Festuca rubra* and *Agrostis capillaris* as dominant species. The meadow is cut annually in late summer and there is a minimal amount of available soil phosphorus due to management applied in the past (5 cuts per year). Two treatments were established: present management (one late cut in September/October) and cut with P+K fertilization. The average number of plant species was about 18 per a 4 m² plot. The study is aimed at discovering suitable management for the increase of plant species biodiversity.

2.9 Jonsdorf – Schmetterlingshaus

The experiment was established in 2017 in a relatively wet upland meadow (Fig. 6) with *Carex brizoides* and *Bistorta officinalis* as dominant species. The meadow is annually cut in

late summer. Four treatments were established: present management (one late cut), two cuts (mid-June and mid-August), two cut and hay transfer (donation site Leutersdorfer Folge), two cut and soil disturbance (milling) and hay transfer. The average number of plant species was about 28 per a 4 m² plot. The aim of the study is to discover suitable management for the increase of plant species biodiversity and development of species rich wet meadow.



Source: Henning Haase

Fig. 6: Experiment in meadow “Schmetterlingshaus” after first cutting in June 2017

2.10 Waltersdorf – Lausche

The experiment was established in 2017 in a species-poor mesophytic mountain meadow with *Festuca rubra*, *Holcus mollis*, and *Agrostis capillaris* as dominant species. It has low species diversity with about 12 species per a 4 m² plot. The meadow is cut annually in late summer and there is a minimal amount of available soil phosphorus. Four treatments were established: present management (one cut in August), one cut with hay transfer (donation site: species rich meadow nearby), one cut with hay transfer and disturbance (raking), one cut with hay transfer and top-soil removal (Fig. 7). The aim of the study is to find suitable management for increase of plant species biodiversity.

2.11 Spitzkunnendorf – Neuwiese

The experiment was established in 2017 in a fresh wet forest meadow with high dominance of *Carex brizoides*. In the locality some members of Orchidaceae family exist. This area was cut in the past as a part of a big meadow complex until the 1940s [23]. Probably in the 1950s, the biggest part was afforested and the meadow in recent dimensions was left [52]. After 2010 it was abandoned for a few years. Presently, the meadow is cut annually in late term. Two treatments were established: present management (one late cut) and two cuts in the beginning of June and August. The average number of plant species was about 23 per a 4 m² plot. The aim of the study is to find suitable management for the increase of plant species biodiversity especially of target species like *Dactylorhiza fuchsii* and to reduce the dominance of *Carex brizoides*.



Source: Henning Haase

Fig. 7: Hay transfer at Lausche

2.12 Mittelherwigsdorf – Spitzberg

The experiment was established in 2017 on a basalt hill. Although the meadow has still *Festuca rubra* and *Agrostis capillaris* as dominant species, relatively rich occurrence of the rare species such as *Carlina acaulis*, subsp. *acaulis* are found. This area had been grazed by sheep and goats until the middle of the 20th century when it was converted to an intensive pasture for cattle; and after the change in political leadership it was abandoned for a few years [44]. Now, the meadow is cut yearly in late term. There is a dense (~ 10 cm) layer of rotten material which prevents establishment of low competitive species. Additionally, there are signs of acidification (*Vaccinium myrtillus*) which are not typical for this kind of a meadow. Two treatments were established: present management (one late cut in September) and early cut (in June) followed by sheep grazing (Fig. 8). The average number of plant species was about 26 per a 4 m² plot. The study is aimed at discovering suitable management for promoting some herbaceous target species and to change the current structure of the sward for an enriched sward.



Source: Henning Haase

Fig. 8: Aftermath grazing at Spitzberg

Conclusion

The cross-border area comprising the Jizerské hory Mts (CZ), the Lužické hory Mts (CZ) and the Zittauer Gebirge Mts (D) had similar historical land use and nowadays there are similar problems in nature conservation in relation to grasslands plant species diversity. Despite various subsidies, there is a remarkable decrease of plant species diversity in grasslands habitats. In the view of these, twelve manipulative management experiments were established in DiverGrass project on different types of grasslands to find long term sustainable management supporting plant species diversity.

Acknowledgements

The described project is funded by the program Interreg VA SN-CZ 2014-2020, Nr. 100264999.

Literature

- [1] HEYWOOD, V. H. (ed.) *Global Biodiversity Assessment*. Cambridge University Press, Cambridge, 1995.
- [2] BUTCHART, S. H. M.; WALPOLE, M.; COLLEN, B.; Van STRIEN, A.; SCHARLEMANN, J. P. W.; ALMOND, R. E. A.; BAILLIE, J. E. M.; BOMHARD, B.; BROWN, C.; BRUNO, J.; CARPENTER, K. E.; CARR, G. M.; CHANSON, J.; CHENERY, A. M.; CSIRKE, J.; DAVIDSON, N. C.; DENTENER, F.; FOSTER, M.; GALLI, A.; GALLOWAY, J. N.; GENOVESI, P.; GREGORY, R. D.; HOCKINGS,

- M.; KAPOS, V.; LAMARQUE, J.-F.; LEVERINGTON, F.; LOH, J.; McGEOCH, M. A.; McRAE, L.; MINASYAN, A.; MORCILLO, M. H.; OLDFIELD, T. E. E.; PAULY, D.; QUADER, S.; REVENGA, C.; SAUER, J.; SKOLNIK, B.; SPEAR, D.; STANWELL-SMITH, D.; STUART, S. N.; SYMES, A.; TIERNEY, M.; TYRRELL, T. D.; VIÉ, J.-Ch.; WATSON, R.: Global biodiversity: Indicators of recent declines. *Science*. 2010, Vol. 328, Issue 5982. DOI: [10.1126/science.1187512](https://doi.org/10.1126/science.1187512)
- [3] GOSSNER, M. M.; LEWINSOHN, T. M.; KAHL, T.; GRASSEIN, F.; BOCH, S.; PRATI, D.; BIRKHOFER, K.; RENNER, S. C.; SIKORSKI, J.; WUBET, T.; ARNDT, H.; BAUMGARTNER, V.; BLASER, S.; BLÜTHGEN, N.; BÖRSCHIG, C.; BUSCOT, F.; DIEKÖTTER, T.; RÉ, J. L.; JUNG, K.; KEYEL, A. C.; KLEIN, A.-M.; KLEMMER, S.; KRAUSS, J.; LANGE, M.; MÜLLER, J.; OVERMANN, J.; PAŠALIĆ, E.; PENONE, C.; PEROVIĆ, D. J.; PURSCHKE, O.; SCHALL, P.; SOCHER, S. A.; SONNEMANN, I.; TSCHAPKA, M.; TSCHARNTKE, T.; TÜRKE, M.; VENTER, P. C.; WEINER, C. N.; WERNER, M.; WOLTERS, V.; WURST, S.; WESTPHAL, C.; FISCHER, M.; WEISSER, W. W.; ALLAN, E.: Land-use intensification causes multitrophic homogenization of grassland communities. *Nature*. 2016, Vol. 540, pp. 266–269. DOI: [10.1038/nature20575](https://doi.org/10.1038/nature20575)
- [4] HETTWER, C.; ZÖPHEL U.; WARNKE-GRÜTTNER, R.: Zustand der Arten und Lebensraumtypen zur FFH-Richtlinie in Sachsen 2007–2012. *Naturschutzarbeit in Sachsen*. 2015, Vol. 57, pp. 4–23.
- [5] RYCHNOVSKÁ, M. (ed.): *Structure and functioning of seminatural meadows*. Elsevier Science Publisher, Amsterdam, 1993. ISBN 978-0-444-98669-6. ISSN 0166-2287. DOI: [10.1016/c2009-0-01045-9](https://doi.org/10.1016/c2009-0-01045-9)
- [6] BOSSHARD, A.: *Das Naturwiesland der Schweiz und Mitteleuropas*. Haupt Verlag, Bern, 2016. ISBN 978-3-258-07973-8.
- [7] DIERSCHKE, H.; BRIEMLE, G.: *Kulturgrasland – Wiesen, Weiden und verwandte Staudenfluren*. Ulmer, Stuttgart, 2002. ISBN 3-8001-3816-6.
- [8] JONGEPIEROVÁ, I.; PEŠOUT, P.; JONGEPIER, J. W.; PRACH, K.: *Ecological restoration in the Czech Republic*. Nature Conservation Agency of the Czech Republic, České Budějovice, 2012. ISBN 978-80-87457-32-0.
- [9] HEJCMAN, M.; HEJCMANOVÁ, P.; PAVLŮ, V.; BENEŠ, J.: Origin and history of grasslands in Central Europe – a review. *Grass and Forage Science*. 2013, Vol. 68, Issue 3, pp. 345–363. DOI: [10.1111/gfs.12066](https://doi.org/10.1111/gfs.12066)
- [10] SMIT, H. J.; METZGER, M. J.; EWERT, F.: Spatial distribution of grassland productivity and land use in Europe. *Agricultural Systems*. 2008, Vol. 98, Issue 3, pp. 208–219. DOI: [10.1016/j.agsy.2008.07.004](https://doi.org/10.1016/j.agsy.2008.07.004)
- [11] ROOK, A. J.; DUMONT, B.; ISSELSTEIN, J.; OSORO, K.; WALLISDEVRIES, M. F.; PARENTE, G.; MILLS, J.: Matching type of livestock to desired biodiversity outcomes in pastures: a review. *Biological Conservation*. 2004, Vol. 119, Issue 2, pp. 137–150. DOI: [10.1016/j.biocon.2003.11.010](https://doi.org/10.1016/j.biocon.2003.11.010)
- [12] PÄRTEL, H.; BRUUN, H. H.; SAMMUL, M.: Biodiversity in temperate European grasslands: origin and conservation. In: Lillak, R.; Viiralt, R.; Linke, A.; Geherman, V. (eds.), *Integrating efficient grassland farming and biodiversity*. Estonian Grassland Society, Tartu, 2005, pp. 1–14. ISBN 9985-9611-3-7.

- [13] PAVLŮ, V.; HEJCMAN, M.; PAVLŮ, L.; GAISLER, J.; NEŽERSKOVÁ, P.; GUEROVICH, P.; ANDALUZ, M.: Vegetation changes after cessation of grazing management in the Jizerské Mountains (Czech Republic). *Annales Botanici Fennici*. 2005, Vol. 42, pp: 343–349. ISSN 0003-3847.
- [14] HEJCMAN, M.; KLAUDISOVÁ, M.; HEJCMANOVÁ, P.; PAVLŮ, V.; JONES, M.: Expansion of *Calamagrostis villosa* in sub-alpine *Nardus stricta* grassland: Cessation of cutting management or high nitrogen deposition? *Agriculture, Ecosystems & Environment*. 2009, Vol. 129, Issues 1–3, pp. 91–96. DOI: [10.1016/j.agee.2008.07.007](https://doi.org/10.1016/j.agee.2008.07.007)
- [15] KRISTENSEN, T.; SØEGAARD, K.; KRISTENSEN, I. S.: Management of grasslands in intensive dairy livestock farming. *Livestock Production Science*. 2005, Vol. 96, Issue 1, pp. 61–73. DOI: [10.1016/j.livprodsci.2005.05.024](https://doi.org/10.1016/j.livprodsci.2005.05.024)
- [16] ISSELSTEIN, J.; JEANGROS, B.; PAVLŮ, V.: Agronomic aspects of biodiversity targeted management of temperate grasslands in Europe – A review. *Agronomy Research*. 2005, Vol. 3, Issue 2, pp. 139–151.
- [17] PAVLŮ, V.; HEJCMAN, M.; PAVLŮ, L.; GAISLER, J.: Restoration of grazing management and its effect on vegetation in an upland grassland. *Applied Vegetation Science*. 2007, Vol. 10, Issue 3, pp. 375–382. DOI: [10.1111/j.1654-109X.2007.tb00436.x](https://doi.org/10.1111/j.1654-109X.2007.tb00436.x)
- [18] MANNSFELD, K.; RICHTER, H.: Naturräume in Sachsen. In: Richter, G (ed.) *Forschungen zur deutschen Landeskunde*. Trier, 1995, Vol. 238, pp. 1–230. ISBN: 3-88143-049-0.
- [19] SÄCHSISCHES LANDESAMT FÜR UMWELT, LANDWIRTSCHAFT UND GEOLOGIE (LfULG): Biotoptypen- und Landnutzungskartierung (BTLNK). 2005. Available from WWW: <https://www.umwelt.sachsen.de/umwelt/natur/25140.htm>
- [20] LANDRATSAMT GÖRLITZ, UMWELTAMT, UNTERE NATURSCHUTZBEHÖRDE (UNB Görlitz) (2018): Gesetzlich geschützte Biotope im Landkreis Görlitz, Stand 06.02.2018.
- [21] METEOROLOGISCHER DIENST DER DEUTSCHEN DEMOKRATISCHEN REPUBLIK: Klimatologische Normalwerte 1951/80. *Klimadaten der Deutschen Demokratischen Republik – Ein Handbuch für die Praxis*. 1987, Vol. 14, pp. 1–111.
- [22] Schutzgebiete. In: *Landkreis Görlitz. Geoportal Online*. [online]. Landratsamt Görlitz, 2015. [accessed 2018-03-06]. Available from WWW: <http://gis-lkgr.de/>
- [23] Topographische Karte (Meßtischblätter) Sachsen. Abteilung für Landesaufnahme des Königl. Sächs. Generalstabes. - 1:25000. - 156 Blatt, versch. Auflagen 1905-1942. - Leipzig. - Je Bl. 48 x 45 cm. In: *Deutsche Fotothek* [online]. Sächsische Landesbibliothek – Staats- und Universitätsbibliothek Dresden (SLUB DRESDEN), 2007. [accessed 2018-03-06]. Available from WWW: <http://www.deutschefotothek.de/cms/kartenforum-sachsen-messtischblaetter-alt.xml>
- [24] RICHTER, F.; SCHULZ, D.: *Farn- und Samenpflanzen – Bestandssituation und Schutz ausgewählter Arten in Sachsen*. Sächsisches Landesamt für Umwelt, Landwirtschaft und Geologie, Dresden, Vol. 2, 2016.
- [25] DEMEK, J.; MACKOVČIN, P: *Zeměpisný lexikon ČR. Hory a nížiny*. AOPK, Brno, 2006. ISBN 80-86064-99-9.
- [26] DEMEK, J.: *Hory a nížiny*. Nakladatelství Academia, Praha, 1987.

- [27] TOMÁŠEK, M.: *Půdní mapa ČR (1:50 000)*. List 03-14 Liberec, 1995. Český geologický ústav, Praha.
- [28] KULASOVÁ, A.; BUBENÍČKOVÁ, L.: Podnebí a počasí Jizerských hor. In: Karpaš R et al (eds.), *Jizerské hory, O mapách, kamení a vodě*. Nakladatelství RK, Liberec, 2009. pp 344–367. ISBN 978-80-87100-08-0.
- [29] VETEŠNÍK, P.; VONIČKA, P.: *Správa Chráněné krajinné oblasti Jizerské hory*. Sborník Severočeského muzea. Severočeské muzeum, Liberec, 1999, Vol. 21, pp. 247–252. ISBN 80-238-3934-9.
- [30] AOPK ČR: *Plán péče o Chráněnou krajinnou oblast Jizerské hory na období 2011-2020*. AOPK ČR, SCHKO Liberec, 2010.
- [31] VIŠŇÁK, R.: Rostlinstvo Jizerských hor. In: Karpaš R.; Višňák R.; Vonička P. (eds.), *Jizerské hory – o rašeliništích, květeně a zvířené*. Nakladatelství RK, Liberec, 2013, pp. 73–169. ISBN 978-80-87100-23-3.
- [32] PECH, P.: *Landforms and Rock Formations in Lusatian*. Liberec, Bachelor thesis. Technická univerzita v Liberci. 2012.
- [33] AOPK ČR: *Plán péče o CHKO Lužické hory na období 2015-2024*. AOPK ČR, SCHKO Liberec, 2013.
- [34] Chráněná krajinná oblast Lužické hory. In: *Wikipedia*. [encyclopedia online]. Wikimedia Foundation Inc., updated 10 February 2018, at 22:14. [accessed 2018-02-23]. Available from WWW: https://cs.wikipedia.org/wiki/Chráněná_krajinná_oblast_Lužické_hory
- [35] KAUTER, D.: “*Sauergras*” und “*Wegbreit*” – *Die Entwicklung der Wiesen in Mitteleuropa zwischen 1500 und 1900*. Berichte des Institutes für Landschafts- und Pflanzenökologie der Universität Hohenheim, Stuttgart, 2002. ISBN 3-935380-05-4.
- [36] HEMPEL, W.: Die historische Entwicklung des Wirtschaftsgrünlandes in Sachsen. Berichte der Naturforschenden Gesellschaft der Oberlausitz. 2008, Vol. 16, pp. 3–18. ISSN 0941-0627.
- [37] POSCHLOD, P.: *Geschichte der Kulturlandschaft*. Ulmer, Stuttgart (Hohenheim), 2015. ISBN 978-3-8001-7983-1.
- [38] HEJCMAN, M; PAVLŮ, V.: Historie pastevního obhospodařování (History of grazing management). In: Mládek J.; Pavlů V.; Hejčman M.; Gaisler J. (eds.), *Pastva jako prostředek údržby trvalých travních porostů v chráněných územích (Grazing as a method of grasslands management in protected areas)*. VÚRV, Praha, pp. 7–9. ISBN 80-86555-76-3.
- [39] Aplikace pro prohlížení naskenovaných archiválií. In: *Ústřední Archiv Zeměměřictví a Katastru (Úazk)* [online]. 2017, Český Úřad Zeměměřičský a Katastrální. [accessed 2017-04-23]. Available from WWW: <http://archivnimapy.cuzk.cz/uazk/pohledy/archiv.html>
- [40] GAISLER, J.; HEJCMAN, M.; MIKULKA, J.; PAVLŮ, L.; PAVLŮ, L.; ŠTROBACH, J.: Zemědělské využívání krajiny. In: Karpaš R.; Hušek J. (eds.), *Jizerské hory o lesích, dřevu a ochraně přírody*. Nakladatelství RK, Liberec, 2014, pp. 498–507. ISBN 978-80-87100-26-4.

- [41] SÄCHSISCHES MINISTERIUM FÜR UMWELT UND LANDWIRTSCHAFT (SMUL) *Richtlinie des Sächsischen Staatsministeriums für Umwelt und Landwirtschaft zur Förderung von Vorhaben der umweltgerechten Flächenbewirtschaftung im Freistaat Sachsen (Förderrichtlinie Agrarumwelt- und Klimamaßnahmen – RL AUK/2015)*. [online] 2015. [accessed 2018-03-06]. Available from WWW: <https://www.revosax.sachsen.de/vorschrift/16239/25377>
- [42] BUSCHMANN, P.: *Dokumentation und Pflegerichtlinie für das Flächennaturdenkmal Hänschberg am Kottmar*. Unpublished investigation, 1987.
- [43] GLÄSER, P.: *Zustandserfassung und Behandlungsrichtlinien für ausgewählte Landschaftspflegeobjekte im Landkreis Löbau-Zittau (2004)*. Unpublished investigation, Bautzen, 2004.
- [44] LANDSCHAFTSARCHITEKTURBÜRO SCHÜTZE UND PARTNER: *Managementplan für das pSCI 113 „Mandautal“*. Unpublished investigation, Bautzen, 2004.
- [45] JANSEN & PARTNER: *Managementplan für das SCI 032E „Hochlagen des Zittauer Gebirges“*. Unpublished investigation, Bautzen, 2006.
- [46] BUNDESAMT FÜR NATURSCHUTZ (BFN): ...Grünlandnutzung nicht vor dem 15. Juni... Sinn und Unsinn von behördlich verordneten Fixterminen in der Landwirtschaft. Dokumentation einer Tagung des Bundesamtes für Naturschutz und des Naturschutz-Zentrums Hessen (NZH) in Wetzlar am 16. / 17. September 2003. *BfN-Skripten*. 2004, Vol. 124, pp. 1–90
- [47] BRIEMLE, G.: Landschaftsökologisch sinnvolle Mindestpflege von artenreichem Grünland und dessen erfolgsorientierte Bewertung. In: Reiter, K.; Schmidt, A.; Stratmann, U. (eds) ...*Grünlandnutzung nicht vor dem 15. Juni...*. BfN-Skripten, Vol. 124, Bonn, Bad-Godesberg, 2004. pp. 33–56.
- [48] NITSCHKE, S.; NITSCHKE, L.: *Extensive Grünlandnutzung*. Neumann, Radebeul, 1994, ISBN 978-3740201494.
- [49] HUŠEK, J.: Zonace území CHKO Jizerské hory. In: Karpaš R.; Hušek J. (eds.), *Jizerské hory – o lesích, dřevu a ochraně přírody*. Nakladatelství RK, Liberec, 2014. ISBN 978-80-87100-26-4.
- [50] HUŠEK, J.: Jizerské hory. *Ochrana přírody*. 2008, Vol. 63, Issue 3, pp. 2-5. ISSN 1210-258X.
- [51] Katalog biotopů. In: *Katalog biotopů České republiky*. [online]. AOPK, 2010, AOPK. [accessed 2018-02-21]. Available from WWW: <http://geoportal.gov.cz/web/guest/home>
- [52] Topographische Karte 1 : 25 000 - Ausgabe Staat (DDR). In: *GeoViewer.Sachsen* [online]. Staatsbetrieb Geobasisinformation und Vermessung, 2017. [accessed 2018-03-06]. Available from WWW: <https://geoviewer.sachsen.de/mapviewer2/index.html?map=359463cd-0222-49ba-bad2-c9f84a6fb1ca&lang=de>

Ing. Jan Titěra; Henning Haase, MSc; Ing. Teowdroes Kassahun Teka;
 Ing. Chukwudi Nwaogu, MSc; Ing. Klára Pavlů, Ph.D.; Dr. Matthias Kändler;
 Ing. Lenka Pavlů, Ph.D.; Ing. Jan Gaisler, Ph.D.; František Paška; Heike Heidenreich;
 Dipl.-Ing (FH) Gerlinde Liepelt; Irena Jonášová; Prof. Dr. Vilém Pavlů

DIVERGRASS – PŘESHraniČNÍ PROJEKT PRO PODPORU UDRŽITELNÉHO MANAGEMENTU TRAVNÍCH POROSTŮ

Většina evropských luk a pastvin patří k polopřirozeným nebo dočasným intenzivním travním porostům. Polopřirozené, většinou druhově bohaté travní porosty byly po staletí udržovány pomocí zemědělských aktivit. Nicméně, v dnešní době jsou modernějším, ale rozšířeným jevem intenzivní travní porosty. Pastva skotu je klíčovým způsobem obhospodařování pro pastviny a pravidelné sečení pro louky. Kombinace pasení a sečení je typická pro spásané louky. Absence defoliace travních porostů, extenzifikace nebo příliš intenzivní hospodaření může vést k poklesu druhové diverzity, doprovázeným mizením ohrožených druhů rostlin. Snížení druhové rozmanitosti travních porostů na přírodních stanovištích je jedním z klíčových problémů současné ochrany přírody na obou stranách česko-německé hranice. V přeshraniční oblasti zahrnující Jizerské hory (CZ), Lužické hory (CZ) a Zittauer Gebirge s předhůřím (D) bylo v rámci projektu DiverGrass na různých typech travních porostů založeno 12 manipulativních managementových experimentů s cílem nalézt optimální opatření pro zastavení poklesu nebo zvýšení biodiverzity rostlin na stanovištích s travními porosty.

DIVERGRASS – EIN GRENZÜBERGREIFENDES PROJEKT ZUR FÖRDERUNG NACHHALTIGEN MANagements VON GRASLAND

Der Großteil der europäischen Wiesen und Weiden kann dem halbnatürlichen Grasland oder dem eingesäten Intensiv-Grasland zugeordnet werden. Halbnatürliches oft artenreiches Grasland entstand aus der jahrhundertelangen landwirtschaftlichen Tätigkeit des Menschen. Intensiv-Grasländer hingegen sind eine relativ moderne aber sehr weit verbreitete Erscheinung. Während die Beweidung für Weiden typisch ist und regelmäßiges Mähen für Wiesen, wird bei Mähweiden die Mahd mit einer Vor- oder Nachbeweidung kombiniert. Die Nutzungsaufgabe, zu extensive oder zu intensive Nutzung führt in der Regel zu einer Reduktion der Pflanzenvielfalt und Verlust von gefährdeten Pflanzenarten. Der Verlust der Diversität halbnatürlicher Grasländer ist derzeit eines der größten Probleme des Naturschutzes beiderseits der Deutsch (D)-Tschechischen (CZ) Grenze. In der grenzüberschreitenden Region bestehend aus dem Isergebirge (CZ), dem Lausitzer Gebirge (CZ) und dem Zittauer Gebirge und Vorland (D) wurden im Rahmen des Projektes DiverGrass 12 Experimentalflächen auf verschiedenen Grasland-Typen eingerichtet. Auf denen werden verschiedene Maßnahmen zur Stabilisierung und Förderung eines guten Erhaltungszustandes der Grasländer erprobt, um den weiteren Verlust seltener Arten entgegenzuwirken und die Diversität der Standorte bestenfalls zu erhöhen.

DIVERGRASS – PROJEKT TRANSGRANICZNY NA RZECZ ZRÓWNOWAŻONEGO ZARZĄDZANIA ZBIOROWISK TRAWIASTYCH

Większość europejskich łąk i pastwisk to intensywnie użytkowane, półnaturalne i tymczasowe użytki zielone. Półnaturalne, w większości gatunkowo bogate, zbiorowiska trawiaste były na przestrzeni wieków utrzymywane poprzez rolniczą działalność człowieka. Jednak obecnie bardziej nowoczesnym i powszechnym zjawiskiem jest intensywne użytkowanie zbiorowisk trawiastych. Wypasanie bydła stanowi podstawowy sposób stosowany na pastwiskach, natomiast łąki są regularnie koszone. Połączenie tych dwóch sposobów jest typowe dla wypasanych łąk. Brak defoliacji zbiorowisk trawiastych, ekstensyfikacja lub nadmierna gospodarka intensywna może skutkować zmniejszeniem różnorodności gatunkowej roślin, a także wyplenieniem zagrożonych gatunków roślin.

Zmniejszanie różnorodności gatunkowej zbiorowisk trawiastych na naturalnych stanowiskach stanowi jeden z kluczowych problemów w zakresie ochrony przyrody po obu stronach czesko-niemieckiej granicy. W ramach projektu DiverGrass, realizowanego na terenach transgranicznych obejmujących Góry Izerskie (CZ), Góry Łużyckie (CZ) oraz Góry Żytawskie wraz z ich przedgórzem (DE) założono 12 punktów eksperymentalnych w celu znalezienia optymalnych zabiegów mających na celu zatrzymanie zmniejszania lub zwiększenie różnorodności gatunkowej roślin na stanowiskach ze zbiorowiskami trawiastymi.

LIST OF AUTHORS

Name	E-Mail and Page Number of Contribution
Jiří Beneš	benes@ipp.cas.cz 7
Michal Špína	spina@ipp.cas.cz 7
František Procháska	prochaska@ipp.cas.cz 7
Jiří Hlubuček	hlubucek@ipp.cas.cz 17
Jiří Budasz	budasz@ipp.cas.cz 17
Jan Václavík	vaclavik@ipp.cas.cz 17
Karel Žídek	zidek@ipp.cas.cz 17
Jiří Hlubuček	hlubucek@ipp.cas.cz 24
Karel Žídek	zidek@ipp.cas.cz 24
Pavel Psota	psota@ipp.cas.cz 33
Vít Lédl	ledl@ipp.cas.cz 33
Roman Doleček	dolecek@ipp.cas.cz 33
Ondřej Matoušek	ondrej.matousek@tul.cz 33
Jan Kredba	jan.kredba@tul.cz 33
Jana Urbánková	jana.urbankova@vuts.cz 43
Alexander Prošek	alexander.prosek@vuts.cz 53
Jan Titěra	titeraj@fzp.czu.cz 61
Henning Haase	henning.haase@tu-dresden.de 61
Teowdroes Kassahun Teká	teka@fzp.czu.cz 61
Chukwudi Nwaogu	cnwaogu@gmail.cz 61
Klára Pavlů	kpavlu@fzp.czu.cz 61
Matthias Kändler	matthias.kaendler@tu-dresden.de 61
Lenka Pavlů	pavlul@fzp.czu.cz 61
Jan Gaisler	gaisler@vurv.cz 61
František Paška	paska@vurv.cz 61
Heike Heidenreich	heike.heidenreich@tu-dresden.de 61
Gerlinde Liepelt	gerlinde.liepelt@tu-dresden.de 61
Irena Jonášová	jonasova@vurv.cz 61
Vilem Pavlů	pavlu@vurv.cz 61

GUIDELINES FOR CONTRIBUTORS

Guidelines for contributors are written in the form of a template which is available as a Word document at http://acc-ern.tul.cz/images/journal/ACC_Journal_Template.docx.

EDITORIAL BOARD

<i>Editor in Chief</i>  Prof. Ing. Pavel Mokrý, Ph.D.	Technical University of Liberec pavel.mokry@tul.cz
<i>Assistant of the Editor in Chief</i>  Prof. Ing. Miroslav Žižka, Ph.D.	Technical University of Liberec miroslav.zizka@tul.cz
<i>Executive Editor</i>  PaedDr. Helena Neumannová, Ph.D.	Technical University of Liberec helena.neumannova@tul.cz phone:+420 734 872 413

Other Members of the Editorial Board

 Doc. PaedDr. Hana Andrášová, Ph.D.	University of South Bohemia in České Budějovice andras@pf.jcu.cz
 Doc. PhDr. Tomáš Kasper, Ph.D.	Technical University of Liberec tomas.kasper@tul.cz
 Prof. Ing. Jiří Militký, CSc.	Technical University of Liberec jiri.militky@tul.cz
 Doc. Ing. Iva Petříková, Ph.D.	Technical University of Liberec iva.petrikova@tul.cz
 Doc. Dr. Ing. Miroslav Plevný	University of West Bohemia in Pilsen plevny@fek.zcu.cz
 Doc. Ing. Petr Šidlof, Ph.D.	Technical University of Liberec petr.sidlof@tul.cz
 Dr. Eckhard Burkatzki	TU Dresden / IHI Zittau burkatzki@tu-dresden.de
 Prof. Dr.-Ing. Frank Hentschel	Hochschule Zittau / Görlitz f.hentschel@hszg.de
 Prof. Dr. phil. PhDr. (MU Brno) Annette Muschner	Hochschule Zittau / Görlitz a.muschner@hszg.de
 Dr. Piotr Gryszel	Universitet Ekonomiczny we Wrocławiu Wydział Ekonomii Zarządzania i Turystyki piotr.gryszel@ue.wroc.pl
 Prof. UE Dr. hab. Elżbieta Sobczak	Universitet Ekonomiczny we Wrocławiu Wydział Ekonomii Zarządzania i Turystyki elzbieta.sobczak@ue.wroc.pl
 Prof. UE Dr. hab. Grażyna Węgrzyn	Universitet Ekonomiczny we Wrocławiu Wydział Ekonomii Zarządzania i Turystyki grazyna.wegrzyn@ue.wroc.pl

Assistant of the editorial office:

Ing. Dana Nejedlová, Ph.D., Technical University of Liberec, Department of Informatics,
phone: +420 485 352 323, e-mail: dana.nejedlova@tul.cz

Název časopisu (<i>Journal Title</i>)	ACC JOURNAL
Rok/Ročník/Číslo (<i>Year/Volume/Issue</i>)	2018/24/1 (2018/XXIV/Issue A)
Autor (<i>Author</i>)	kolektiv autorů (<i>composite author</i>)
Vydavatel (<i>Published by</i>)	Technická univerzita v Liberci Studentská 2, Liberec 1, 461 17 IČO 46747885, DIČ CZ 46 747 885
Schváleno rektorem TU v Liberci dne	18. 1. 2018, č. j. RE 3/18
Vyšlo (<i>Published on</i>)	30. 6. 2018
Počet stran (<i>Number of pages</i>)	83
Vydání (<i>Edition</i>)	první (<i>first</i>)
Číslo publikace (<i>Number of publication</i>)	55-003-18
Evidenční číslo periodického tisku (<i>Registry reference number of periodical print</i>)	MK ČR E 18815
Počet výtisků (<i>Number of copies</i>)	60 ks (<i>pieces</i>)
Adresa redakce (<i>Address of the editorial office</i>)	Technická univerzita v Liberci Akademické koordinační středisko v Euroregionu Nisa (ACC) Studentská 2, Liberec 1 461 17, Česká republika Tel. +420 485 352 318, Fax +420 485 352 229 e-mail: acc-journal@tul.cz http://acc-ern.tul.cz
Tiskne (<i>Print</i>)	Vysokoškolský podnik Liberec, spol. s r.o. Studentská 1402/2, Liberec 1 460 01, Česká republika

Upozornění pro čtenáře

Příspěvky v časopise jsou recenzovány a prošly jazykovou redakcí.

Readers' notice

Contributions in the journal have been reviewed and edited.

Předplatné

Objednávky předplatného přijímá redakce. Cena předplatného za rok je 900,- Kč mimo balné a poštovné. Starší čísla lze objednat do vyčerpání zásob (cena 200,- Kč za kus).

Subscription

Subscription orders must be sent to the editorial office. The price is 40 € a year excluding postage and packaging. It is possible to order older issues only until present supplies are exhausted (8 € an issue).

Časopis ACC JOURNAL vychází třikrát ročně (červen, září, prosinec).

Three issues of ACC JOURNAL are published every year (June, September, December).

Liberec – Zittau/Görlitz – Wrocław/Jelenia Góra

© Technická univerzita v Liberci – 2018

ISSN 1803-9782 (Print)

ISSN 1803-9790 (CD-ROM)

ISSN 2571-0613 (Online)